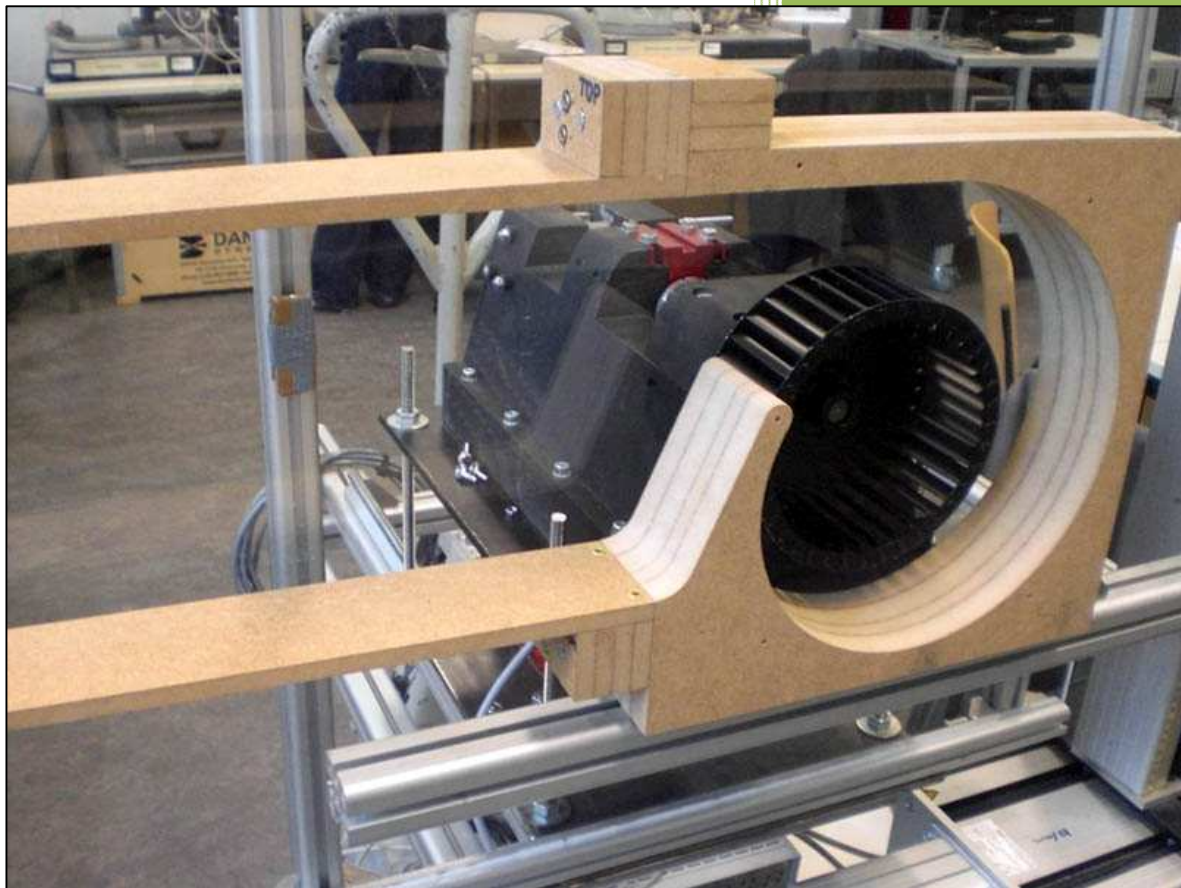


Anexo

Proyecto fin de carrera completo en inglés

Title:

Experimental investigation on the influence of the scroll housing on the performance of Sirocco type fan



Director:

Prof. Dr.-Ing. Stefan Frank
Area of Mechanical engineering
HTW Berlin

Author:

Ricard Terés Duaso
Matr.Num.: 528090
HTW Berlin
6/1/2011

Experimental investigation on the influence of the scroll housing on the performance of Sirocco fans

Abstract

The aim of this work was to perform an experimental investigation on the influence of the scroll housing on the performance of Sirocco type fan (i.e. Radial fans with forward curved blades). It was developed under the Research funding of “Numerical Calculations and Designing of Sirocco Fans” in German “Numerische Berechnung und Auslegung von Trommelläufer-Ventilatoren” (NUBAT) at the University of Applied Sciences Berlin (HTW Berlin).

The main goal of this work was to evaluate the behavior of the Sirocco type fan for different configurations regarding on the parameters of the scroll housing and the relative position of the rotor inside it. It was expected to find a better performance of the fan and achieve a higher static efficiency. Common Sirocco fans are about 30-55%.

To achieve this goal, three main tasks were necessary. The first task was the development and manufacturing of appropriate test models of Sirocco type fan. The second was the design, organization and implementation of a measurement campaign based on an existing test rig. The final task was the compilation and evaluation of the results.

After a deep review of the literature and by using the advices of the members of the team, six new models of the fan were designed by using appropriate 3D software. The sketches of these designs were sent to an external workshop in order to be manufactured. After receiving the new pieces it was necessary to assembly them and to polish them to ensure a good surface finish.

A measurement campaign was organized in order to evaluate the models. The whole measurement matrix regarded the amount of 144 different variations in the configuration of the fan to be checked. By using technologically-advanced equipment i.e. high-accuracy chamber test rig, contactless torque sensor and multifunctional fan test rig, the measurements were recorded.

All the data was compiled and evaluated. The measurements were converted in graphs to easy appreciate the behavior of the fan. The characteristic curves for the pressure rise, torque on shaft and static efficiency were drawn. An extensive static efficiency study was developed to find the configuration with the best static efficiency. The influences of the parameters of design were evaluated.

Interesting information on the behavior of the new model of Sirocco type fan has been found. The best static efficiency recorded rises to 69% for a rotational speed of 1000 rpm. Moreover some influences and trends were found while evaluating the characteristic curves and were included in this work.

Acknowledgement

I would like to express my sincere gratitude to Prof. Dr.-Ing. Stepan Frank who brought me the chance to develop my Master thesis in the team of research of mechanical engineering in HTW Berlin. I appreciate specially his support and guidance during all the development of my work there.

I am grateful to Adam Stuchlik for his constant advices and assistance, to all the members of the team for their helping hand in difficult moments and to my tutor in Spain, Mr Guillermo Hauke.

I am grateful also to my family which in the distance always expressed me the love and support that I needed.

Sincerely

Ricard Terés Duaso

Berlin, June 2011

Contents

1 Introduction

1.1 Description of the problem	1
1.2 Objectives of this work	2
1.3 Previous projects	3
1.4 State-of-the-art	3
1.4.1 Chamber test rig	3
1.4.2 Torque sensor	5

2 Designed pieces for the development of this work

2.1 Parameters of design on Sirocco type fan	7
2.1.1 Fixed parameters for the geometry of the rotor	8
2.1.2 Variable parameters for the geometry of the scroll housing	9
2.2 Positioning pieces for the scroll housing	11
2.3 Components for calibrating the torque sensor	11
2.4 Manufacturing the models	12

3 Test rig

3.1 Specifications	15
3.2 Fan test rig	16
3.2.1 Body structure	16
3.2.2 Fan unit	17
3.2.3 Movement of the fan unit through the rail guides	17
3.2.4 Scroll housing integration	18
3.3 Integration into the chamber test rig	19

4 Mathematical foundations

4.1 Introduction	21
4.2 Determination of the characteristics of the fan	22

5 Uncertainty of measurement

5.1 Resume of the sources of uncertainty in the test rig	25
--	----

6 Measurement campaign

6.1 Measurement matrix	27
6.2 Procedure for measuring	29
6.3 Methodology of measuring	30

7 Collected data

7.1 Most relevant data grouped by housing families.....	36
7.1.1 Scroll housing with opening angle of spiral curve of $\alpha_s = 3,0^\circ$	36
7.1.2 Scroll housing with opening angle of spiral curve of $\alpha_s = 3,5^\circ$	38
7.1.3 Scroll housing with opening angle of spiral curve of $\alpha_s = 4,0^\circ$	40
7.1.4 Scroll housing with opening angle of spiral curve of $\alpha_s = 4,5^\circ$	42
7.1.5 Scroll housing with opening angle of spiral curve of $\alpha_s = 5,0^\circ$	44
7.1.6 Scroll housing with opening angle of spiral curve of $\alpha_s = 5,5^\circ$	52

8 Evaluation of the results

8.1 Maximum efficiencies found.....	55
8.1.1 Maximum static efficiency of the whole measurement campaign....	55
8.1.2 Maximum static efficiencies by opening angle families.....	56
8.1.3 Maximum static efficiencies by width families	59
8.1.4 Maximum static efficiencies by gap rotor-housing families.....	60
8.1.5 Maximum static efficiencies by angle of eccentricity families.....	63
8.1.6 Maximum static efficiencies for each point of flow rate	65
8.2 Resume of trends and influences found.....	67
8.2.1 Influence of the opening angle	67
8.2.2 Influence of the width of housing	69
8.2.3 Influence of decentering the rotor	70

9 Comparison of the results

9.1 Comparison with CFD's results.....	73
9.2 Comparison with Roth's results.....	75

10 Conclusions 79

11 Bibliography

11.1 Written references.....	81
11.2 Electronic references	81

12 Nomenclature..... 83

Appendix A. Tool for obtaining the points of the spiral curve.....	II
Appendix B. Values for decentering the rotor.....	III
Appendix C. Data provided by the chamber test rig.....	V
Appendix D. Study of maximal static efficiencies.....	VI
Appendix E. Details of the configuration with highest static efficiency.....	VIII

Appendix F. Data collected from Roth's graphs.....	IX
Appendix G. Specifications of the components.....	X

1 Introduction

1.1 Description of the problem

Sirocco type fan is a centrifugal fan (also called “blower” or “squirrel cage”). It has mainly two forming parts. The first is a moving component, the rotor that is basically a central shaft in which a set of forward curved blades are positioned. The second is a scroll housing responsible to collect the various air streams leaving the blades and lead them into a single air flow that leaves the unit. In Sirocco type fan, the operating principle is a combination of two effects: centrifugal force and the deflection of the air flow by the blades. An actual picture of Sirocco type fan is shown in Figure 1.1



Figure 1.1: Sirocco type fan (source: www.jouning-blower.com)

Sirocco type fan is used nowadays in a big range of commercial and domestic products. Computers, dryers, projectors, cars and cooling systems are some examples. The strengths of this type of fan are the low operating noise level and the low manufacturing costs. But not all is favorable in Sirocco type fan. It presents very poor static efficiencies. When to the total efficiency provided by the fan, the dynamic pressure is subtracted; the highest static efficiency is fluctuating around 30–55%. This means that the electrical or hydraulic power necessary for their operation is too high in comparison to the useful power at the outlet. This fact is especially important to be considered in the actual context where more strict regulations about high efficiencies are requested.

The main reason for its low efficiency is due to the high turbulent and tridimensional flow that normally presents on its operation. According to CFD

(Computational Fluid Dynamics) simulations, the air flow leaves the blades at the very beginning and it is not guided anymore. The result is a big amount of turbulences that produce high energy losses. Blades impact in a mass of air that is moving in all directions.

The behavior of this kind of fans cannot be deduced directly from Euler's equation. That is one of the reasons of the lack of study on Sirocco type fan. Experimental investigations are requested to improve in this area of knowledge.

Research funding of "Numerical Calculations and Designing of Sirocco Fans" in German "Numerische Berechnung und Auslegung von Trommelläufer-Ventilatoren" (NUBAT) at the University of Applied Sciences Berlin (HTW) has been working for three years with this type of fan. The purpose of this research is to optimize its performance by using both CFD simulations and experimental investigations.

1.2 Objectives of this work

As a student collaborator into this ambitious project, I carry on with a subpart of it. My task is to investigate the influence of the scroll housing on the performance of Sirocco type fan in order to elevate its low efficiency.

To achieve this aim several subtasks are necessary. Firstly I submerge along the actual literature to have a big view about the topic. With the knowledge provided by these books and with the great advices of the director and the members of the team of the project, I am able to start this work. If it's possible to increase the static efficiency of the Sirocco type fan by optimizing the scroll housing, I know in which way to experiment it could be possible. Secondly, it is necessary to choose the parameters of design for the scroll housing for the study. After that, a campaign with 144 configurations it ready to develop. Some new mechanical pieces need to be drawn with 3D-design-software in order to be sent to the manufacturing company because this is an experimental study. By using the advanced installations in the laboratory of fluid dynamics of the HTW Berlin, the new models are evaluated within a measurement campaign. Subsequently all data is compiled and evaluated to check out the expectations of increment the static efficiency. Finally we will be able to say if the aim of this work has a successfully end. Additionally after this study it is possible to advice about some trends that are favorable for better performance on the Sirocco type fan.

As a resume we can number the objectives of this work below:

1. To design new scroll housings adapted to a multifunctional fan test ring by using adequate analysis tools and 3D software.
2. To obtain the sketches and other data necessary for manufacturing the pieces into an external enterprises or in the workshop of HTW Berlin.
3. To assembly and to verify the manufactured pieces.
4. To design, to organize and to perform a measurement campaign according to the equipment of the fluid dynamic laboratory at HTW.
5. To compile and to evaluate the data obtained with the new designs regarding operating and efficiency performance.

1.3 Previous projects

As mentioned before this project is a part of a bigger investigation about Sirocco type fan. Some students have contributed with the next works:

Monteiro Sotelo, Iago. **Analysis of the air flow in a tumble dryer by means of laser Doppler and hotwire anemometry**. Master thesis, Berlin: 2008. Industrial engineer by the University of Vigo. In this work, the author registered data from velocity and turbulences of a commercial Sirocco type fan. This information was used as a data base for simulations with finite elements.

López Martínez, José Ramón. **Analysis and design of Sirocco fans using different philosophies**. Master thesis, Berlin: 2009. Industrial engineer by the University of Vigo. In his work, the author designed three different Sirocco type fans following the criteria of three authors. The final aim was to check the differences in design and performance of these three different types.

Lückemann, Andreas. **Laseroptische Strömungsmessungen an Trommelläufnern**. Master thesis, Berlin: 2009. Master in mechanical engineering by HTW Berlin. In this work, the author designed and built a scroll housing of methacrylate and some other components to perform a measurement campaign by using PIV technology and high-accuracy test rig.

Salinas Cortés, David. **Measurement of Velocity and Turbulence in the Scroll housing of a Sirocco type fan by means of Laser Doppler Velocimetry**. Master thesis, Berlin: 2010. Industrial engineer by the University of Zaragoza. In his work, the author performed a measurement campaign on the Scroll housing of Sirocco type fan by using the Laser Doppler Velocimetry. Afterwards, the author compared the plausibility of the experimental data recorded with the CFD simulations.

Darvish, Manoochehr. **Numerical Investigations on the Performance Characteristic of Radial Fans with Froward curved blades by means of CFD**. Master thesis, Berlin: 2010. The author performed a study by using CFD on the Sirocco type fan. The main goal was to predict the performance curves of this type of fans and compare it to the experimental results. The author used for that purpose different turbulence models and mesh configurations.

1.4 State-of-the-art

1.4.1 Chamber test rig

Chamber test rigs are used to determine characteristic curves and to study flows in fans and other HVAC (Heating, Ventilating and Air Conditioning) parts. The study of the performance is executed by a test that will fling the flow rate, pressure rise, power consumption and efficiency for every operating point.

Afterwards should be possible to continue detailed flow studies thanks to this database by matching with the characteristic resistance curve from the fans or other components.

Chamber test rigs for small fans are usually designed according to the DIN 24163 and have a testing capacity starting at a flow rate of 11 m³/h up to 1600 m³/h, until an increment of pressure of 2500 Pa.

The main components of a test chamber stand are the volume measuring equipment associated to inlet and outlet sections, a support fan, a hermetically sealed housing with flow conditioner, a cabinet for measuring and the Control technology.

The determination of volume flow will be done by the volume measuring equipment according to DIN EN ISO 5167. To cover the entire range of flow rates, different pipe inlets with different sections can be switch.

The pressure loss in the inlet pipe will be compensated by the support fan and it will not affect to the measurement.

To set the desired pressure or the desired flow rate on the suction side of the DUT (Device under Test), the required air flow generated through the support fan and the DUT, is guided into the measuring chamber through a motorized throttle valve and a diffuser.

A flow conditioner is located in the hermetically sealed chamber which ensures that the airflow moves evenly to the outlet. In the outlet is positioned the Test fan.

The sensors are connected to the main panel by using the appropriated data bus. The detailed measurements are recorded by a computer and appropriate software.

The chamber test rig provided by ILK Dresden ensures high-accuracy data to determinate the performance curves on test. With precise and well adapted sensors is providing a uncertainty for the flow rate less than 1% and for pressure differences less than 0,5%. A scheme of the parts of the test chamber stand is shown in Figure 1.2.

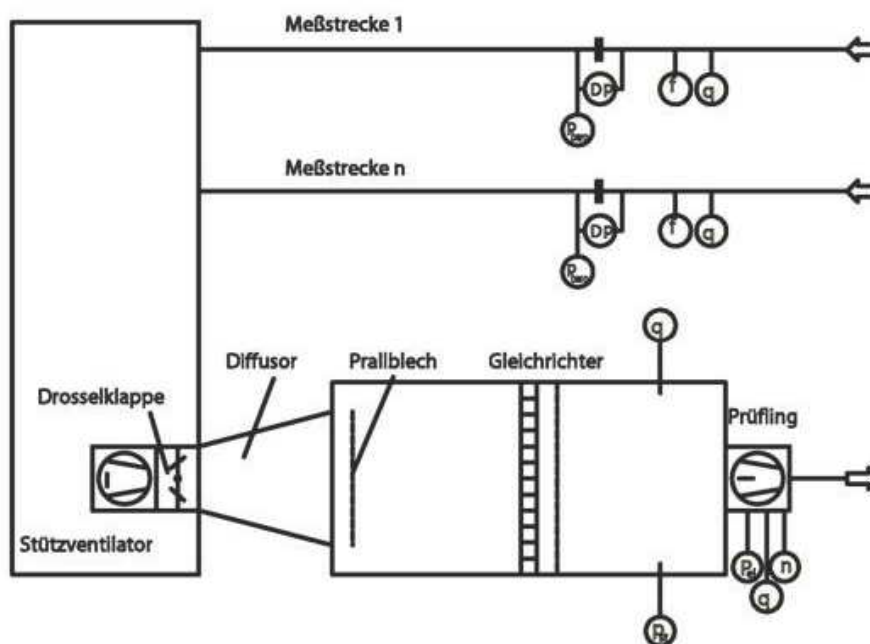


Figure 1.2: Scheme of the Test chamber rig by ILK Dresden

1.4.2 Torque sensor

A torque sensor is used for monitoring the torque that is contributing on the shaft. The applications of torque sensors are diverse: They are used in assemblies to monitor a maximum torque such as engines, crankshafts, gearboxes and transmissions, or in quality control in measuring the power output of a machine.

In general, torque sensors are combined with others type of sensors at the same time, for example to determine the rotational speed or the rotation angles. That allows to record certain angle positions that could be useful in the case of Sirocco type fans or to save rotational speeds in order to check out the performance of this kind of fans.

Torque sensors of the latest generation effectuate the required readings by using non-contact technology, so that losses and uncertainties are reduced. These torque sensors operate on the principle of strain gage technology. The torque signal is transmitted from the rotating shaft via frequency modulation and is processed as an analog signal.

These torque sensors also give the rotation angle signal as a transistor-transistor logic signal levels (TTL) from which allows the transmitted square wave frequency as a function of other devices to control the angle of rotation signal. This signal is read twice during the 360 degrees. So that means that the sensors provide two signals for every degree arranged from 1 to 360. The angle of positioning is determined by the amount offset of the two tracks.

Common torque sensors start at a range of 0,35 Nm and depending on size, can reach 30 kNm. The accuracy classes are between 0,2% and 0,01% (accuracy relative to full scale). Thus, an absolute measurement uncertainty is less than 0,005 Nm. The ranges of these torque sensors reach up to 30,000 rpm. A picture of the torque sensor used in this project can be appreciated in Figure 1.3:



Figure 1.3: Rotational torque sensor (source: <http://www.kistler.com>)

2 Designed pieces for the development of this work

To achieve the objectives of this work, new mechanical pieces need to be design. We need six new scroll housings, their own positioning pieces to center them, and some auxiliary pieces to calibrate the torque sensor. In this chapter all the details of these new pieces can be found.

2.1 Parameters of design on Sirocco type fan

By collecting the inheritance from Werner Roth in his comprehensive study of Sirocco type fan (Roth, 1980) we can use his description of the variables involved in the design of that kind of fans. Refer to Figure 2.1.

Geometry of the scroll housing:

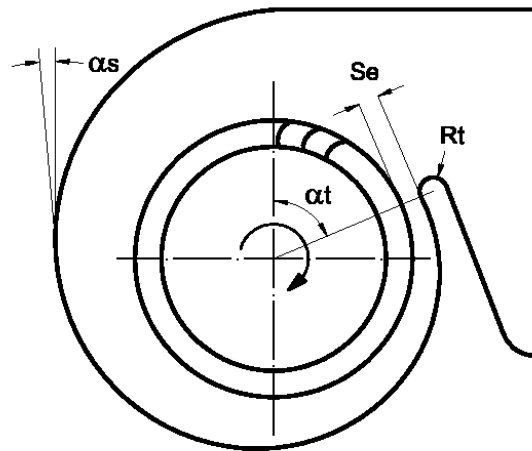
α_s : Opening angle of spiral curve

α_t : Angle of positioning of the tongue

S_e : Minimum gap between rotor and scroll housing

R_t : Radius of the tongue

B : Width of the scroll housing



Geometry of the rotor:

D_1 : Inner diameter

D_2 : Outer diameter

b : Width of the rotor

R_b : Radius of the blade

β_{s1} : Inlet blade angle

β_{s2} : Outlet blade angle

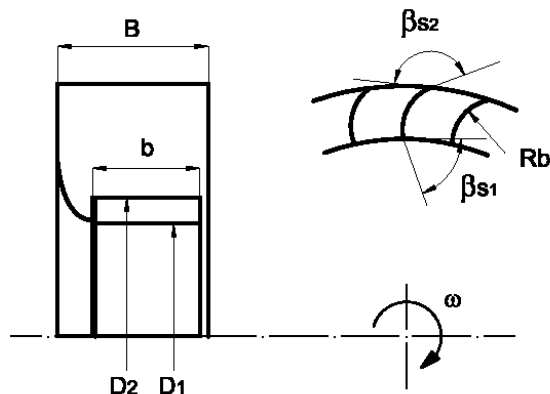


Figure 2.1: Design parameters for Sirocco type fan given by Roth

As this investigation is focused on the influence of the scroll housing on the performance of Sirocco type fan, we work with fix parameters on the rotor design. We will check out the influence of the parameters of the scroll housing. In addition, we evaluate how a slightly decenter from the origin position of the rotor affects on the performance of the fan. In resume:

- Fixed parameters for the geometry of the rotor
- Variable parameters for the geometry of the scroll housing
- Once built the scroll housing, by using decentering the rotor (runout), check out the influence on the performance of the fan.

2.1.1 Fixed parameters for the geometry of the rotor

The rotor used for this work is coming from the company Punker¹. We work with this rotor because we assume that has already an optimized design and because this work is focused on the influence of the scroll housing on the performance of Sirocco type fan.

The model used for the investigation has these properties:

Geometry of the rotor:

$$D_1 = 130 \text{ mm}$$

$$D_2 = 160 \text{ mm}$$

$$b = 62 \text{ mm}$$

$$Rb = 15 \text{ mm}$$

$$\beta_{s1} = 77,3^\circ$$

$$\beta_{s2} = 165,4^\circ$$

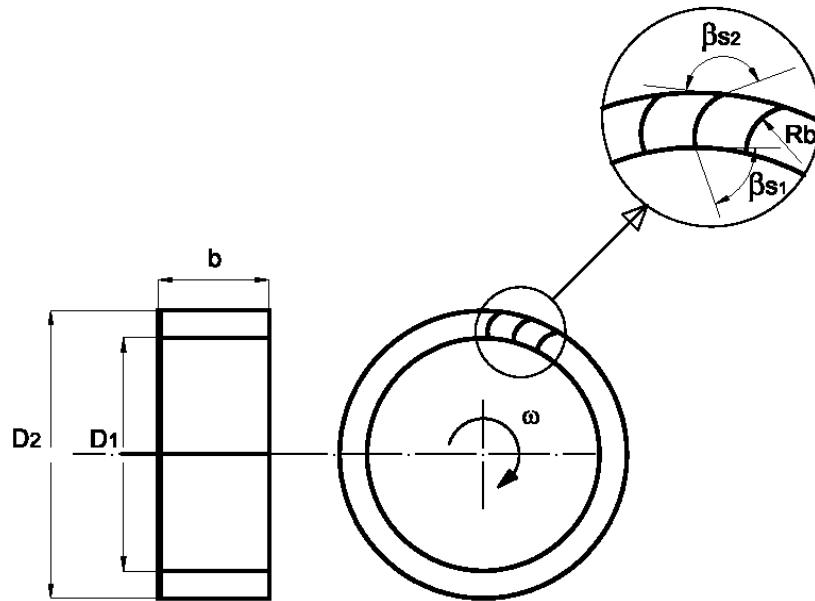


Figure 2.2: Fixed parameters of design for the rotor

These parameters will never change during the measurement campaign therefore there is no need to design for the rotor.

¹ Punker: Blower wheels and Fan Technology (www.punker.de)

2.1.2 Variable parameters for the geometry of the scroll housing

This section is one of the most important points on the design of new pieces. To perform these designs we use for one hand, again the references provided by Roth on his study, and from the other hand the knowledge provided by a previous work from a member of the team (Lückemann, 2009).

Roth has experimented with Sirocco type fan and he arrived to the conclusions that for the best performance, these relations are needed:

$$\alpha_s = 5^\circ$$

$$B/b = 1,08$$

$$Se/D_2 = 0,08$$

$$Rt/D_2 = 0,05$$

$$\alpha_t = 65^\circ$$

Lückemann experimented with the same type of fan on his work with good results following the next criteria:

$$\alpha_s = 7^\circ$$

$$B/b = 1,08$$

$$Se/D_2 = 0,075$$

$$Rt/D_2 = 0,05$$

$$\alpha_t = 67^\circ$$

As we see the relations for obtaining high efficiencies are practically the same ones.

The interest of this work is born in the fact that Roth did an exhaustive experimentation in all the aspects of the Sirocco fan: rotor, blades, housing, nozzles, tongue, etc. But with that amount of experimentation he could not practice as much detailed as to arrive a definitive conclusions. He is expressing this fact on his own words besides empathizing the lack of experimentation in this kind of fans.

For instance, when he is checking the influence of the opening angle of spiral curve (α_s), he uses on his measurements different angles for this purpose. These angles are $\alpha_s = 3^\circ, 5^\circ, 7^\circ, 9^\circ$ and 11° , that is every 2 degrees. The opening angle that is giving the best efficiency for him is 5° . But could happen that the real maximum is for another angle near this one for example for $4,5^\circ$ or $5,5^\circ$. That is why in this work we experiment with short divisions around that maximum.

For the new investigation we experiment with divisions in every $0,5$ degree in the range from 3° to $5,5^\circ$. More precisely the opening angles of spiral curves involved in the new study are: $\alpha_s: 3,0^\circ; 3,5^\circ; 4,0^\circ; 4,5^\circ; 5,0^\circ; 5,5^\circ$.

We check as well two values for the width of housing that is for 67 mm and 87 mm. By using the dimensionless parameter $B/b = 67/62; 87/62 = 1,08; 1,4$. According

to Roth, the relation $B/b = 1,08$ should be better, but we want to repeat the experiment and check out this results for ourselves.

About the value of the gap between rotor and housing we design by using the criteria of $Se/D_2 = 0,075$. As the outer diameter of the rotor is $D_2 = 160$ mm, this gap should be $Se = 0,075 \cdot 160 = 12$ mm.

The radius of the tongue is fixed according the relation $Rt/D_2 = 0,05$. As long as we know the D_2 , the value of this radius is $Rt = 0,05 \cdot 160 = 8$ mm

For the angle of positioning of the tongue we use the criteria of $\alpha_t = 67^\circ$

As a resume of the design of the new scroll housings, a final scheme is shown in Figure 2.3:

Geometry of the scroll housing:

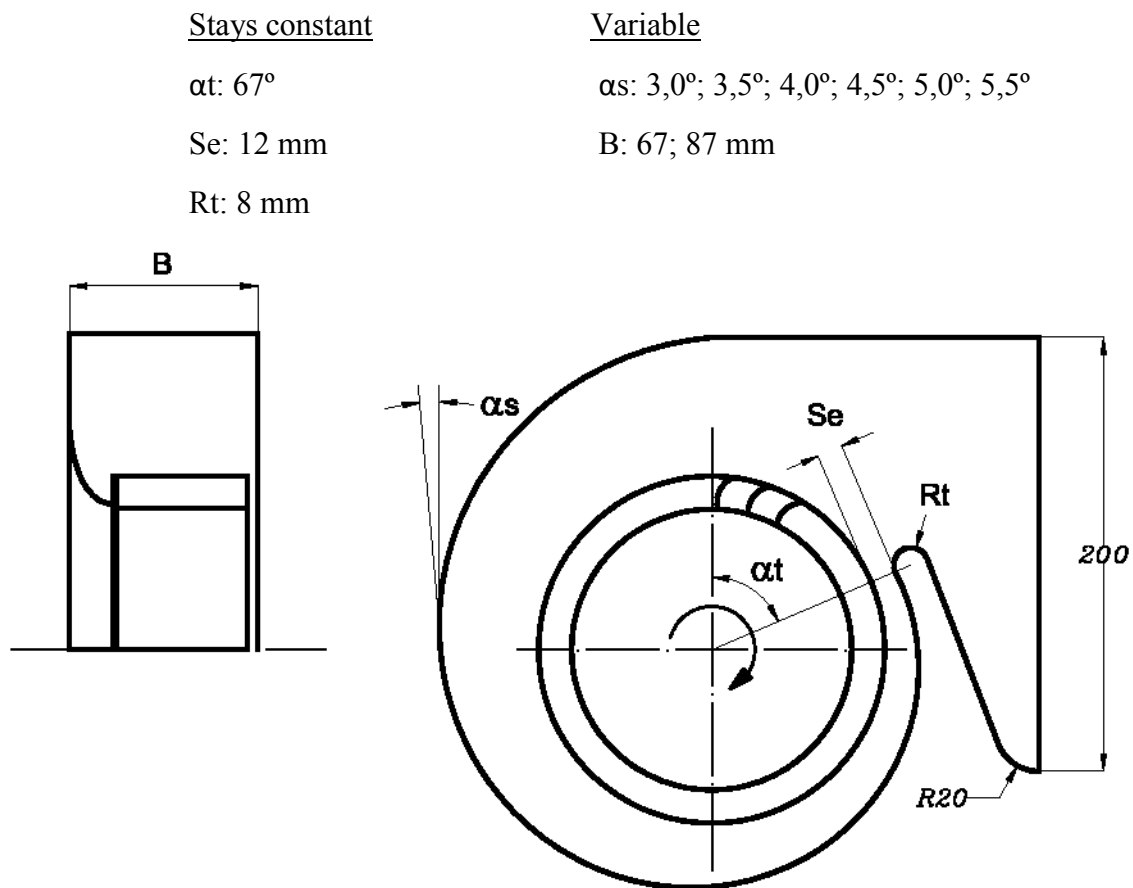


Figure 2.3: Parameters of design for the scroll housing

For obtaining the points to drawn the logarithmic spiral contour with the different values of α_s , we created a sheet tool that allows exporting these points to 3D-design software. We have a view of this tool in *Appendix A. Tool for obtaining the points of the spiral curve.*

2.2 Positioning pieces for the scroll housing

This piece is used to align the scroll housing in the origin position on the desk from the fan test rig in order to proceed with the measurement.

As we built six scroll housings we need six positioning pieces as well. The design of this piece is easy to obtain after having the corresponding design of the housing. This part has to match inside the cavity of the housing. In addition, it is needed a hole with the diameter of the shaft of the rotor in the central point of the spiral curve that is 10 mm.

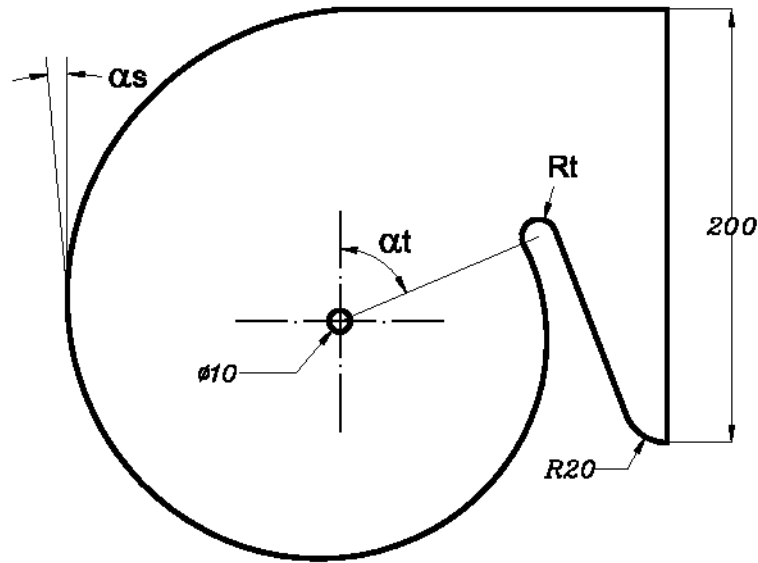


Figure 2.4: Positioning piece for 5° housing

An example of a positioning piece for the scroll housing of 5 degree is shown in Figure 2.4.

2.3 Components for calibrating the torque sensor

The torque sensor allows to record the torque present in the shaft and afterwards to calculate the efficiency of the fan.

Before mounting the torque sensor in his placement in the fan test rig, we execute a manual verification of the accuracy of the values given by this sensor although we have a regulatory certificate of calibration of it.

We need a new part for this pre-calibration that has to stop the shaft in order to record the static moment created when a mass is hanging on the bar opposite side of the shaft. Refer to Figure 2.5.



Figure 2.5: Pre-calibration set for the torque sensor

This new piece that we need has to be able to fix or free the shaft as own necessity.

2.4 Manufacturing the models

The piece to calibrate the torque sensor was manufactured in the workshop of the HTW Berlin. For manufacturing this piece, used in the calibration of the torque sensor, we created and sketch 2-d by hand. Then we wrote the regulatory sheet to send to the Workshop of the HTW Berlin.

For manufacturing the scroll housings, these were sent to an extern workshop. We decided to cut it from an external company specialized in wood material. In order to cut the housing we send a file with the sketches drawn with software for designing and subsequently we create and sketch 2-d with the profile of each housing. In total are six sketches: for the housing of $3,0^\circ$ - $3,5^\circ$ - $4,0^\circ$ - $4,5^\circ$ - $5,0^\circ$ and $5,5^\circ$. Additionally another six sketches for manufacturing the six positioning pieces for the housings.

The restrictions for the design of the housings were to cut the piece in a block of wood of 300 x 300 mm. All the designs are adapted to this geometry. As an example, we can appreciate the sketch for the housing of 5 degree in Figure 2.6.

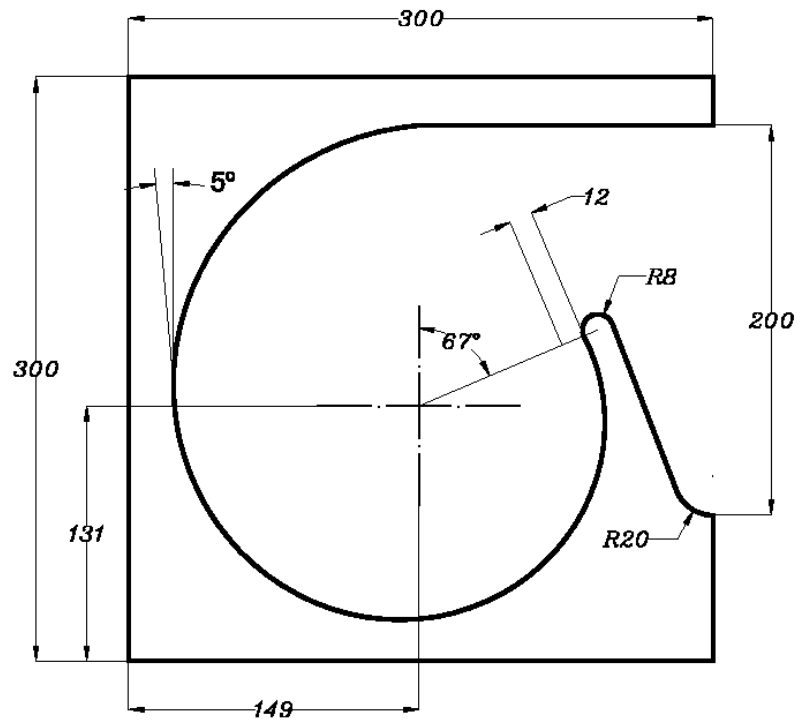


Figure 2.6: Scroll housing of 5 degrees

For more details about the final geometry of the scroll housings and the positioning pieces please refer to *Appendix G. Specifications of the components*.

To conclude this chapter, we have a picture of the all pieces manufactured for the measurement campaign.

In Figure 2.7 we can appreciate the full set of manufactured pieces for this work. In foreground there are the six positioning pieces for the housings. In middle view the complementary pieces to increase the width of housing to 87mm. Finally, in the background of the picture, the six housings of 67 millimeter width.

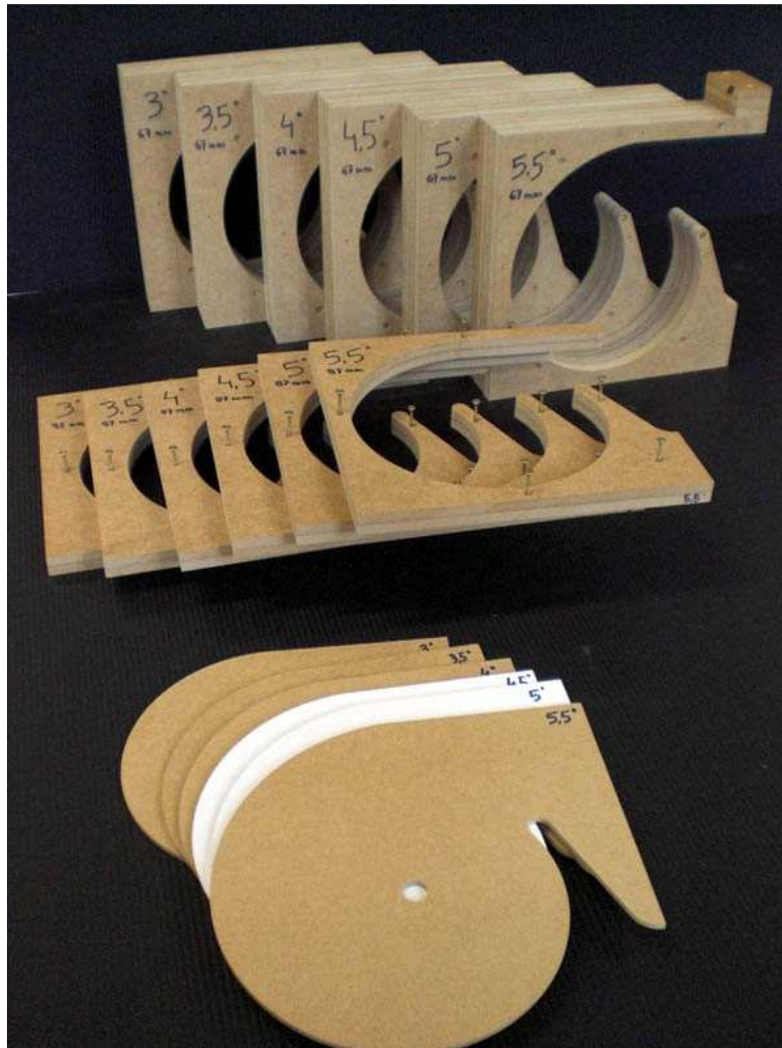


Figure 2.7: Full set of designed pieces for this work

Just to conclude this part, Figure 2.8 shows the detail of the difference in the opening angle of spiral curve on the manufactured scroll housings.

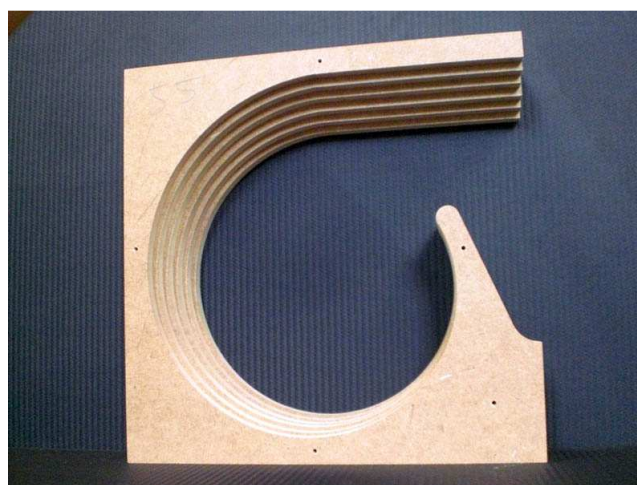


Figure 2.8: Detail of the increase of the value of opening angle for the housings

3 Test rig

We refer as a test rig to all the technical equipment necessary to develop the measurement campaign on the new designed pieces. It is described in this chapter.

3.1 Specifications

We can divide all the equipment necessary to achieve the objective of this work in two main parts: the chamber test rig and the fan test rig.

The first one, which is described also in *Chapter 1, State-of-the-art*, is a high-accuracy chamber test rig that allows to evaluate and to save all the performance data from the fan test rig. We have a full view of the chamber test rig in Figure 3.1.



Figure 3.1: Chamber test rig

The second part is the fan test rig. This is a multifunctional test rig for fans. Its design allows us to assembly and to test different fan configurations. The other members of the team used it for the aims of their projects as I am using it for the objectives of my work. In Figure 3.2 we can appreciate the fan test rig.

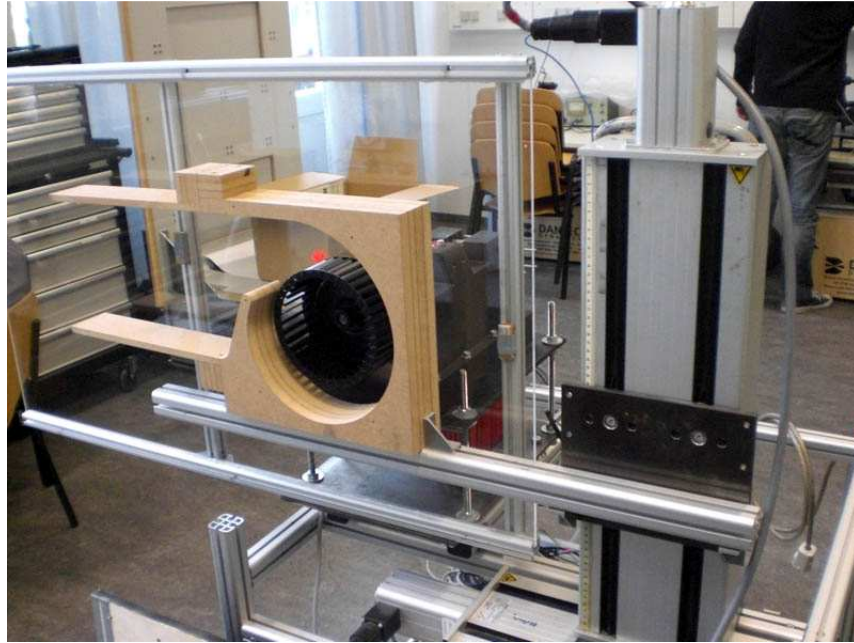


Figure 3.2: Fan test rig

The fan test rig can be subdivided in several parts as we explain in the next subchapter.

3.2 Fan test rig

3.2.1 Body structure

The body structure of the fan test rig is shown in Figure 3.3. It consists of a structure made with metallic profiles on which a wooden base plate is mounted. This structure is strong enough to sustain the entire fan unit in order to have a properly stability.

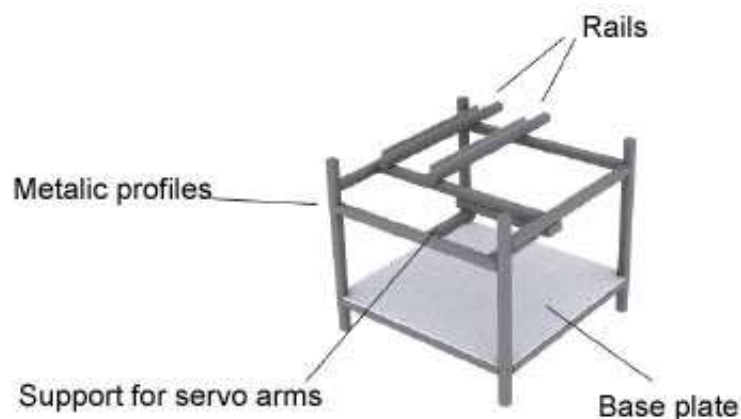


Figure 3.3: Body structure of the fan test rig

On this body structure we can see also two rails that guides the fan unit to slide in order to assembly/disassembly the fan.

This construction allows mounting a system of two servo arms which supports the scroll housing and allows it to move in two axes as desired.

3.2.2 Fan unit

The parts concerning the fan unit are detailed in Figure 3.4. The main parts of the unit are the motor and the rotor. In order to provide the rotor the power to run are necessary some parts.

Firstly we need a right angle gear in order to connect the shaft of the motor and the shaft of the rotor. This part is used to connect these shafts that are positioned in angle of 90 degrees of difference. A flexible coupling is mounted between the motor and the right angle gear.

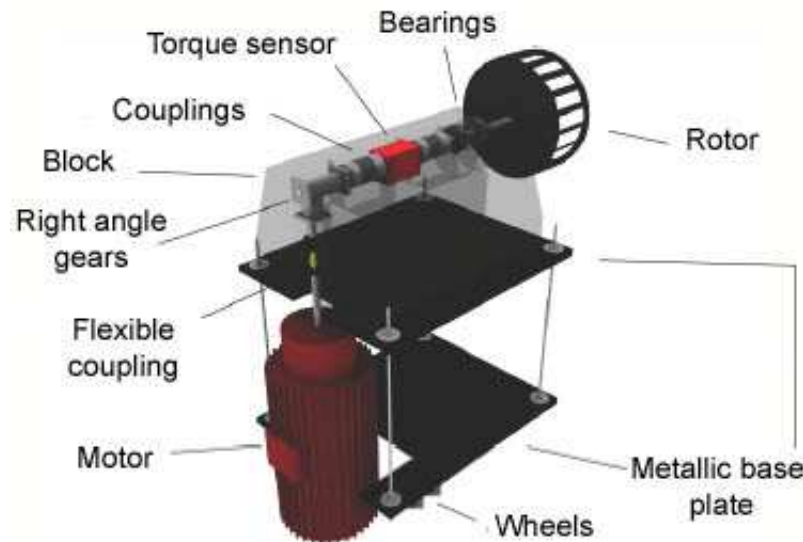


Figure 3.4: Fan unit

Afterwards, we have an important piece for the evaluation of the static efficiency that is the torque sensor. It is mounted in the shaft of the rotor. In both sides there are flexible couplings to avoid possible misalignments between axes. All this pieces have their placement inside a static block that provides them unity.

The fan unit is completed with two base plates that give it stability and allow it to be mounted in the body structure.

3.2.3 Movement of the fan unit through the rail guides

The rail guides are designed to allow linear movement from the fan unit through the body structure. That makes easy the possibility to assembly/disassembly the fan unit and to connect with the chamber test rig. In Figure 3.5 we show and scheme of that movement.

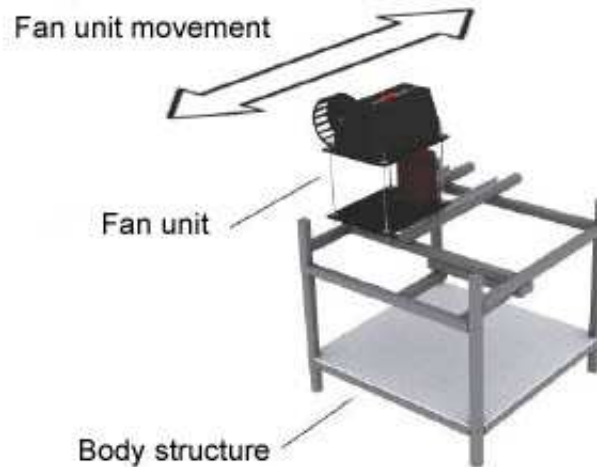


Figure 3.5: Movement through the rail guides

The movement of the fan unit is according to the rail guides in direction to the outlet of the chamber test rig.

3.2.4 Scroll housing integration

So far we can proceed with the integration of the scroll housing on the fan test rig. Firstly the servo mechanism with two arms, according to X-Y-axes referenced in Figure 3.6, is placed in the body structure. Subsequently we can fix the scroll housing on it.

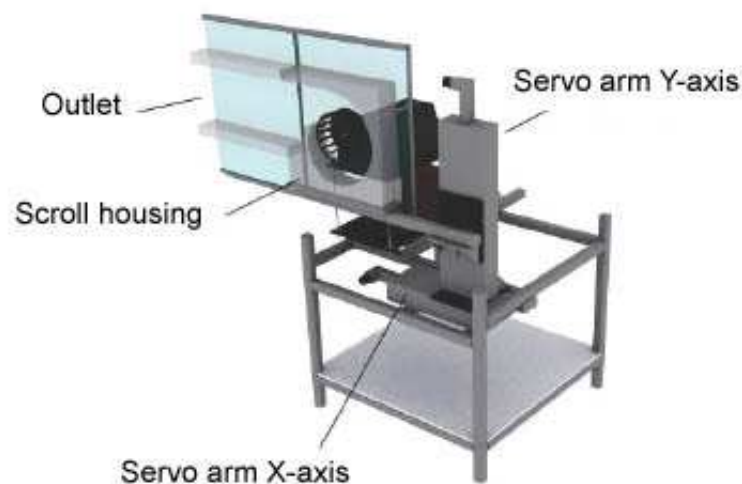


Figure 3.6: Scroll housing integration to the fan test rig

The scroll housing rests on the servo mechanism and can be displaced with high-accuracy on X-Y axes by using the software that controls the servo arms. This suitable software is RSterm

3.3 Integration into the chamber test rig

The final step is the integration of the fan test rig into the chamber test rig in order to have the whole test rig ready for the measurement as we see in Figure 3.7.

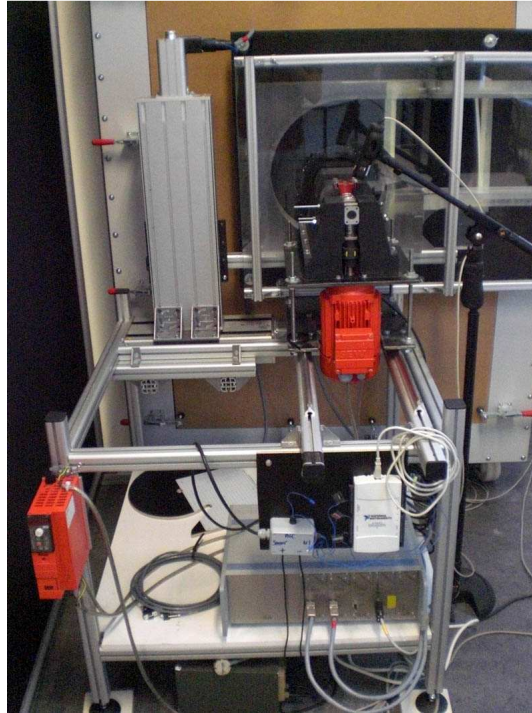


Figure 3.7: Complete test rig

Before the integration we have to be sure that the shaft of the fan is aligned properly.

After assembling the desk panel on the chamber test rig, we use a green piece designed by Andreas Lückemann in order to align the shaft of the rotor to the chamber test rig as we see in Figure 3.8:

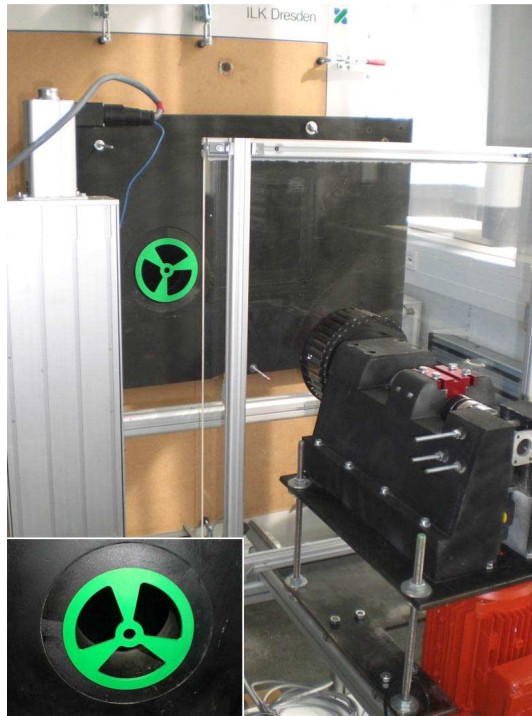


Figure 3.8: Alignment of the shaft of the fan test rig to the chamber outlet

To proceed with the alignment to the test chamber we have to place manually the fan test rig. The shaft of the fan test rig has to be coincident in direction to the hole of the green centering piece of the chamber.

Afterwards the test rig is ready to develop the measurements.

4 Mathematical foundations

In this chapter we describe all the mathematical equations and relations that we use to process and to compare the data of this work.

4.1 Introduction

To compare flow machines of different sizes and different operating conditions, it is necessary to normalize the measured data.

For this purpose, are used the similarity laws of mechanical models and the dimensionless ratios. Examples are the similarity fan laws: the relation between flow rate, pressure rise and power consumption. Also the dimensionless ratios like: Number of Reynolds, dimensionless ratio of pressure, dimensionless ratio of flow rate, or dimensionless ratio of performance.

The results of the measurements made (see Chapter 7 Collected data) are comparable to other flow machines by using these relations. Can be also classified entering for example in the Cordier² diagram.

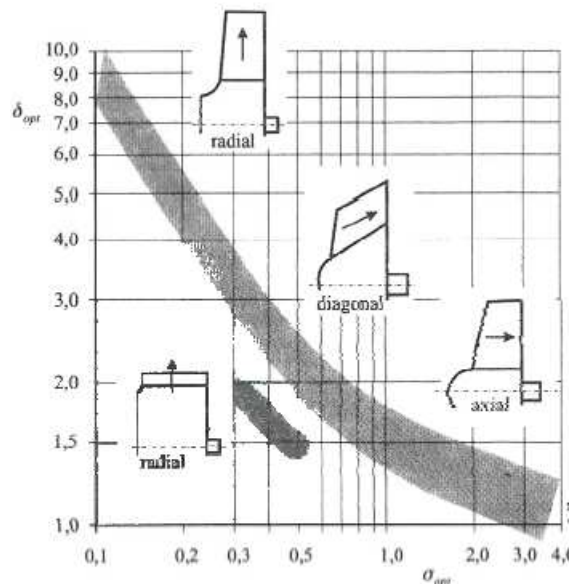


Figure 4.1: Cordier diagram (source: Carolus, 2003)

In the Cordier diagram, the best points of efficiency for different flow machines are registered by using the dimensionless ratio of rotational speed σ and the dimensionless ratio of diameter δ . For the registration of the performance of Sirocco

² Otto Cordier, German engineer

type fans are necessary to be saved e.g. the flow rate, the increase of static pressure, torque on shaft and the static efficiency. Afterwards is possible to determine dimensionless ratios such as dimensionless ratio of flow rate (φ), dimensionless ratio of pressure rise (ψ) and the efficiency η (See Roth, 1980).

4.2 Determination of the characteristics of the fan

In this section we specify the equations for determining the characteristics and sizes of the investigated fan that will be needed for the evaluation and registration of this fan.

Using the chamber test rig it is possible to obtain for each operating point the following data:

- The flow rate in m^3/h (Q)
- The increase of static pressure or pressure rise in Pa (Δp_{st})
- The torque on shaft in Nm (M)
- The rotational speed in rpm (n)

In addition, the following data are recorded by the chamber test rig:

- Density of the air in the chamber in kg/m^3
- Pressure of the barometer in Pa
- Temperature in the chamber in $^{\circ}\text{C}$
- Relative humidity of the air in%
- Mass flow in kg/h
- Absolute humidity of the air g/m^3
- Temperature of the room in $^{\circ}\text{C}$
- Reynolds number

Flow rate (Q) and increase of static pressure (Δp_{st}) of the Sirocco type fan are determined by the test chamber in m^3/h and in Pa and can be used unchanged.

The static efficiency (η_{st}) of the fan is calculated as the ratio between the delivered power on the shaft (P_{mec}) by the motor and the hydraulic useful hydraulic power provided by the fan (P_{hyd}):

$$P_{mec} = M \cdot n \cdot 2\pi \quad (4-1)$$

$$P_{hyd} = \Delta P_{st} \cdot Q \quad (4-2)$$

$$\eta_{st} = (P_{hyd}/P_{mec}) \cdot 100 \quad (4-3)$$

To determine the dimensionless ratios commented above, the following metrics and connections are necessary:

To calculate the dimensionless ratio of flow rate $(\varphi_r)^3$ is necessary to use the flow rate (Q), the geometry of the rotor (D_2) and the rotational speed (n). There are different philosophies, such as the geometry of the flow machine is respected. Cordier has entered the turbo-machines in the chart named after him only with the diameters. Since the width of the rotor plays a critical size, the width is included in the geometry:

$$\varphi_r = \frac{4 \cdot Q}{\pi^2 \cdot D_2^3 \cdot n} \quad (4-4)$$

$$\varphi_r = \frac{Q}{\pi^2 \cdot D_2^2 \cdot b \cdot n} \quad (4-5)$$

To calculate the dimensionless ratio of static pressure rise (ψ_{st}) is necessary the increase of static pressure (ΔP_{st}), the density of the medium (ρ), the geometry of the fan (D_2) and the rotational speed (n), as follows:

$$\psi_{st} = \frac{2 \cdot \Delta P_{st}}{\rho \cdot \pi^2 \cdot D_2^2 \cdot n^2} \quad (4-6)$$

Finally, if we want to enter our data in Cordier diagram we need also to evaluate two more parameters: dimensionless ratio of the speed of the fan (σ) and dimensionless ratio of the geometry of the fan (δ):

$$\sigma = \frac{\varphi^{1/2}}{\psi^{3/4}} \quad (4-7)$$

$$\delta = \frac{\psi^{1/4}}{\varphi^{1/2}} \quad (4-8)$$

³ Sub index “r” refers to radial fans

5 Uncertainty of measurement

The uncertainty in the measurement of a physical value delimits a range of values within which the true value of the parameter is assumed to be. In this chapter, the uncertainty of the measurements is determined. Here we review the deviations from the flow rate, the increase of pressure of the chamber test rig, the deviations from the torque and from the speed of the torque sensor.

5.1 Resume of the sources of uncertainty in the test rig

By ILK Dresden the following deviations in the chamber test rig are known:

Table 5-1: Uncertainty in the chamber test rig

Chamber test rig		
Sensors	Measurement range	Relative uncertainty
Flow rate	11...1600 m ³ /h	1% from reading
Pressure rise	+2500 Pa	0,5% from reading
Temperature		±0,3 °C
Relative air humidity		± 1%

By the specifications of the torque sensor we know:

Table 5-2: Uncertainty of the torque sensor

Torque sensor		
Sensors	Measurement range	Relative uncertainty
Torque	0...2 Nm	0,2% full scale
Rotational speed	0...7000 min ⁻¹	0,2% full scale

Finally the combined uncertainties are resumed subsequently:

Table 5-3: Combined uncertainties for the measurements

Combined uncertainty	
Measurement	Relative uncertainty
(Q, ΔP_{st})	1,1% from reading
(Q, η_{st})	7,6% from reading

For more details about the quantification of the uncertainty in the test rig please refer to the literature: [10] FRANK, S. STUCHLIK, A.: Numerical analysis and design of sirocco fans with ideal and disturbed inflow and outflow. 2011.

6 Measurement campaign

The aim of the measurement campaign is to record the performance of the new designed scroll housings. After this campaign we have the necessary data to develop a precise study about the designs and we will be able to analyze the data searching for the best static efficiencies and influence of the parameters of design on Sirocco type fan.

6.1 Measurement matrix

This measurement campaign regards on one hand the evaluation of the new scroll housings and on the other hand the evaluation of effects on the performance of the fan when the rotor is slightly decentered from the design position. All this variations are consolidated in this measurement campaign. We detail its parts below.

We have six scroll housings according to the values of the opening angle of spiral curve that we want to check out.

Table 6-1: Values for evaluating the opening angle of spiral curve

α_s : Opening angle of spiral curve					
3,0°	3,5°	4,0°	4,5°	5,0°	5,5°

We have six complementary parts for the scroll housings for increasing their width from 67 mm to 87 mm which is the same than increase B/b from 1,08 to 1,4.

Table 6-2: Values for evaluating the dimensionless ratio of housing width

B/b: Dimensionless ratio of housing width	
1,08	1,4

To decenter the rotor from the design position, we use as a reference the minimum gap between rotor and housing (Se). The original design is according to the relation $Se/D_2 = 0,075$. We want to decenter the rotor to the positions $Se/D_2 = 0,025$; 0,050; 0,010 and 0,015. That means to move the rotor to have the minimum gap of $Se = 4$; 8; 16 and 20 mm.

Table 6-3: Values for evaluating the dimensionless ratio of the gap

Se/D_2 : Dimensionless ratio of the gap between rotor and housing				
0,025	0,050	0,075	0,010	0,015

In addition we want to set these five positions of minimum gap in two additional angles. A part from the original position (23°), we want to set the minimum gap at 0° and -23° according to general angles. In order not to confuse with the angle of positioning of the tongue (α_t), we create a new variable named α_e (angle of eccentricity) to define the position of the minimum gap between rotor-housing (Se). In Figure 6.1 we can appreciate more clearly in which way we want to decenter the rotor position for the measurement campaign.

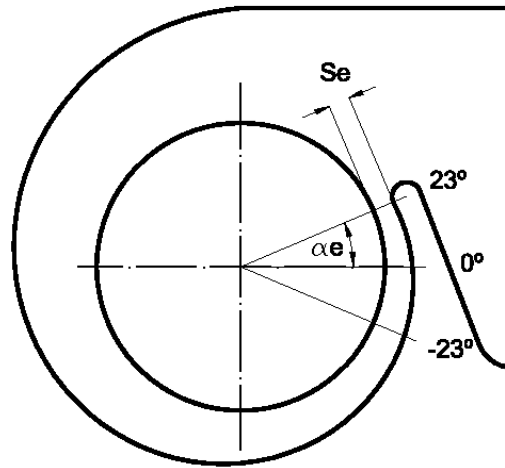


Figure 6.1: Decentering the rotor position according to the parameters Se and α_e

Although this way of decenter the rotor it has polar coordinate definition (Se, $\alpha_e = 4\text{ mm}$, 0° , for instance), we have to set the positions in Cartesian coordinates in Y-X-axes according to the software that controls the servomechanism. For detailed values about the positioning on X-Y-axes, please refer to *Appendix B. Values for decentering the rotor*.

Table 6-4: Values for evaluating the angle of eccentricity of the gap

α_e : angle of eccentricity of the minimum gap rotor-housing		
23°	0°	-23°

Grouping all these parameters, we can summarize all the measurement campaign as it follows. Configurations of sirocco type fan to measure:

1) $\alpha_s = 3,0^\circ; 3,5^\circ; 4,0^\circ; 4,5^\circ; 5,0^\circ; 5,5^\circ$	6 configurations
2) $B/b = 1,08; 1,4$	2 configurations
3) $Se/D_2 = 0,025; 0,050; 0,075; 0,100; 0,150$	5 configurations
4) $\alpha_e = 23^\circ; 0^\circ; -23^\circ$	3 configurations
Total	144 configurations

In resume, we have 144 different configurations to evaluate.

6.2 Procedure for measuring

All the configurations of the Sirocco type fan are evaluated at a rotational speed of 1000 rpm. The procedure for measuring is explained subsequently:

Firstly is needed a warm up for the whole test rig.

The first thing to proceed is to warm up the motor. The nominal rotational speed is 1000 rpm, as said above. The criteria used to warm up this device are to switch on the motor at a rotational speed of 20% from the nominal, which is 200 rpm during 20 minutes.

This warm up is requested for providing to all the assembly parts a right temperature before to start the measurement action. The parts involved in this process are the motor itself, the right angle gear, the shaft, the torque sensor, the couplings and the bearings.

The chamber test rig has a process of warm up at the same time. Again by using with the same criteria of 20%, the flow rate is set to 100 m³/h during 20 minutes.

This is necessary to raise the temperature of the internal parts of the chamber such as auxiliary support fan, internal conducts through which the air stream flows, etc.

Once the system reaches the operating temperature, the next step is to locate the scroll housing into the fan test rig. When the scroll housing is assembled to the servo arms, it is needed to find the origin position. The servomechanism is digitally controlled and uses two servo arms to move the scroll housing both in X and Y axis. But the initial position has to be set manually.

For this purpose the positioning pieces are used. Firstly, the positioning piece is introduced into the scroll housing of the corresponding opening angle, as we see in Figure 6.2:

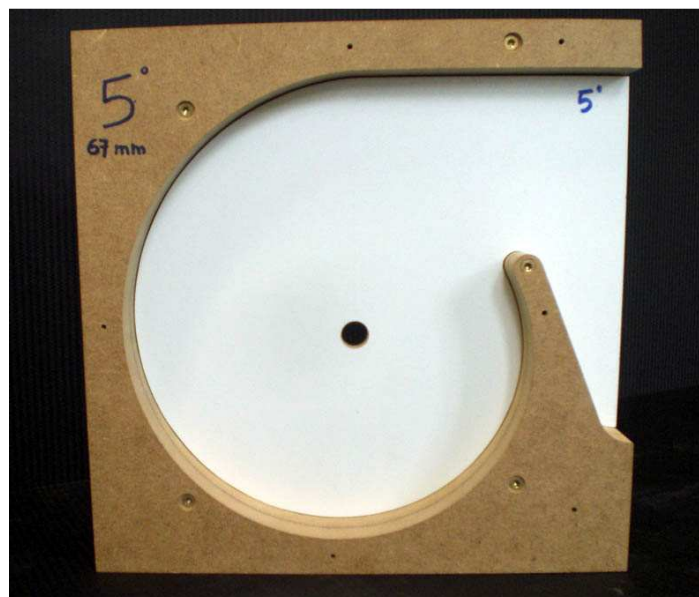


Figure 6.2: Setting the scroll housing of 5° to the reference position

6.3 Methodology of measuring

Afterwards, we act manually the servo arms to find the origin. We can adjust the mechanism in X-Y axes by using the corresponding buttons at the top of the servo arms. The shaft should be aligned with the hole of the positioning piece. We have to save this position. Once is recorder we can send the order to move the housing to the position that we want to measure.

The next step is to assembly the rotor in the shaft. After that we can move the fan unit until the whole fan test rig is assembled.

The whole system is now ready for the measurement. One important thing to do is to reset the pressure sensors. Subsequently we can switch on the motor and start with the measurements.

The measurement is done manually by using the software of control of the chamber test rig. The criteria to record each point of the performance of the fan is to wait in the operating point since when arrive to steady state and then wait ten seconds on this point. The software is taking the average values for ten seconds.

The step used to record the performance curves is to raise the flow rate in 25 m³/h from point to point. That means 0; 25; 50; 100; 150; m³/h ... etc.

6.3 Methodology of measuring

To control the chamber test rig and achieve the measurements we use suitable software⁴ provided by the same company that has manufactured the chamber test rig (ILK Dresden).



Figure 6.3: Front panel of the software used to control the test chamber

⁴ Volumenstromprüfstand/ILK Dresden software

In Figure 6.3 we have a general view of the software that controls the chamber test rig. On the picture we can appreciate five parts that we describe below.

The first part on the top left of the screen is the operating panel.

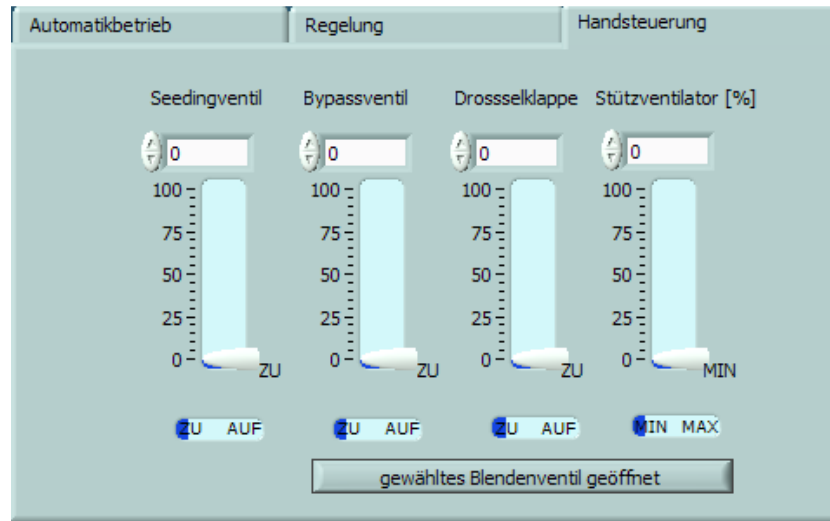


Figure 6.4: Panel of manual settings

As we see in Figure 6.4, we have different options to regulate the flow rate that we want to set in the chamber test rig. We use the manually set option (Handsteuerung) to record the performance curves because with this option you have a full control of the flow rate.

The most important buttons in the manually set panel are the ones which regulates the opening of the throttle valve (Drosselklappe) and the one which regulates the power of the support fan (Stützventilator).

The first point to record for a particular fan configuration is for zero flow rate. For this point, both the throttle valve and the support fan have to be set to 0. That means that the throttle valve is totally closed and the support fan is switch off.

When we want to progress on the characteristic curve of the fan, we have to increase the flow rate provided for the chamber test rig to the next point that is 25 m³/h. To achieve this flow rate the first is to proceed to open the throttle valve. If this is not enough, we can use the support fan.

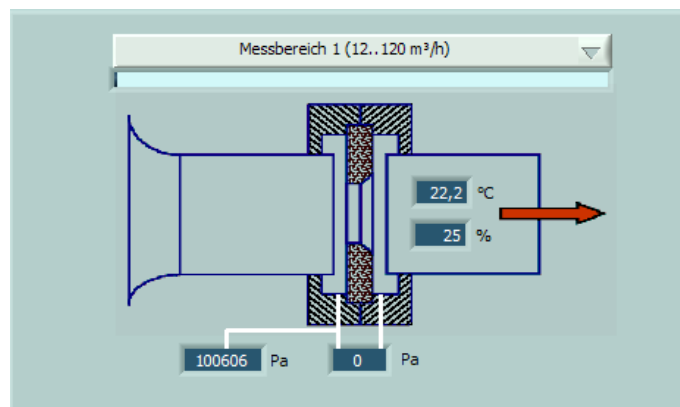


Figure 6.5: Panel of system indicators

If we want to go further in flow rate values, the panel shown in Figure 6.5 should be considered.

As we say in *Chapter 1 Introduction* when we spoke about it, the chamber test rig has three measurement ranges. For flow rates from 12 to 120 m³/h we use the first measuring duct. From 70 to 680 m³/h we use the second measuring duct. Finally, from 150 to 2000 m³/h we use the third measuring duct. We can switch from measuring ducts on this panel. By clicking on the arrow placed on the top right.

On top right side we have the panel of instantaneous values. On it we can see the state of the values involved in the measurement. In Figure 6.6 we have a view of that panel.

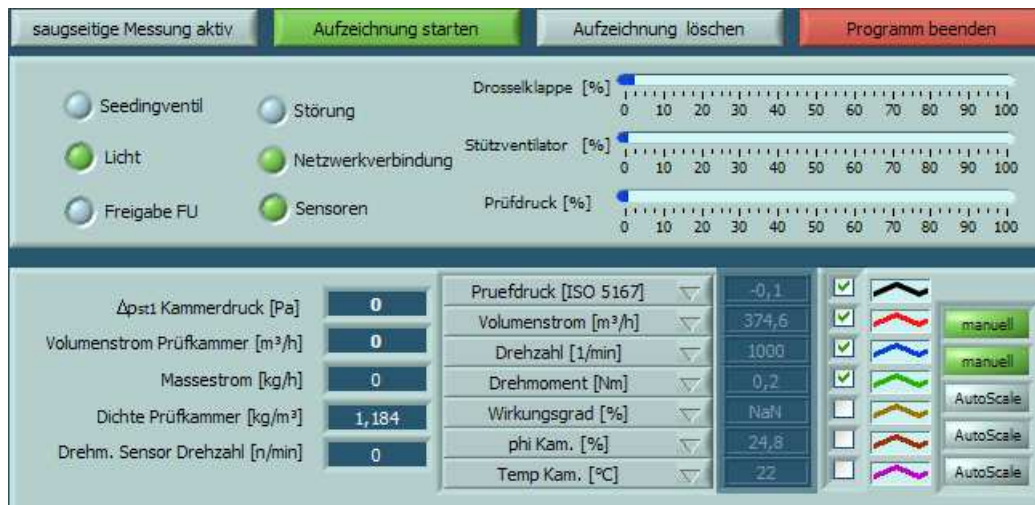


Figure 6.6: Panel of instantaneous values

In the top half part of the panel, there are the indicators of the state of the throttle valve, support fan and pressure rise (Prüfdruck) registered on the chamber. They are shown in percentage values. Evidently when a magnitude is at 100% it means that it is the maximum assumed in the chamber test rig.

Just next to it, on the left there are some indicators represented by circles. Among them, the most important indicators are: Connection between chamber and PC (Netzwerkverbindung), Sensors are successfully connected to the chamber (Sensoren) and the power on the chamber (Licht).

In the bottom half part, there are represented the instantaneous values that the sensors are providing to the chamber. The most important are: Pressure rise (Prüfdruck), Flow rate (Volumenstrom), Rotational speed (Drehzahl) and Torque on shaft (Drehmoment). By clicking next to the name of the value it can be added to the graph panel.

The pannel of graphs is shown in Figure 6.7, here it can be represented the values we explain above in different x-axis: Time (Zeit) or Flow rate (Volumenstrom). This pannel is very usefull to have a global view of the whole measurement.



Figure 6.7: Graphics panel

In the example of Figure 6.7 the next parameters are shown over the time (x-axis):

- Pressure rise in Pa (Black line)
- Flow rate in m³/h (Red line)
- Torque on shaft in Nm (Green line)
- Rotational speed in rpm (Blue line)

We can see for the flow rate (red line) that it raises by steps of 25 m³/h. There is a fall in the flow rate after rising 100 m³/h. The reason is that range of the first measuring duct is pretty close to its maximum. If we want to go ahead for higher flow rate values, we have to switch to the next measuring duct. When we want to switch between measuring ducts, it is necessary to have zero flow rate or nearly zero. Otherwise the chamber test rig could be damaged.

The last part is the panel of the data recorded manually. We can appreciate it in Figure 6.8, where the values recorded for this configuration are shown. They are recorded in steps of 25 m³/h. For each point the software is giving us the next information:

- Time of measurement in s
- Flow rate in m³/h
- Pressure rise in Pa
- Density in the chamber in Kg/m³
- Temperature in the chamber in °C
- Mass rate in Kg/h
- Humidity in the chamber in g/Kg
- Temperature in the room in °C
- Rotational speed in 1/min
- Torque on shaft in Nm

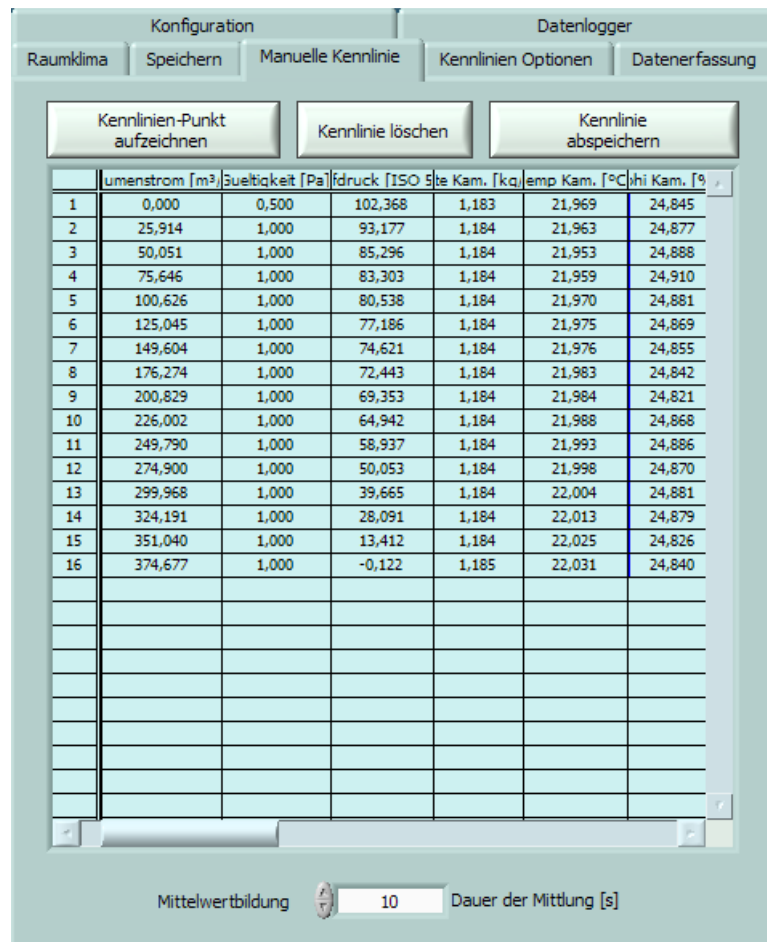


Figure 6.8: Manually recorder data panel

This data can be exported as a data sheet for more suitable treatment. For more detailed information about the data and the format of this export, please refer to *Appendix C. Data provided by the chamber test rig*.

7 Collected data

This chapter is a recompilation of data from the measurement campaign.

That data is ordered according opening angle families (α_s) and it is given by using graphs which are autocontented. All the details of each graph can be found in the information accompanying that one and in the underline as well. For each section, the next characteristic curves of the Sirocco type fan are shown:

- Increase of static pressure (pressure rise) vs. flow rate
- Torque on shaft vs. flow rate
- Static efficiency vs. flow rate

In addition, at the end of each section more clarifying information can be found i.e. a picture of the scroll housing in 3-D with the configurations of the rotor which are evaluated.

In this chapter only the most relevant data from the measurement camping has added. Since the 144 configurations are an important amount of data, only the most interesting ones according to efficiency, performance and relevancy are shown.

7.1 Most relevant data grouped by housing families

7.1.1 Scroll housing with opening angle of spiral curve of $\alpha_s = 3,0^\circ$

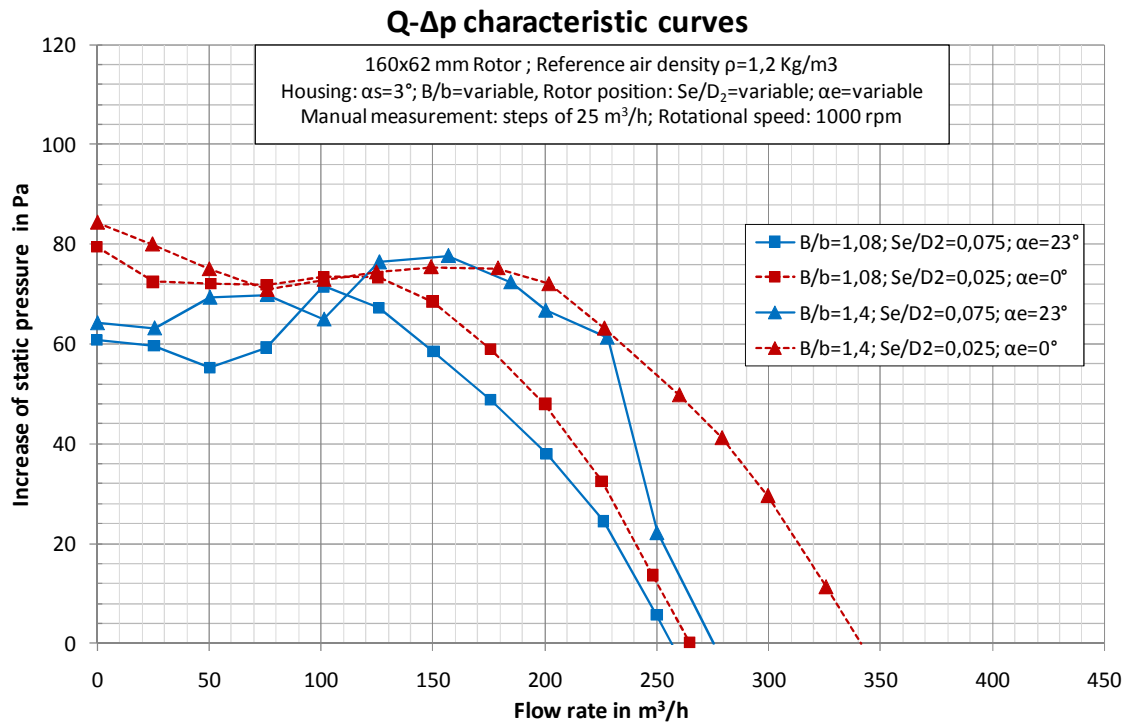


Figure 7.1: Increase of static pressure vs. flow rate curves of the Sirocco type fan D160x62mm at 1000rpm, scroll housing with an opening angle of 3° .

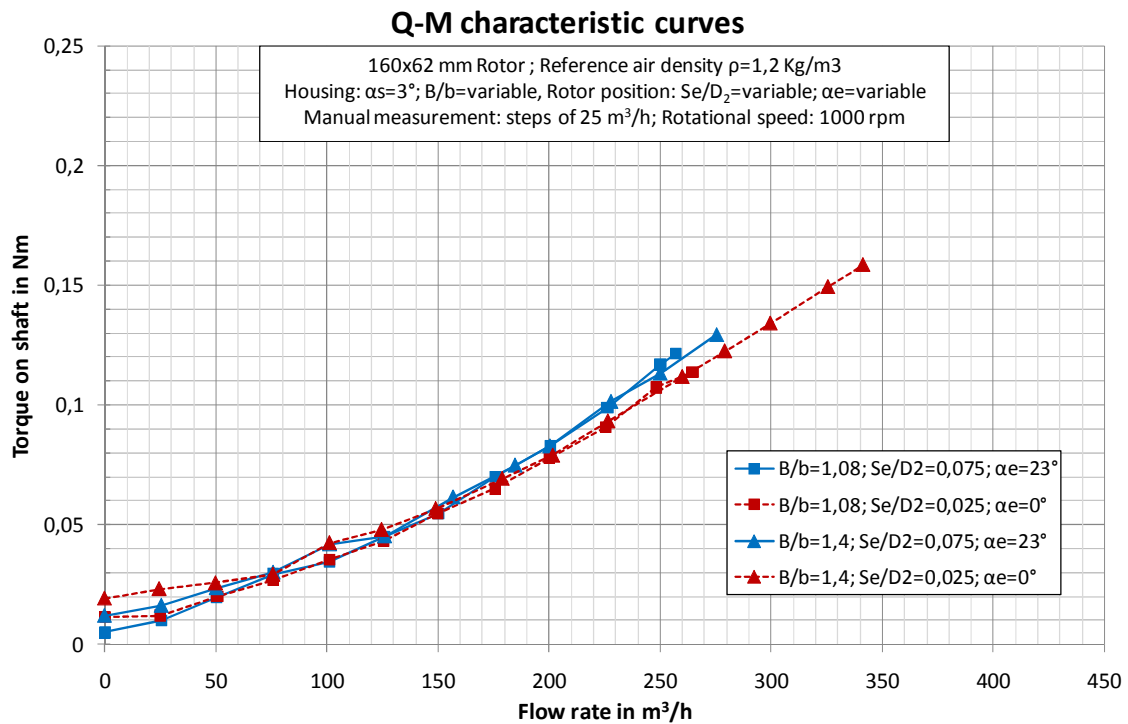


Figure 7.2: Torque on shaft vs. flow rate curves of the Sirocco type fan D160x62mm at 1000rpm, scroll housing with an opening angle of 3° .

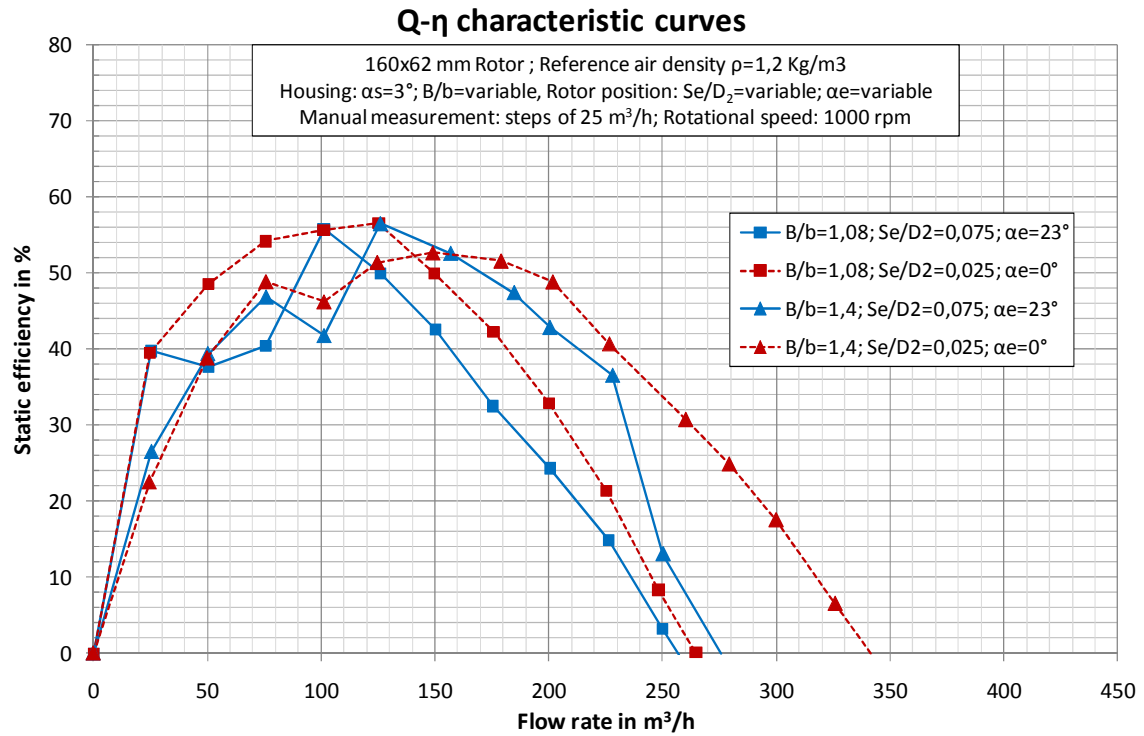


Figure 7.3: Static efficiency curves of the Sirocco type fan D160x62mm at 1000rpm, scroll housing with an opening angle of 3° .

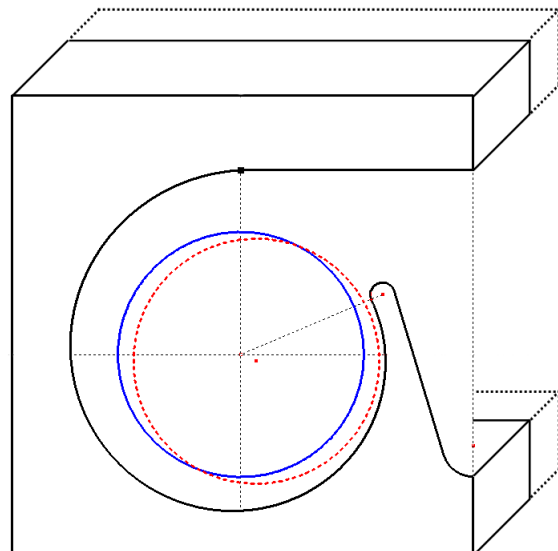
Spiral opening angle: $\alpha_s = 3^\circ$

$B/b = 1,08$

$B/b = 1,4$

$Se/D_2 = 0,075$; $\alpha_e = 23^\circ$

$Se/D_2 = 0,025$; $\alpha_e = 0^\circ$



7.1.2 Scroll housing with opening angle of spiral curve of $\alpha_s = 3,5^\circ$

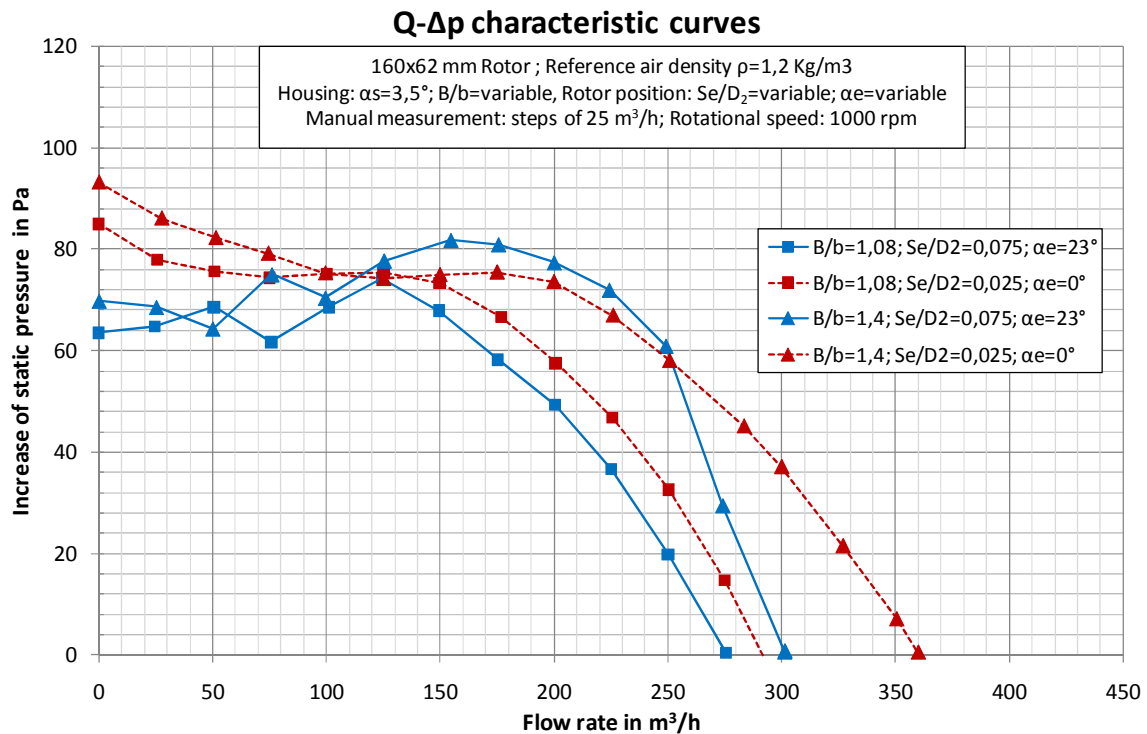


Figure 7.4: Increase of static pressure vs. flow rate curves of the Sirocco type fan D160x62mm at 1000rpm, scroll housing with an opening angle of 3,5°.

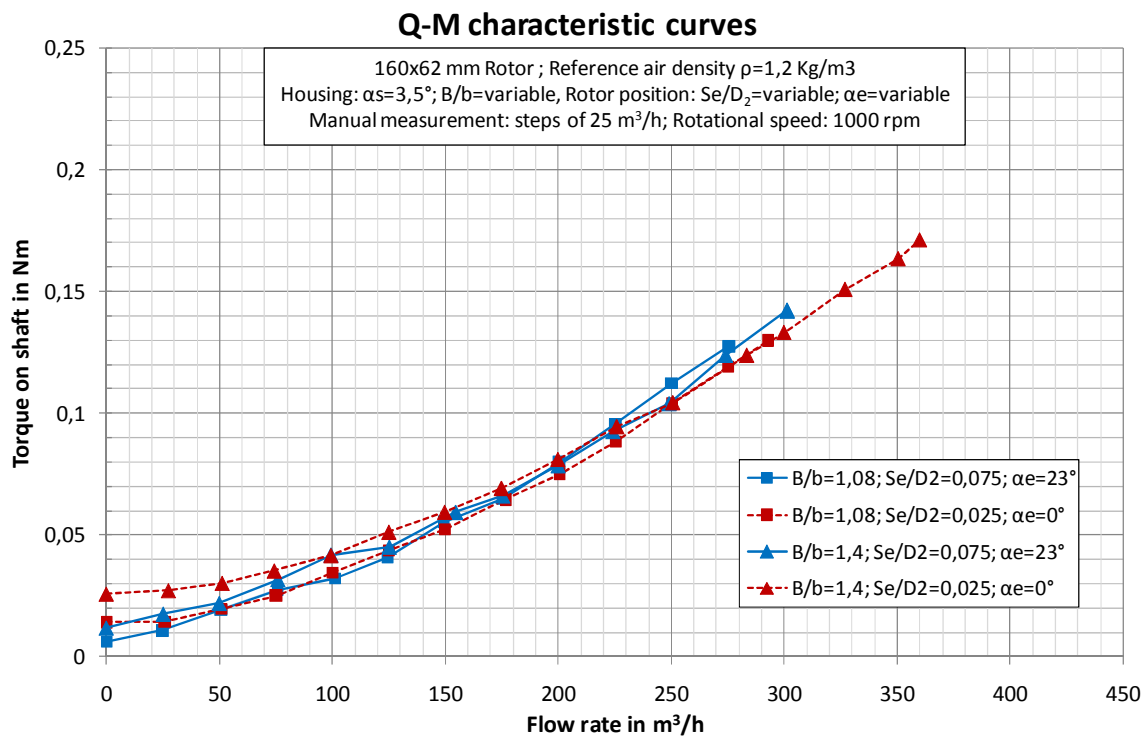


Figure 7.5: Torque on shaft vs. flow rate curves of the Sirocco type fan D160x62mm at 1000rpm, scroll housing with an opening angle of 3,5°.

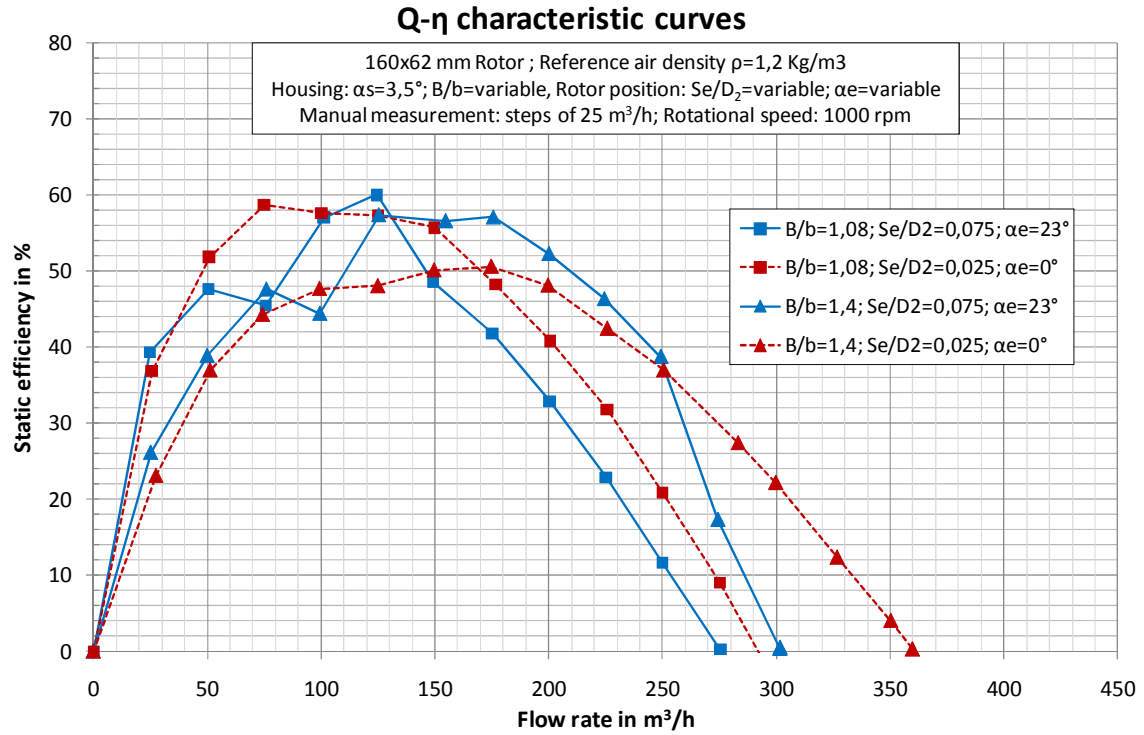


Figure 7.6: Static efficiency curves of the Sirocco type fan D160x62mm at 1000rpm, scroll housing with an opening angle of $3,5^\circ$.

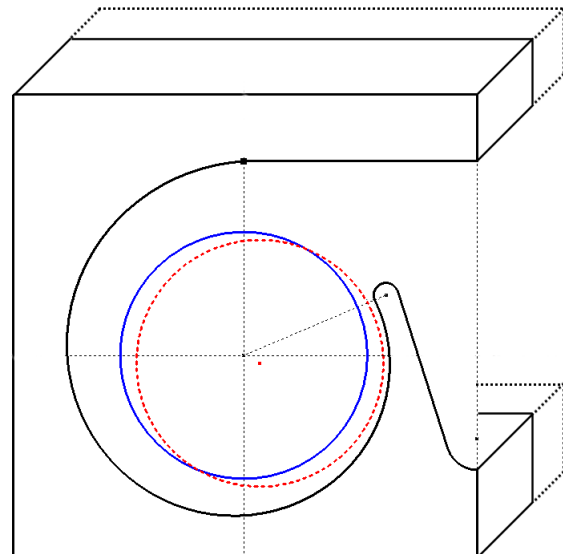
Spiral opening angle: $\alpha_s = 3,5^\circ$

—□— $B/b = 1,08$

—△— $B/b = 1,4$

○ $Se/D_2 = 0,075$; $\alpha_e = 23^\circ$

○ $Se/D_2 = 0,025$; $\alpha_e = 0^\circ$



7.1.3 Scroll housing with opening angle of spiral curve of $\alpha_s = 4,0^\circ$

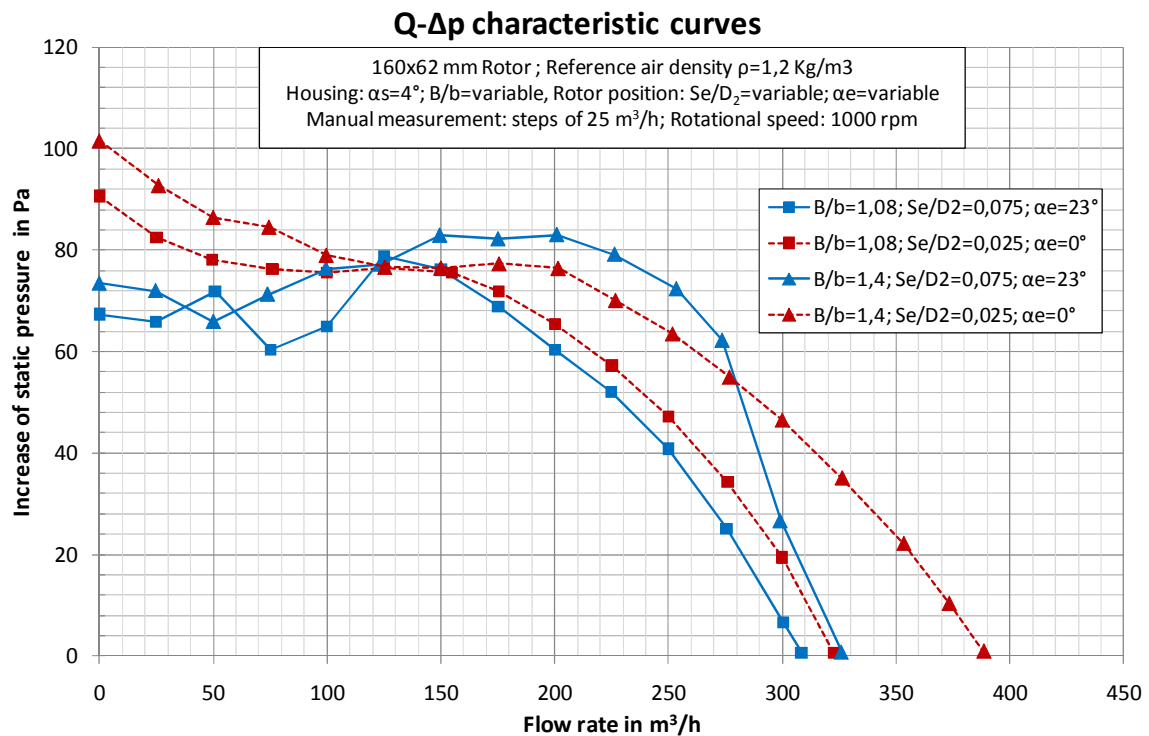


Figure 7.7: Increase of static pressure vs. flow rate curves of the Sirocco type fan D160x62mm at 1000rpm, scroll housing with an opening angle of 4° .

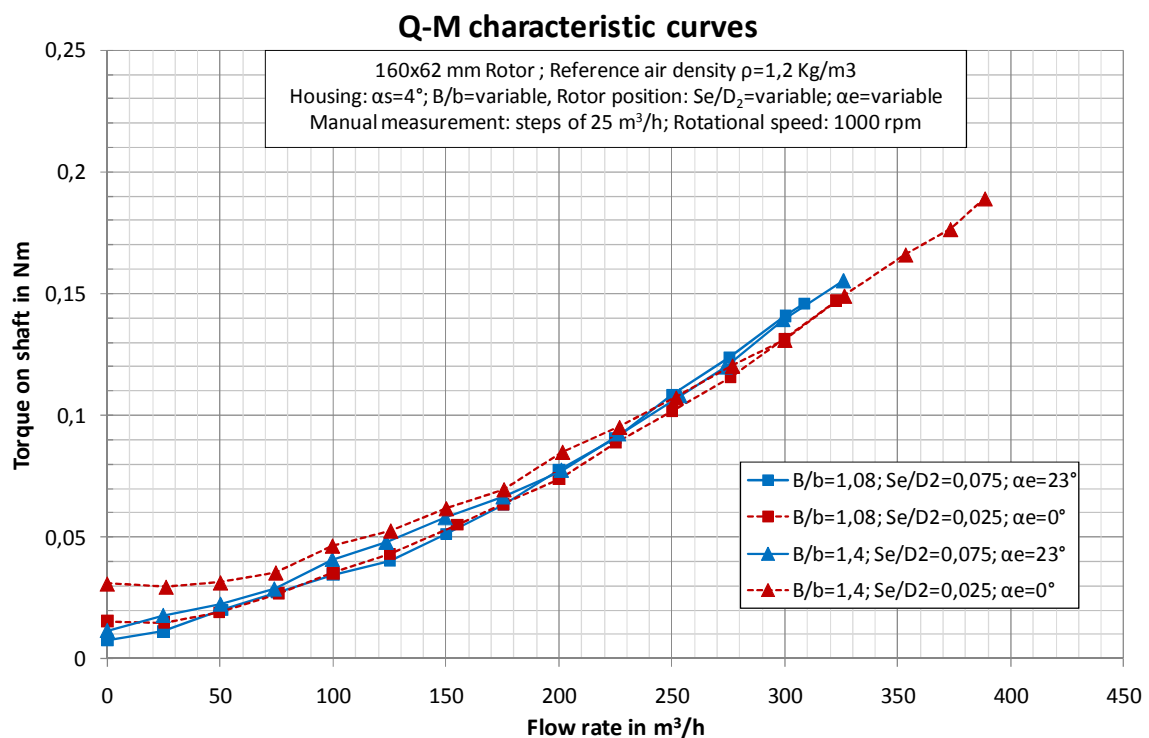


Figure 7.8: Torque on shaft vs. flow rate curves of the Sirocco type fan D160x62mm at 1000rpm, scroll housing with an opening angle of 4° .

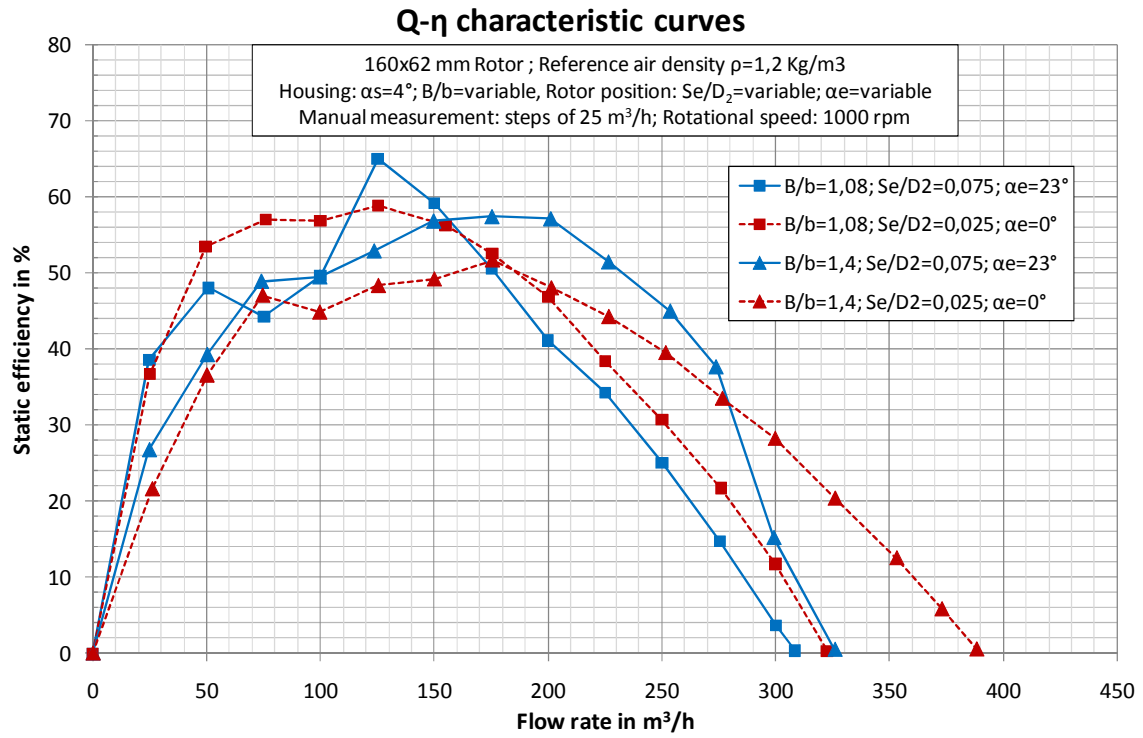


Figure 7.9: Static efficiency curves of the Sirocco type fan D160x62mm at 1000rpm, scroll housing with an opening angle of 4° .

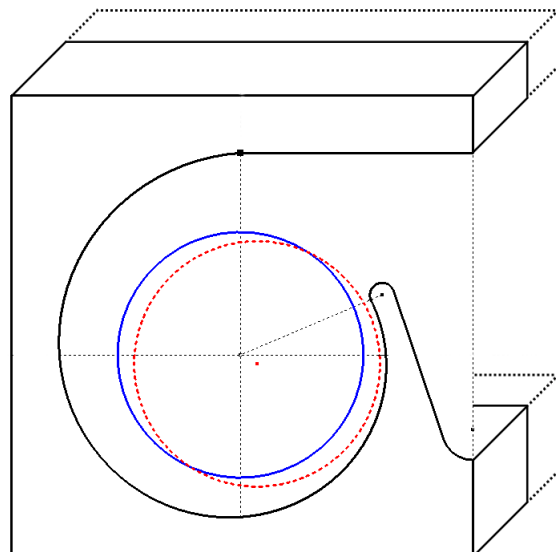
Spiral opening angle: $\alpha_s = 4^\circ$

\square $B/b = 1,08$

\triangle $B/b = 1,4$

\circ $Se/D_2 = 0,075$; $\alpha_e = 23^\circ$

\circ $Se/D_2 = 0,025$; $\alpha_e = 0^\circ$



7.1.4 Scroll housing with opening angle of spiral curve of $\alpha_s = 4,5^\circ$

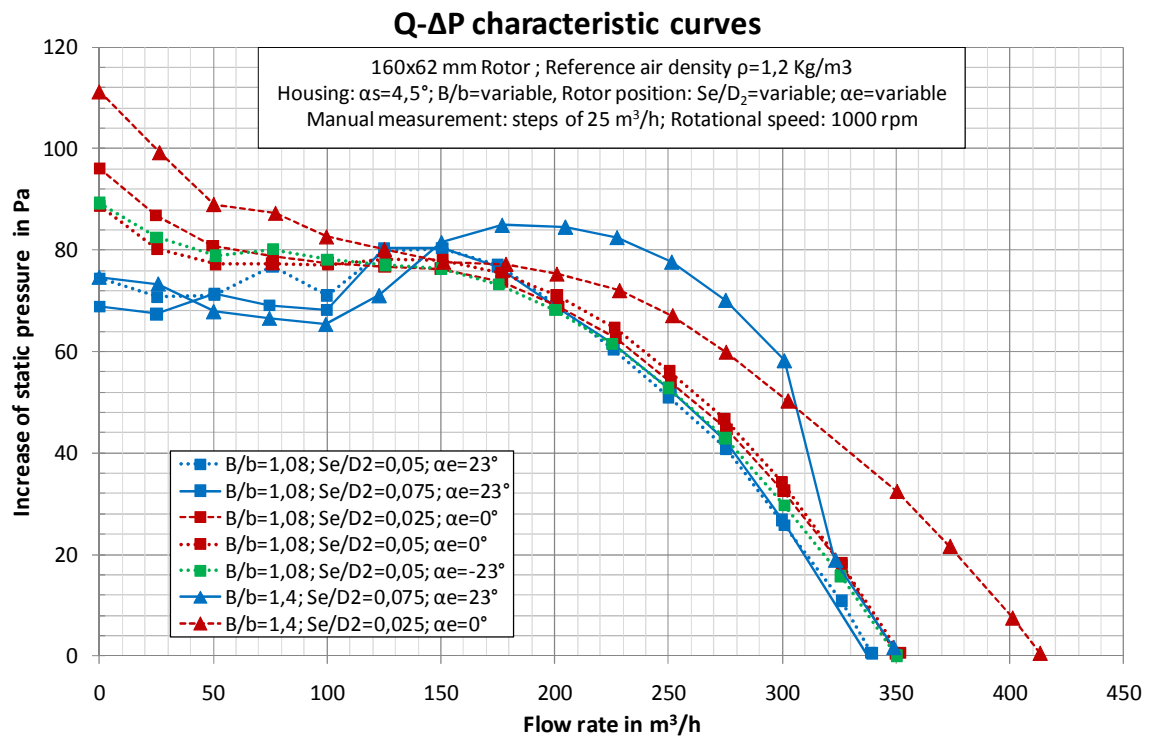


Figure 7.10: Increase of static pressure vs. flow rate curves of the Sirocco type fan D160x62mm at 1000rpm, scroll housing with an opening angle of $4,5^\circ$.

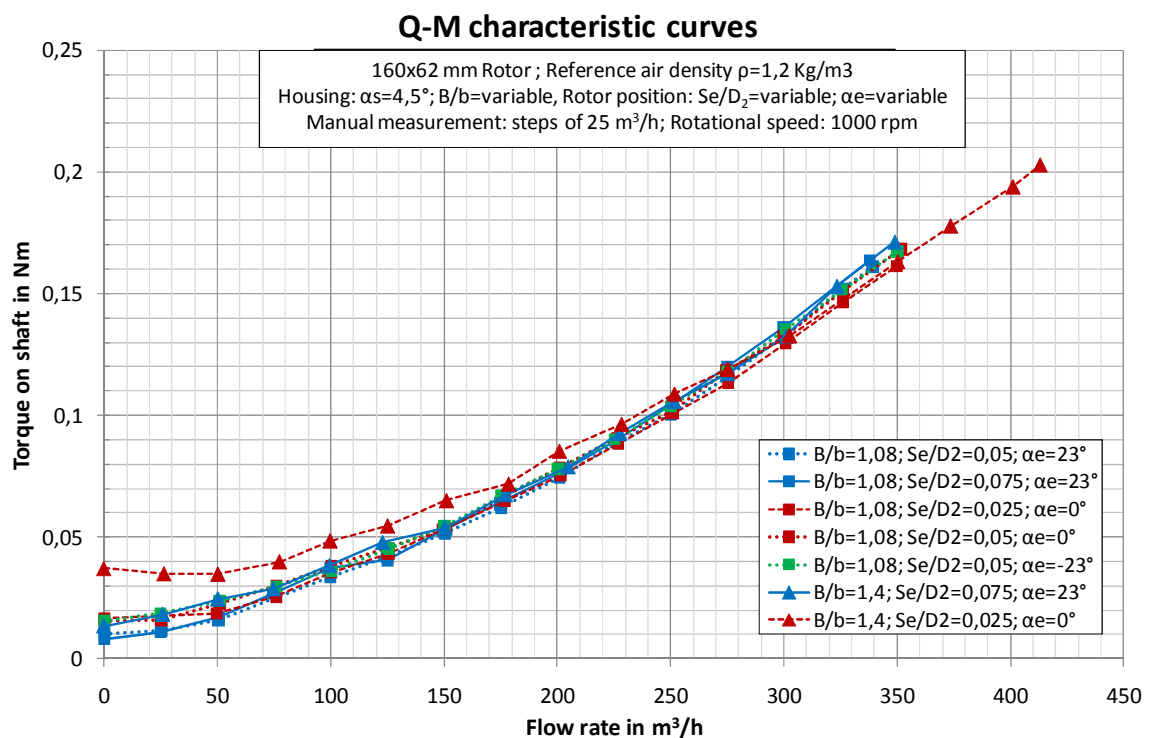


Figure 7.11: Torque on shaft vs. flow rate curves of the Sirocco type fan D160x62mm at 1000rpm, scroll housing with an opening angle of $4,5^\circ$.

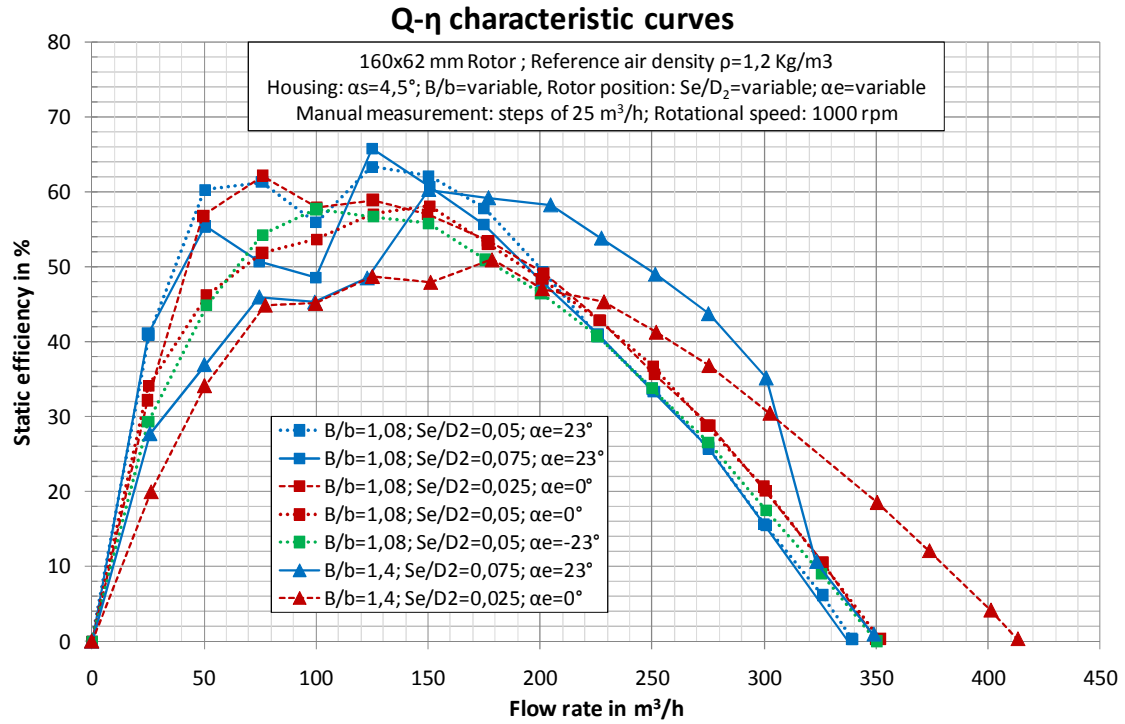
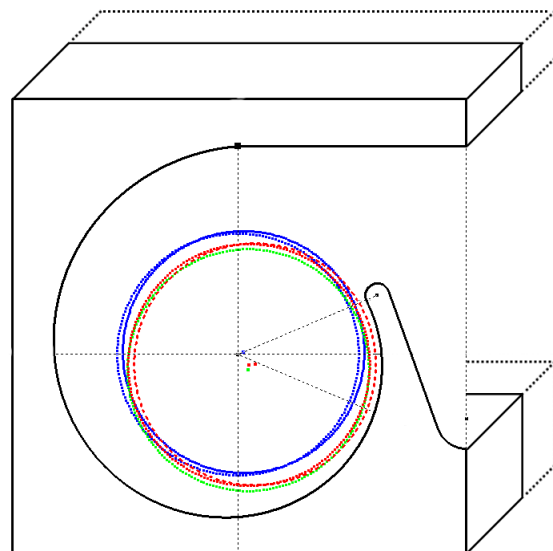


Figure 7.12: Static efficiency curves of the Sirocco type fan D160x62mm at 1000rpm, scroll housing with an opening angle of $4,5^\circ$.

Spiral opening angle: $\alpha_s = 4,5^\circ$

- $\cdots \square \cdots$ $B/b = 1,08$
- $\cdots \triangle \cdots$ $B/b = 1,4$
- $\cdots \circ \cdots$ $Se/D_2 = 0,05$; $\alpha_e = 23^\circ$
- $\cdots \circ \cdots$ $Se/D_2 = 0,075$; $\alpha_e = 23^\circ$
- $\cdots \circ \cdots$ $Se/D_2 = 0,025$; $\alpha_e = 0^\circ$
- $\cdots \circ \cdots$ $Se/D_2 = 0,05$; $\alpha_e = 0^\circ$
- $\cdots \circ \cdots$ $Se/D_2 = 0,075$; $\alpha_e = -23^\circ$



7.1.5 Scroll housing with opening angle of spiral curve of $\alpha_s = 5,0^\circ$

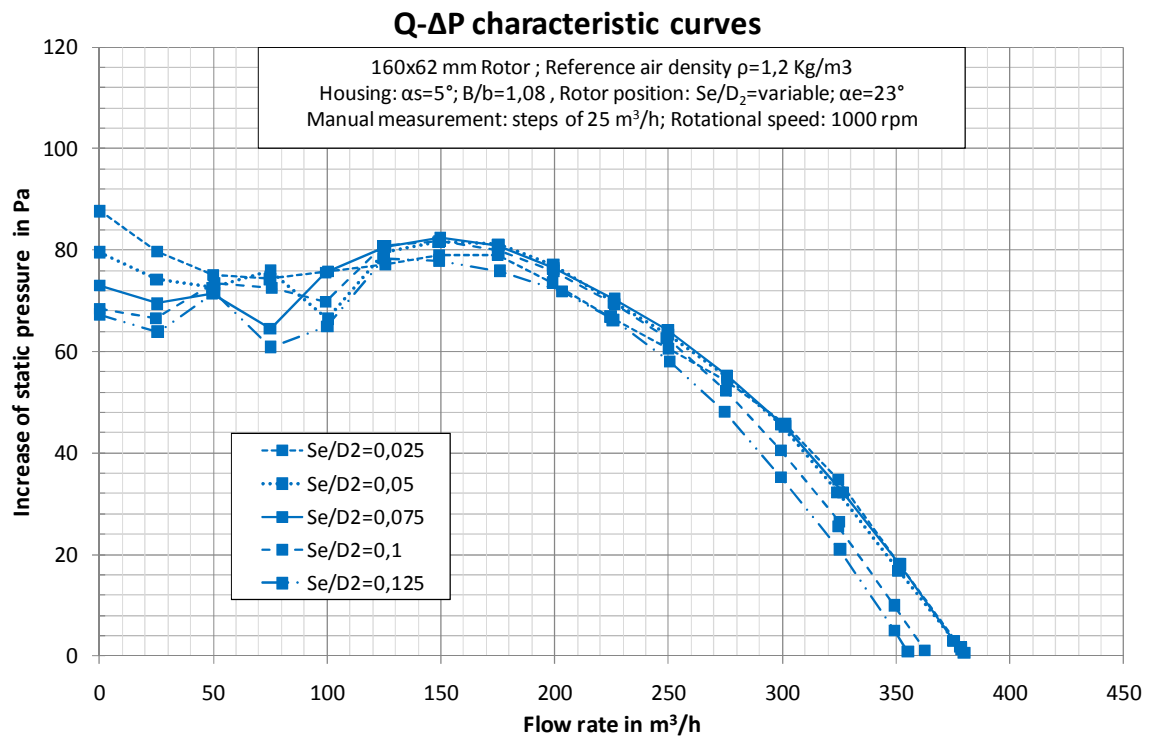


Figure 7.13: Increase of static pressure vs. flow rate curves of the Sirocco type fan D160x62mm at 1000rpm, scroll housing with an opening angle of 5° , width of housing $B/b=1,08$ and angle of eccentricity of gap rotor-housing of 23° .

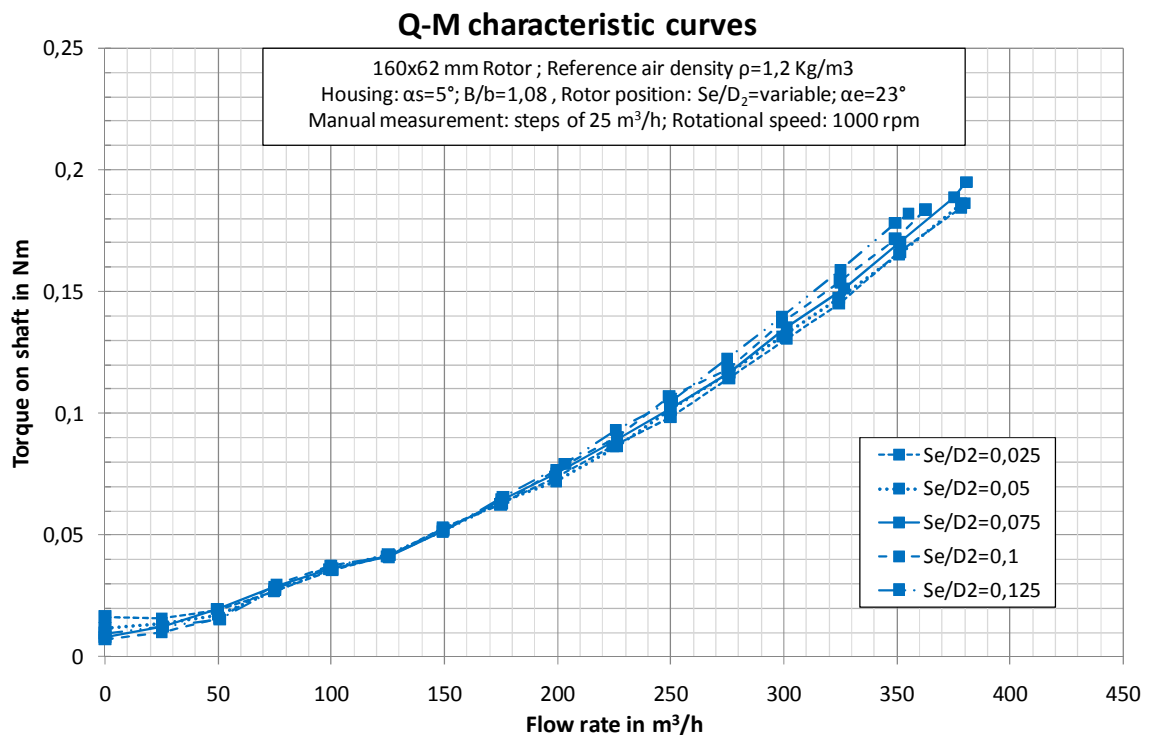


Figure 7.14: Torque on shaft vs. flow rate curves of the Sirocco type fan D160x62mm at 1000rpm, scroll housing with an opening angle of 5° , width of housing $B/b=1,08$ and angle of eccentricity of gap rotor-housing of 23° .

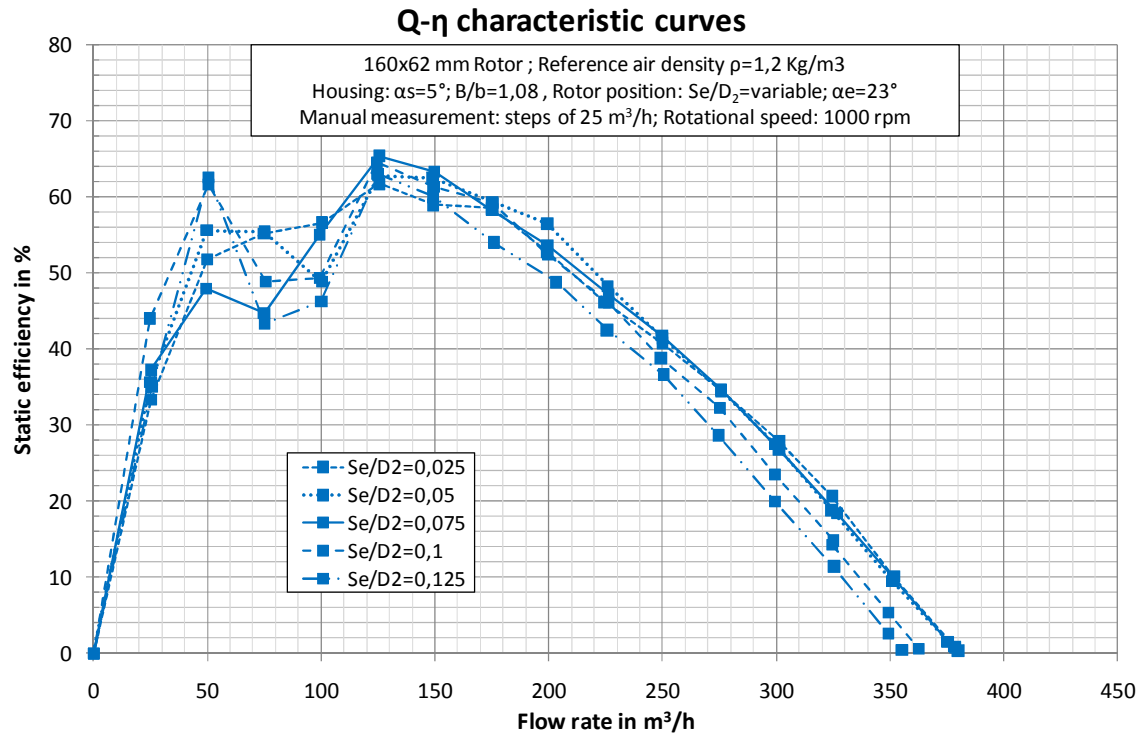


Figure 7.15: Static efficiency vs. flow rate curves of the Sirocco type fan D160x62mm at 1000rpm, scroll housing with an opening angle of 5° , width of housing $B/b=1,08$ and angle of eccentricity of gap rotor-housing of 23° .

Spiral opening angle: $\alpha_s = 5^\circ$

—□— $B/b = 1,08$

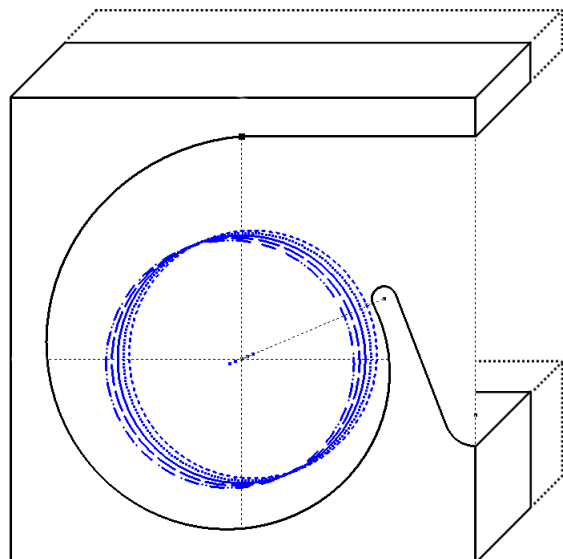
○ $Se/D_2 = 0,025$; $\alpha_e = 23^\circ$

○ $Se/D_2 = 0,05$; $\alpha_e = 23^\circ$

○ $Se/D_2 = 0,075$; $\alpha_e = 23^\circ$

○ $Se/D_2 = 0,1$; $\alpha_e = 23^\circ$

○ $Se/D_2 = 0,125$; $\alpha_e = 23^\circ$



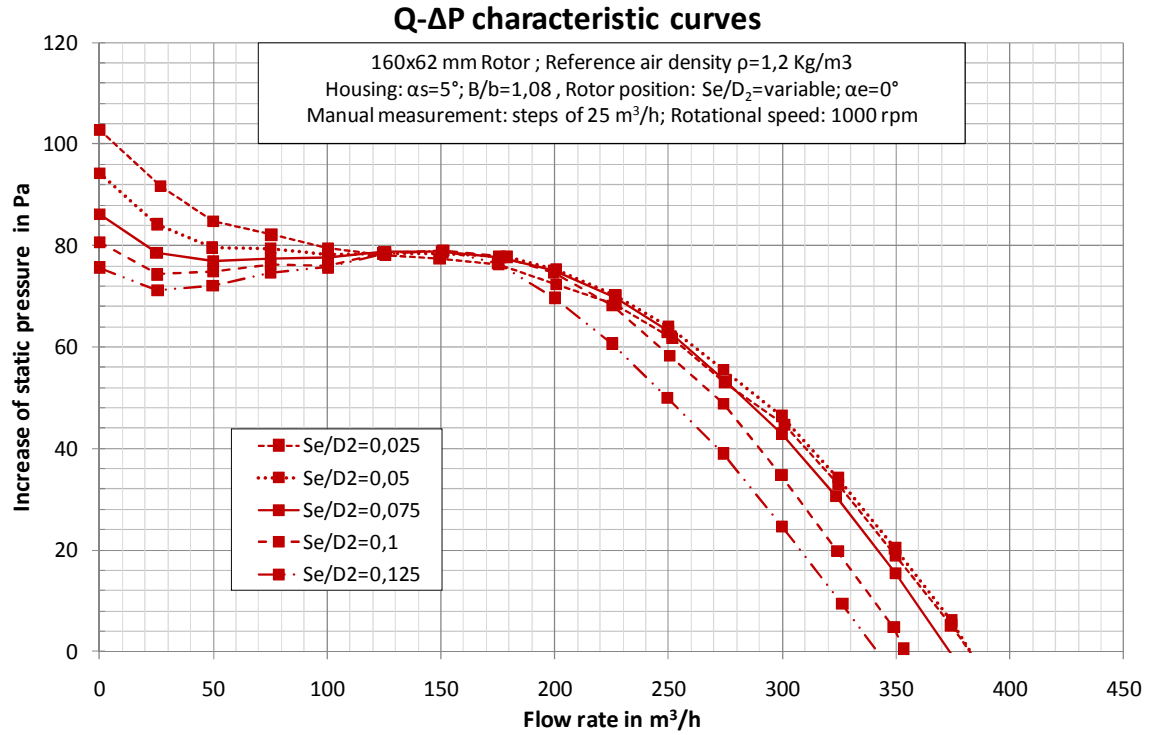


Figure 7.16: Increase of static pressure vs. flow rate curves of the Sirocco type fan D160x62mm at 1000rpm, scroll housing with an opening angle of 5° , width of housing $B/b=1,08$ and angle of eccentricity of gap rotor-housing of 0° .

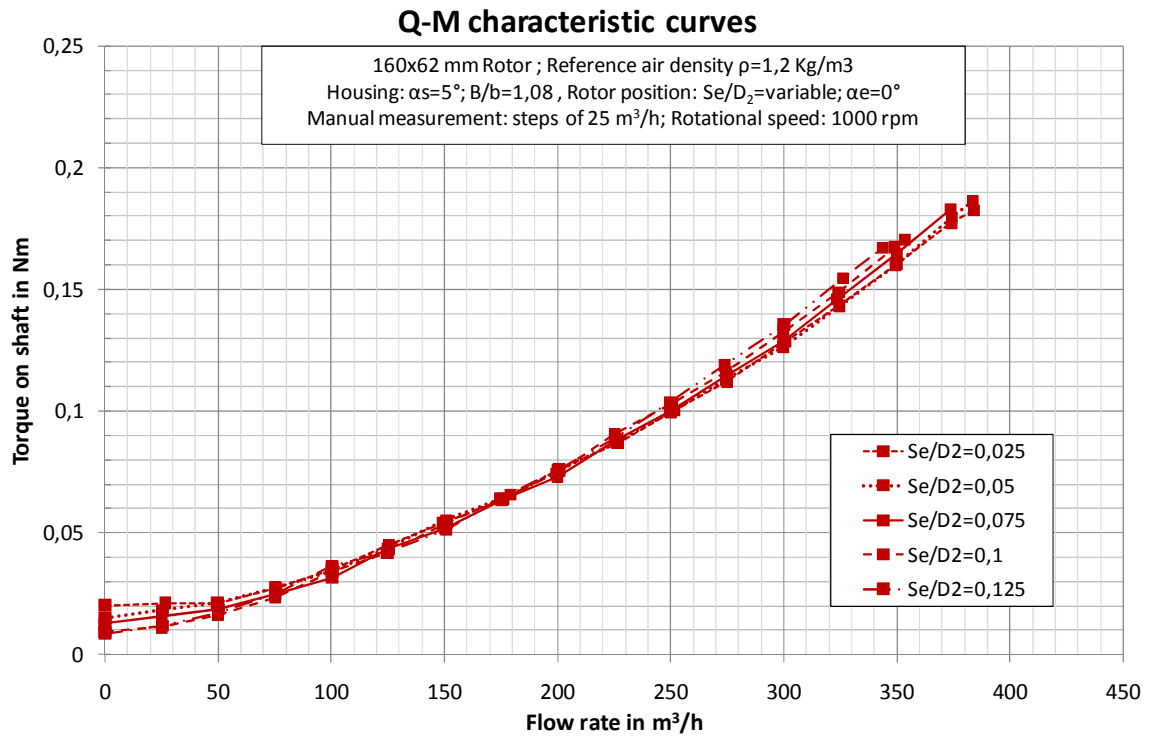


Figure 7.17: Torque on shaft vs. flow rate curves of the Sirocco type fan D160x62mm at 1000rpm, scroll housing with an opening angle of 5° , width of housing $B/b=1,08$ and angle of eccentricity of gap rotor-housing of 0° .

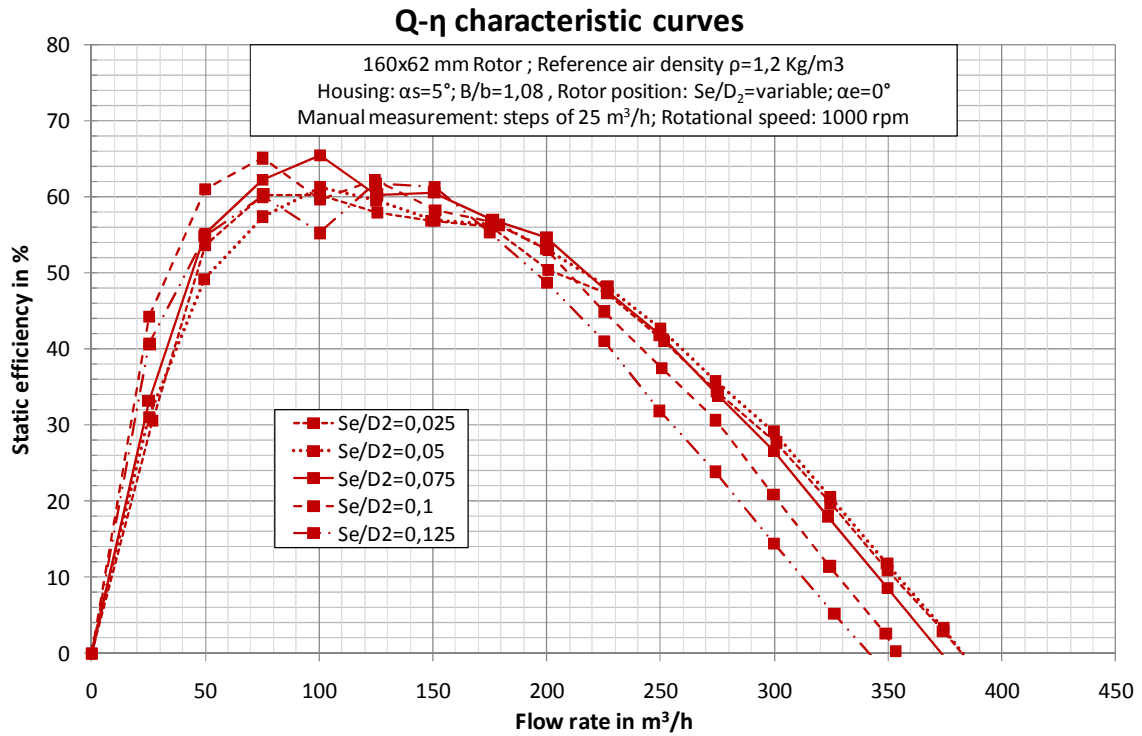


Figure 7.18: Static efficiency vs. flow rate curves of the Sirocco type fan D160x62mm at 1000rpm, scroll housing with an opening angle of 5° , width of housing $B/b=1,08$ and angle of eccentricity of gap rotor-housing of 0° .

Spiral opening angle: $\alpha_s = 5^\circ$

\square $B/b = 1,08$

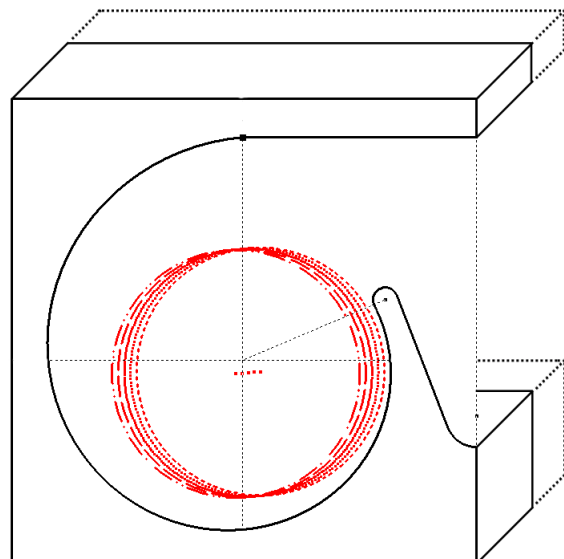
\circ $Se/D_2 = 0,025$; $\alpha_e = 0^\circ$

\circ $Se/D_2 = 0,05$; $\alpha_e = 0^\circ$

\circ $Se/D_2 = 0,075$; $\alpha_e = 0^\circ$

\circ $Se/D_2 = 0,1$; $\alpha_e = 0^\circ$

\circ $Se/D_2 = 0,125$; $\alpha_e = 0^\circ$



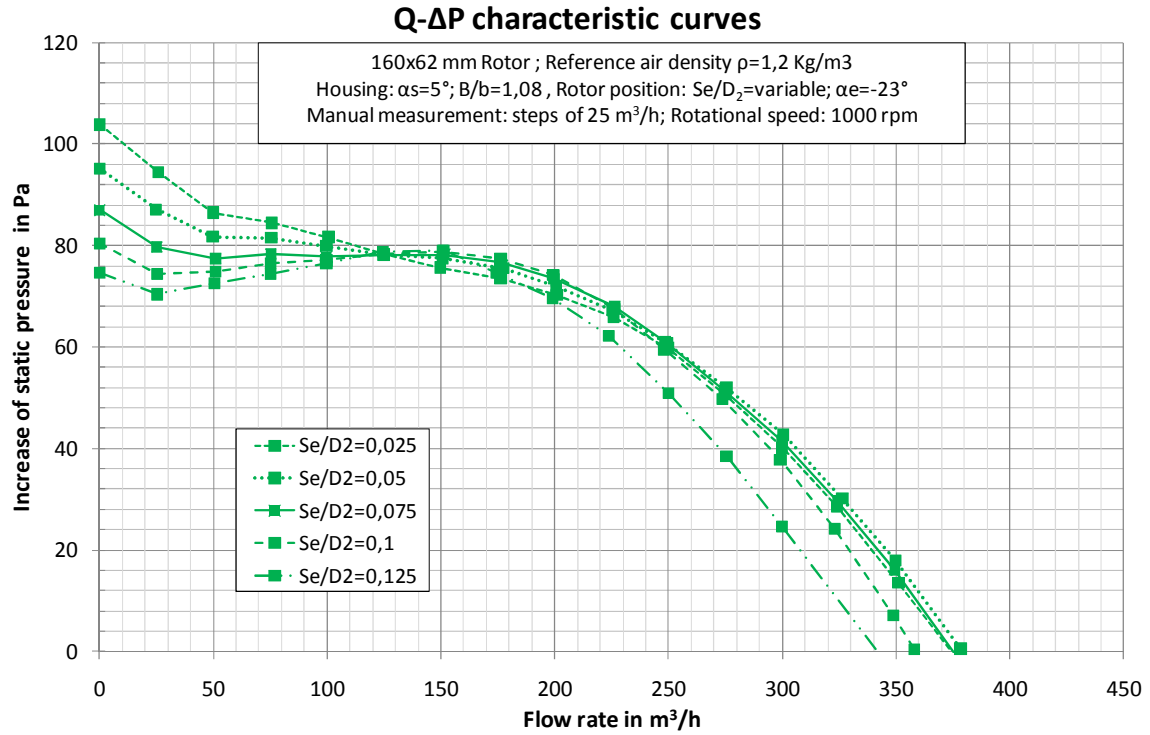


Figure 7.19: Increase of static pressure vs. flow rate curves of the Sirocco type fan D160x62mm at 1000rpm, scroll housing with an opening angle of 5° , width of housing $B/b=1,08$ and angle of eccentricity of gap rotor-housing of -23° .

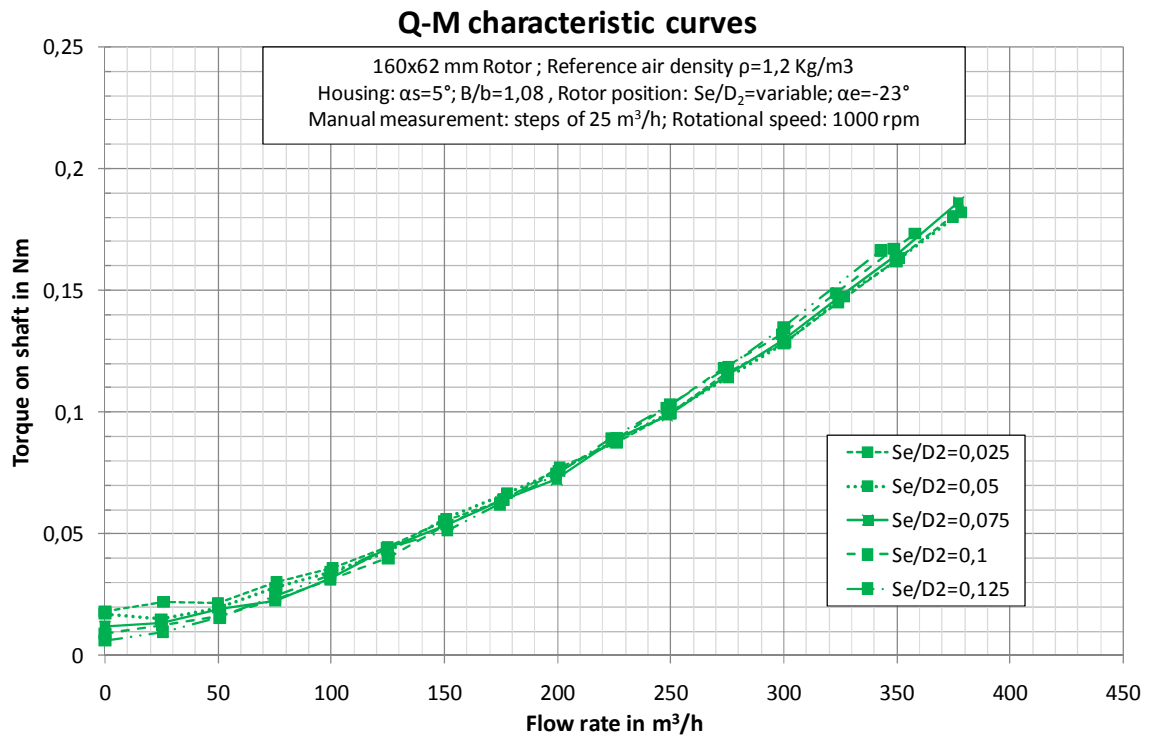


Figure 7.20: Torque on shaft vs. flow rate curves of the Sirocco type fan D160x62mm at 1000rpm, scroll housing with an opening angle of 5° , width of housing $B/b=1,08$ and angle of eccentricity of gap rotor-housing of -23° .

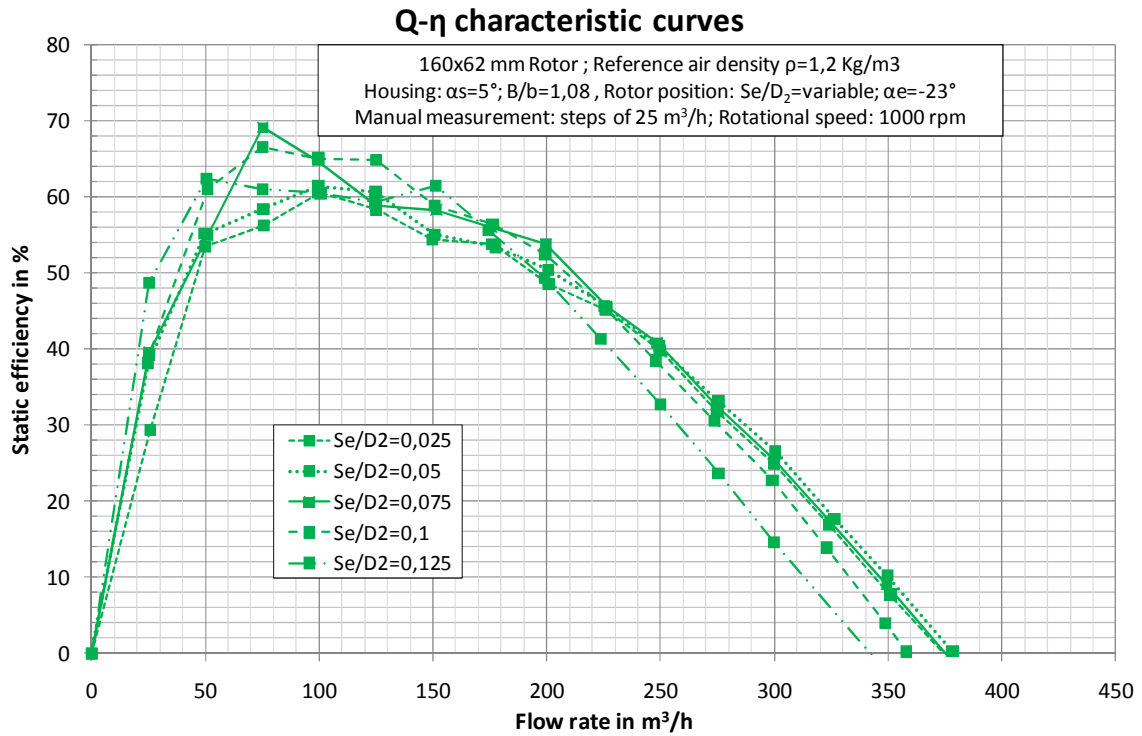
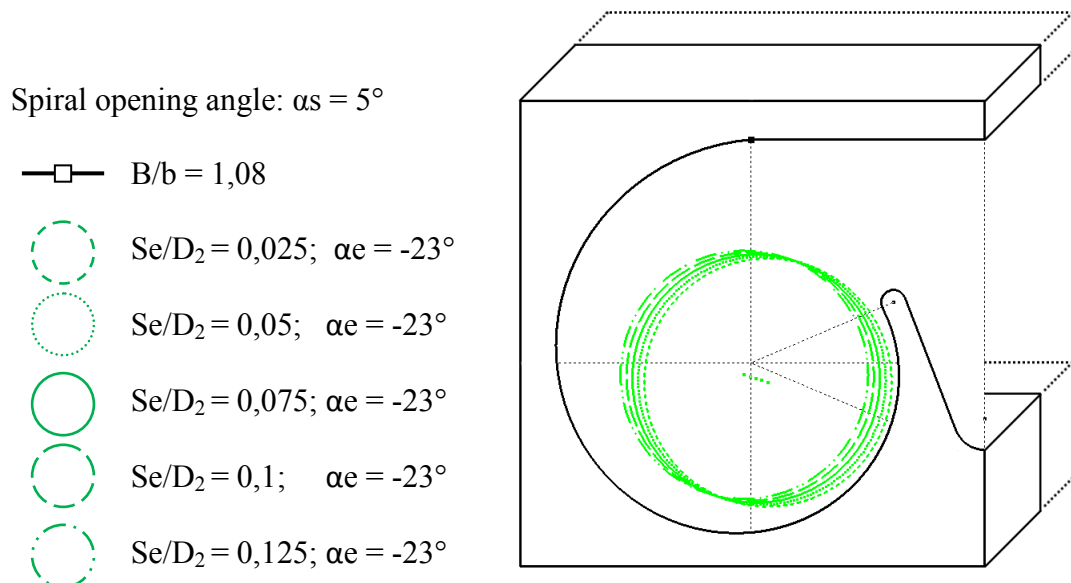


Figure 7.21: Static efficiency vs. flow rate curves of the Sirocco type fan D160x62mm at 1000rpm, scroll housing with an opening angle of 5° , width of housing $B/b=1,08$ and angle of eccentricity of gap rotor-housing of -23° .



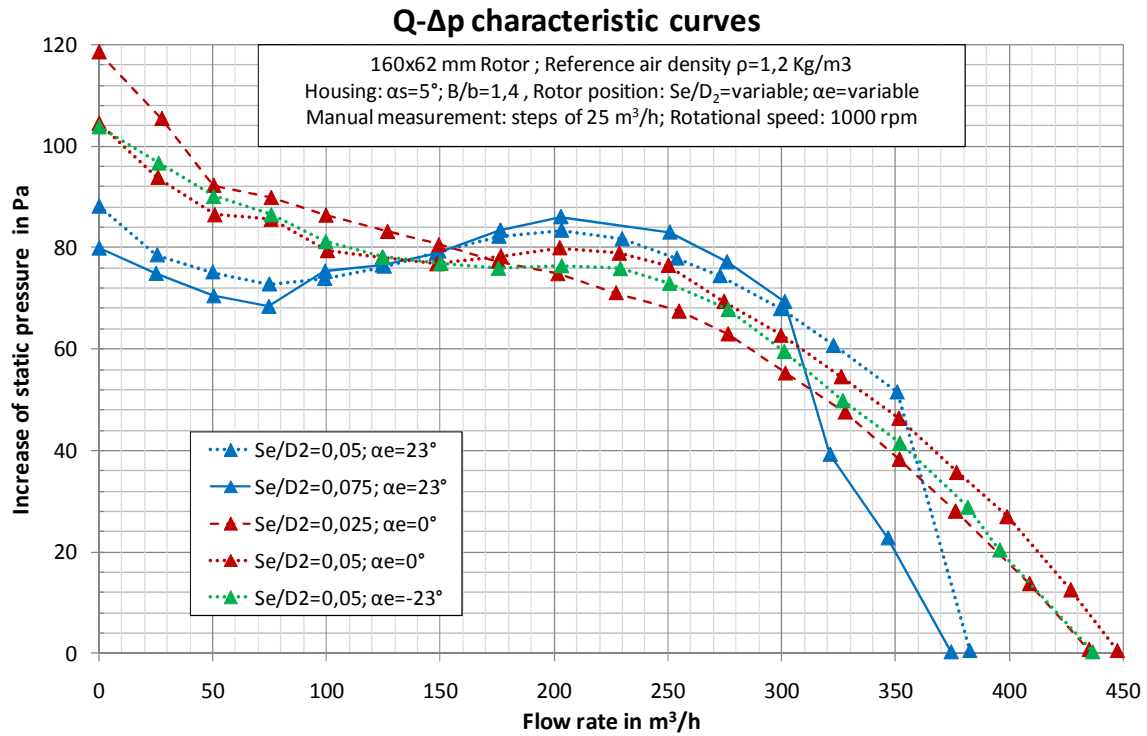


Figure 7.22: Increase of static pressure vs. flow rate curves of the Sirocco type fan D160x62mm at 1000rpm, scroll housing with an opening angle of 5° , width of housing $B/b=1,4$.

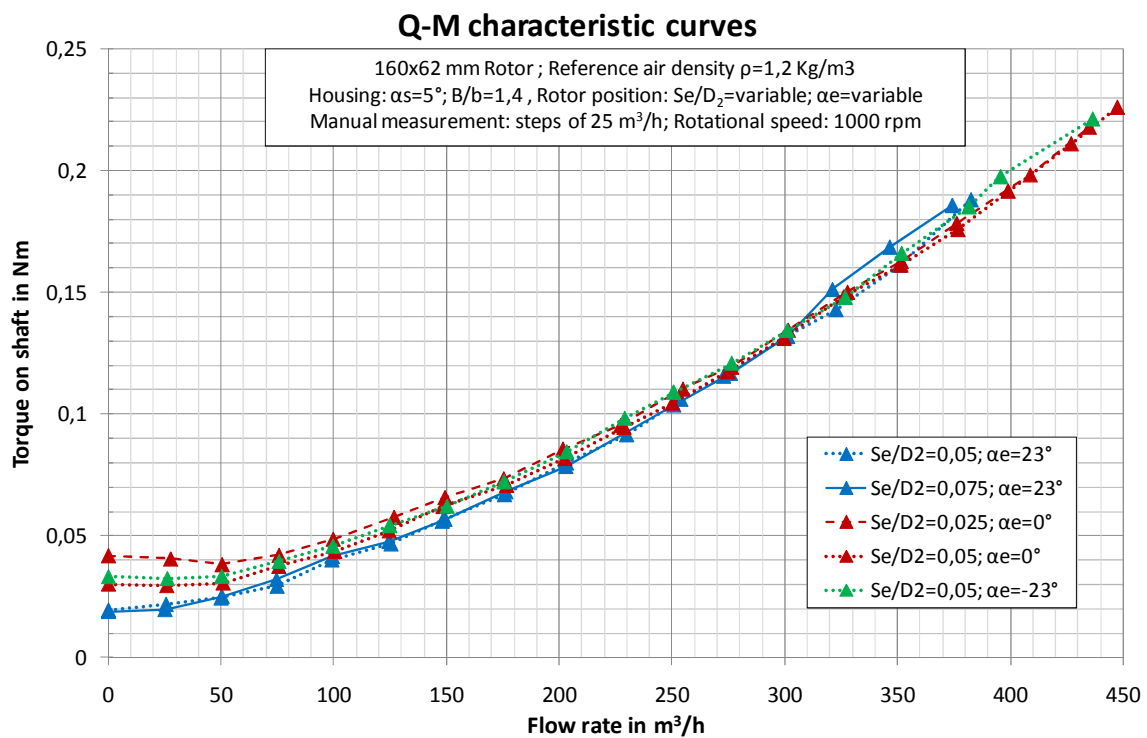


Figure 7.23: Torque on shaft vs. flow rate curves of the Sirocco type fan D160x62mm at 1000rpm, scroll housing with an opening angle of 5° , width of housing $B/b=1,4$.

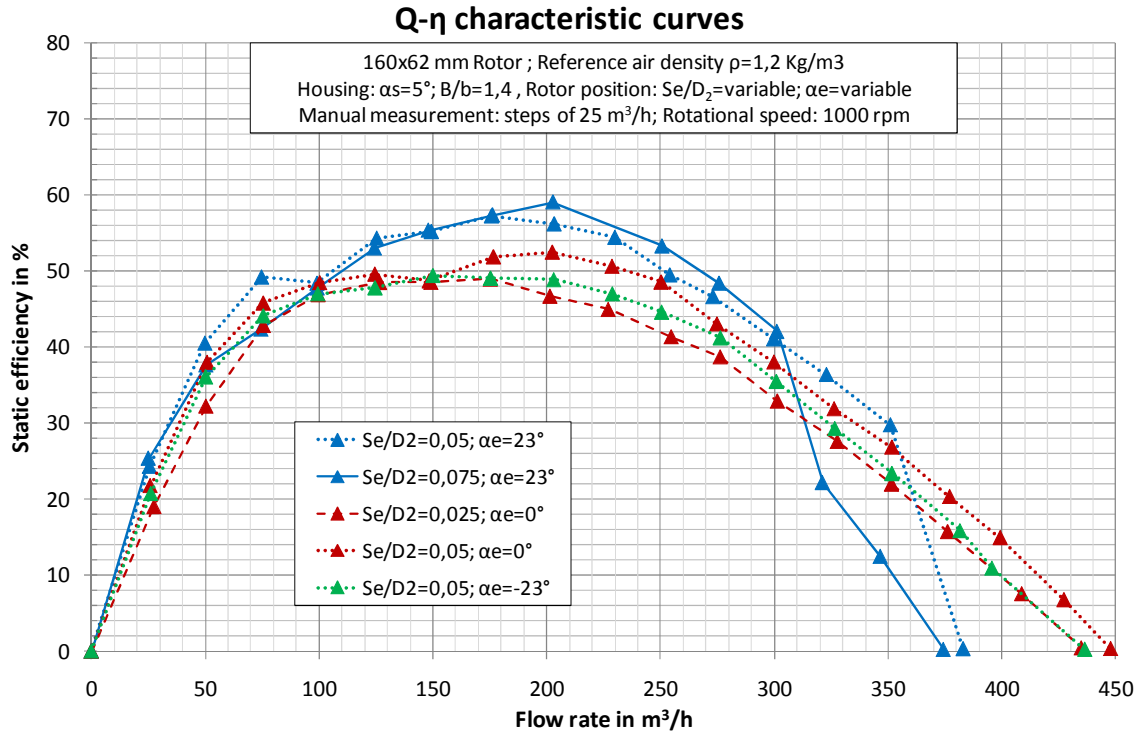
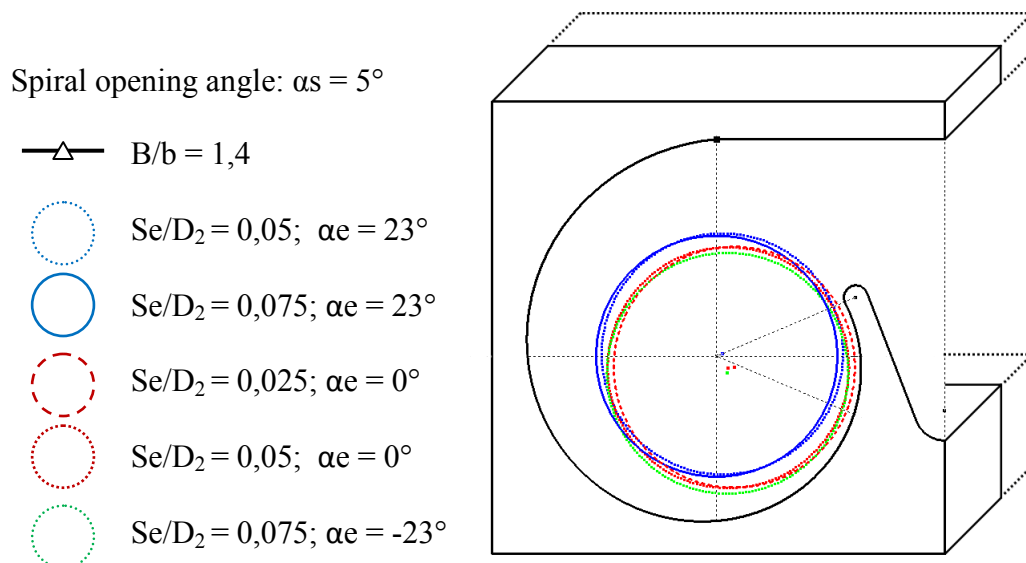


Figure 7.24: Static efficiency vs. flow rate curves of the Sirocco type fan D160x62mm at 1000rpm, scroll housing with an opening angle of 5° , width of housing $B/b=1,4$.



7.1.6 Scroll housing with opening angle of spiral curve of $\alpha_s = 5,5^\circ$

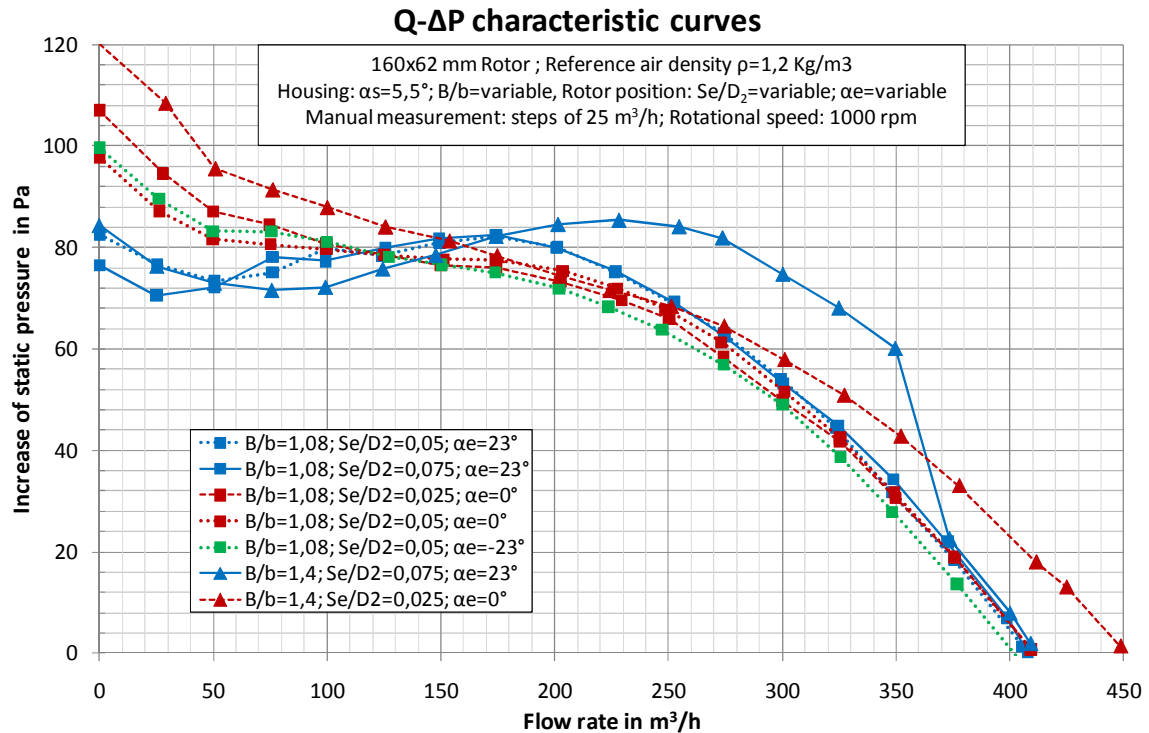


Figure 7.25: Increase of static pressure vs. flow rate curves of the Sirocco type fan D160x62mm at 1000rpm, scroll housing with an opening angle of $5,5^\circ$.

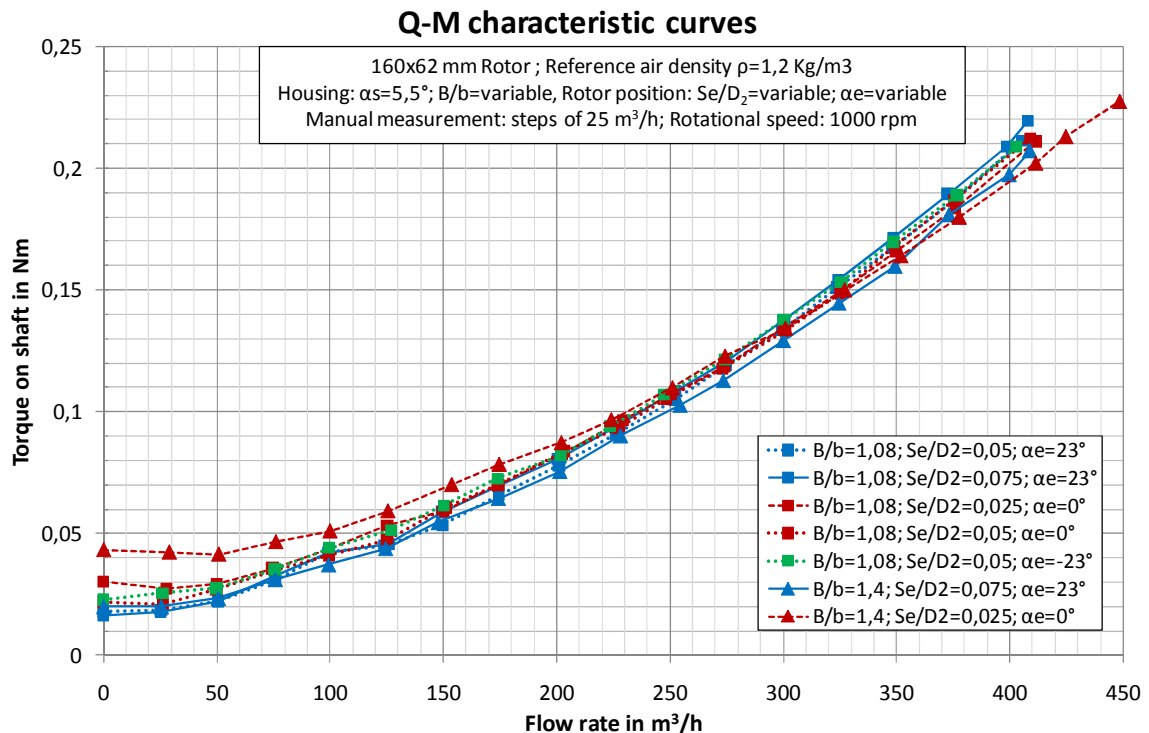


Figure 7.26: Increase of static pressure vs. flow rate curves of the Sirocco type fan D160x62mm at 1000rpm, scroll housing with an opening angle of $5,5^\circ$.

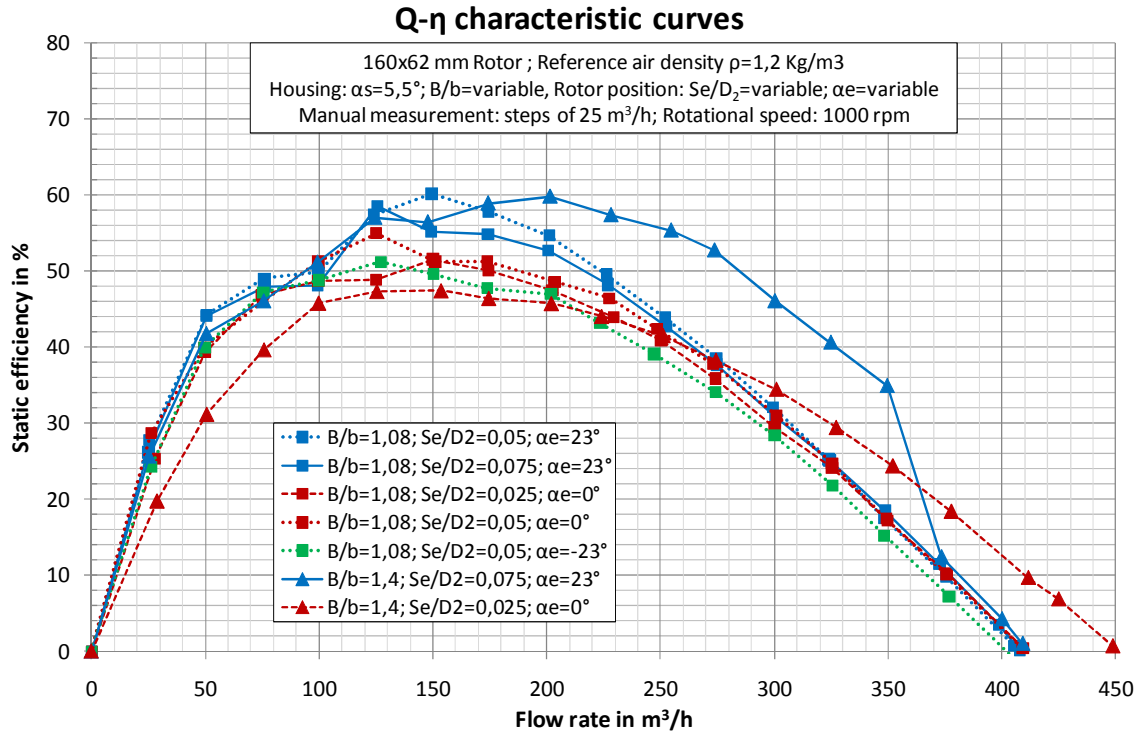


Figure 7.27: Static efficiency curves of the Sirocco type fan D160x62mm at 1000rpm, scroll housing with an opening angle of $5,5^\circ$.

Spiral opening angle: $\alpha_s = 5,5^\circ$

$B/b = 1,08$

$B/b = 1,4$

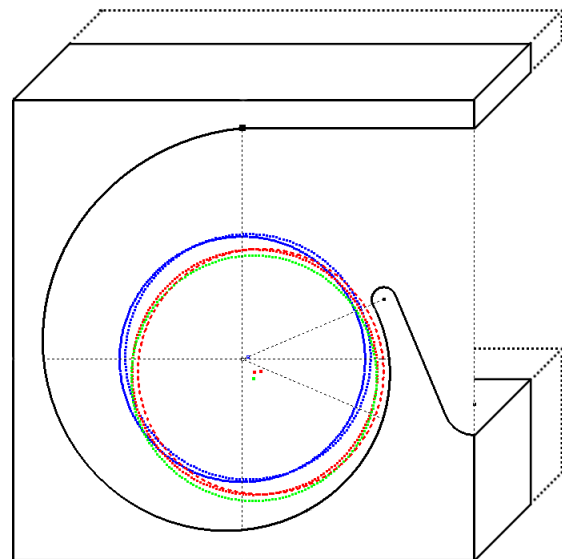
$Se/D_2 = 0,05$; $\alpha_e = 23^\circ$

$Se/D_2 = 0,075$; $\alpha_e = 23^\circ$

$Se/D_2 = 0,025$; $\alpha_e = 0^\circ$

$Se/D_2 = 0,05$; $\alpha_e = 0^\circ$

$Se/D_2 = 0,075$; $\alpha_e = -23^\circ$



8 Evaluation of the results

In this chapter, we analyze all the curves registered in the measurement campaign searching for the best performances on the Sirocco type fan.

The most interesting data for us, in this investigation, is the static efficiency. That is one of the objectives of this work. Therefore, we execute a detailed analysis looking for the highest values. An important issue as well, is to observe which values of the parameters of design are allowing these maximums. We try to find out the most favorable mix of the parameters of design to reach the maximum static efficiencies.

As we have four different parameters of design (α_s , B/b , Se/D_2 , α_e) interacting with each other, this section has four subsections, one per each, in which one we search for their own maximums. Additionally, there are another two more ones. An initial subsection shows the highest efficiency of the whole measurement campaign. A final subsection shows the highest values for static efficiency depending on flow rate points.

Finally, in the last part of this chapter we reveal some influences and trends found concerning the parameters of design on Sirocco type fan.

8.1 Maximum efficiencies found

8.1.1 Maximum static efficiency of the whole measurement campaign

According to the experimental data, the highest static efficiency found is 69,1%. The configuration that provides this maximum is detailed in Table 8-1:

Table 8-1: Maximum static efficiency of the whole measurement campaign.

η_{\max}		Configuration			
α_s	η_{\max}	B/b	Se/D_2	α_e	data file
°	%	-	-	°	-
5	69,1	1,08	0,075	-23	110126_67_5_160x62_-23_12_1000

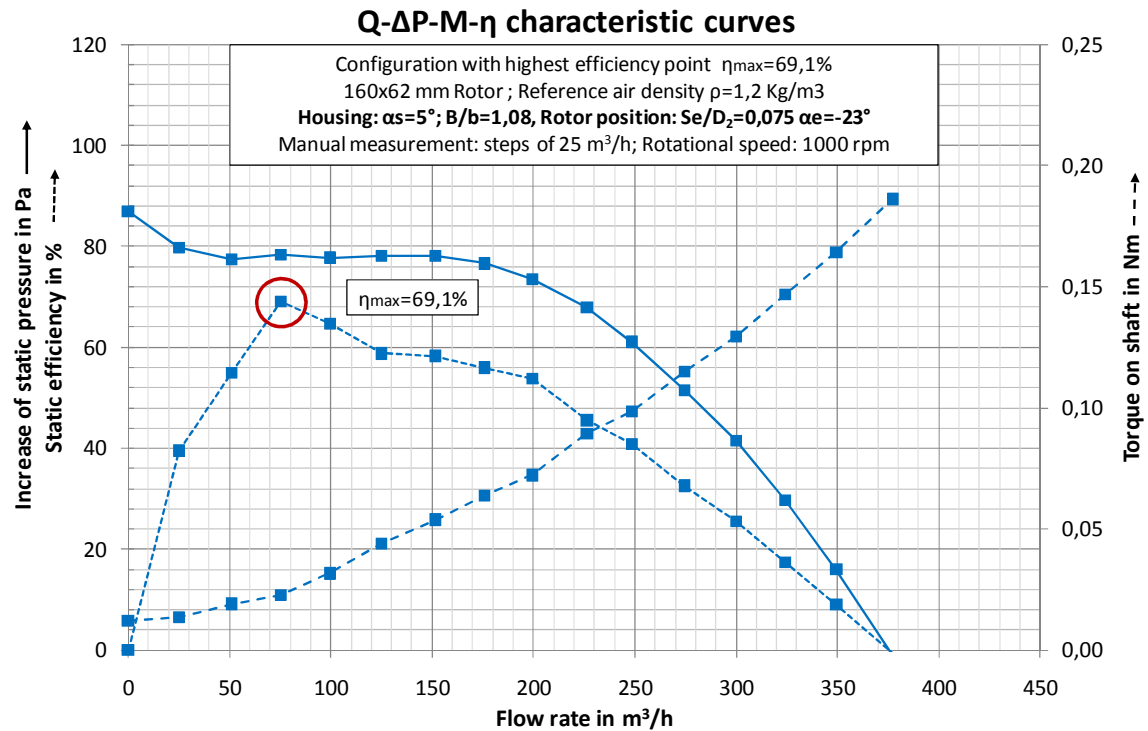


Figure 8.1: Performance curves of the Sirocco type fan D160x62mm at 1000rpm, configuration with maximum static efficiency.

In Figure 8.1, we can appreciate the performance of the configuration of Sirocco type fan with the highest static efficiency of the whole measurement campaign. In the graph, we can see three curves on the behavior of the fan: increase of static pressure, torque on shaft and finally, static efficiency.

Both the curve of increase of static pressure and torque on shaft have a smooth behavior lines. The efficiency curve is more dentate line which presents its maximum for flow rate of $75 \text{ m}^3/\text{h}$.

This value of 69,1% represents a step forward on the study of Sirocco fans type in the department of Fluid dynamics in HTW Berlin. As a reference, the last old highest value for the same type of fan at 1000 rpm found was 50%. That was registered by a student working in the department one year ago.

So that means that we have increased the last old static efficiency in 38,2%, so from 50% to 69,1% according to the experimental measurements.

For more detailed information about the performance of this configuration please refer to *Appendix E. Details of the configuration with highest static efficiency*.

8.1.2 Maximum static efficiencies by opening angle families

We can also have a look on the fluctuation on the static efficiency due to the opening angle of spiral curve α_s .

As we know, we have built six different scroll housings depending on this parameter. We have housings for $\alpha_s = 3^\circ$; $3,5^\circ$; 4° ; $4,5^\circ$; 5° ; $5,5^\circ$. In this subsection, we

notice which are the values of opening angle of spiral curve that are more desirable to obtain higher efficiencies.

We can appreciate as well, which are the configurations that provide the highest efficiencies for each housing.

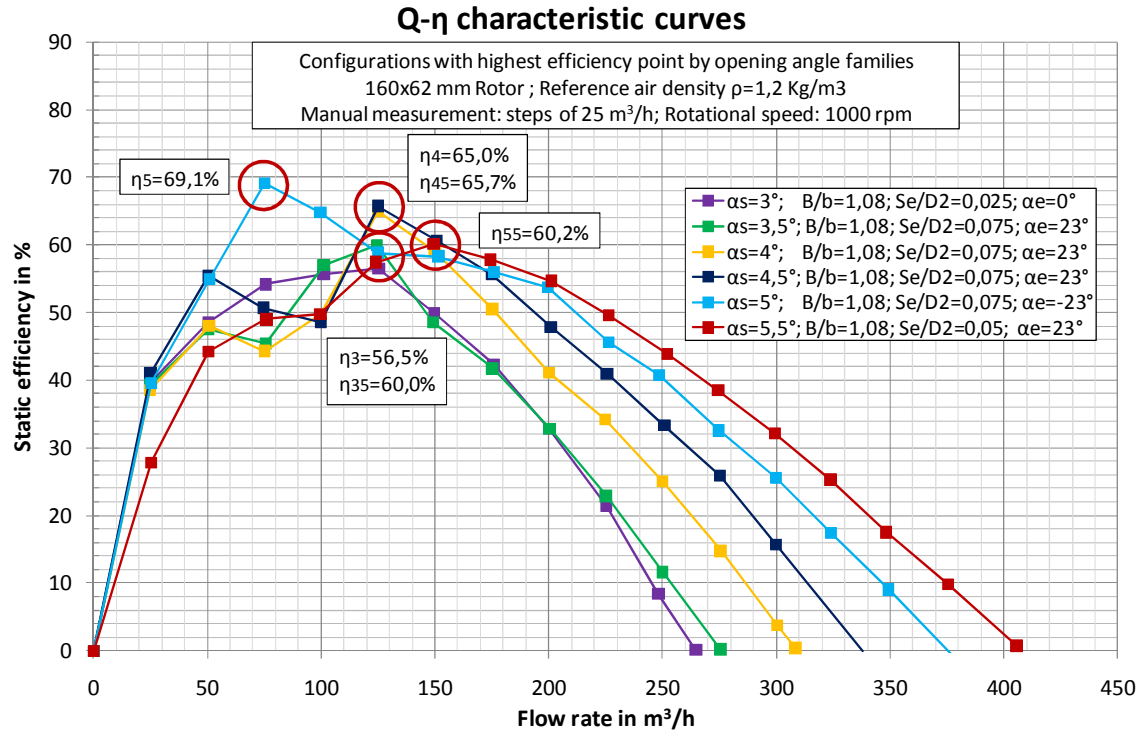


Figure 8.2: Static efficiency vs. flow rate curves of the Sirocco type fan D160x62mm at 1000rpm, maximum static efficiency configuration by opening angle of families.

In Figure 8.2, we can see six different curves of static efficiency vs. flow rate in different colors, each color corresponding to one of the housings. The highest efficiency of each housing is highlighted by using a red circle in the main point accompanied by a small text annotation with each maximum value. Complementing this information, there is a legend on the right side where we can appreciate the configurations that provide these maximums. The maximum static efficiencies each scroll housing reach, are resume below:

Table 8-2: Maximum static efficiencies by open angle families.

η_{\max} by families of α_s		Configuration			
α_s	η_{\max}	B/b	Se/D2	α_e	data file
$^\circ$	%	-	-	$^\circ$	-
3	56,5	1,08	0,025	0	110125_67_3_160x62_0_4_1000
3,5	60,0	1,08	0,075	23	110125_67_35_160x62_23_12_1000
4	65,0	1,08	0,075	23	110125_67_4_160x62_23_12_1000
4,5	65,7	1,08	0,075	23	110125_67_45_160x62_23_12_1000
5	69,1	1,08	0,075	-23	110126_67_5_160x62_-23_12_1000
5,5	60,2	1,08	0,05	23	110127_67_55_160x62_23_8_1000

8.1 Maximum efficiencies found

As we see in Table 8-2, the maximum efficiency is rising from the opening angle of 3° since it reaches the upper point. This maximum is for 5° opening angle. Afterwards, it continues falling for next values.

The most favorable value on the opening angle parameter is $\alpha_s = 5^\circ$ providing an static efficiency of 69,1%. Obviously, this configuration matches with the highest static efficiency of the whole measurement campaign, mentioned in the previous subsection.

It is important to notice that all the maximums are reached by the value of width of scroll housing $B/b = 1,08$.

About the parameter of the gap rotor-housing, we can say that the most repeated configuration on the table is $Se/D_2 = 0,075$. Moreover this value is always moving between the range from 0,025 to 0,075 and never takes higher position.

There is nothing clear to say about the angle of eccentricity because the values are moving in all the range. We can only say that $\alpha_e = 23^\circ$ is the most repeated configuration on Table 8-2.

In addition, to have a full view of these configurations, their curves of increase of static pressure and torque on a shaft vs. flow rate are added. Refer to Figure 8.3 and Figure 8.4.

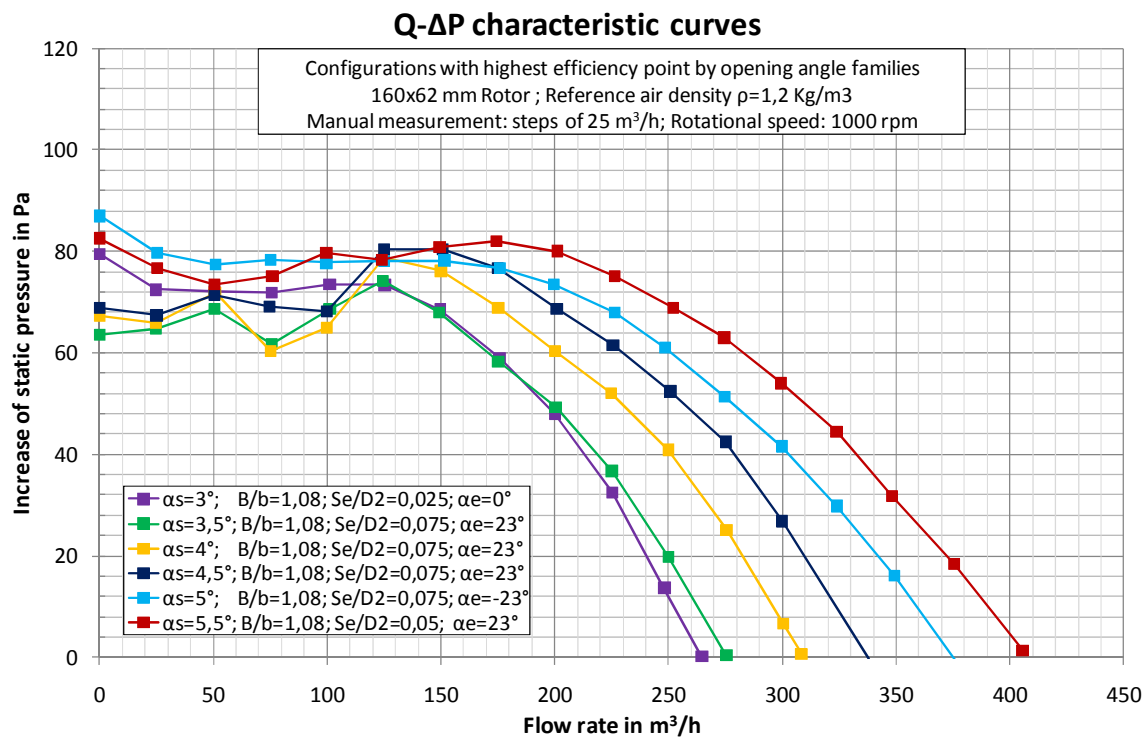


Figure 8.3: Increase of static pressure vs. flow rate curves of the Sirocco type fan D160x62mm at 1000rpm, maximum static efficiency configuration by opening angle of families.

In Figure 8.3 we have the increase of static pressure for the best configurations grouped by angles. We can see on it that in general we can say: the bigger opening angle the larger flow rate, as well, the bigger opening angle the higher initial increase of static pressure. These questions are analyzed with more detail in a further Section 8.2

Resume of trends and influences found. We can appreciate in the same figure, that the configurations according to $Se/D_2=0,075$ and $\alpha_e = 23^\circ$, present a downfall of pressure in the range between $50 - 100 \text{ m}^3/\text{h}$. In the case of figure, that is for the opening angles of $3,5^\circ; 4^\circ; 4,5^\circ$.

Finally the curves for the torque on shaft are shown in Figure 8.4.

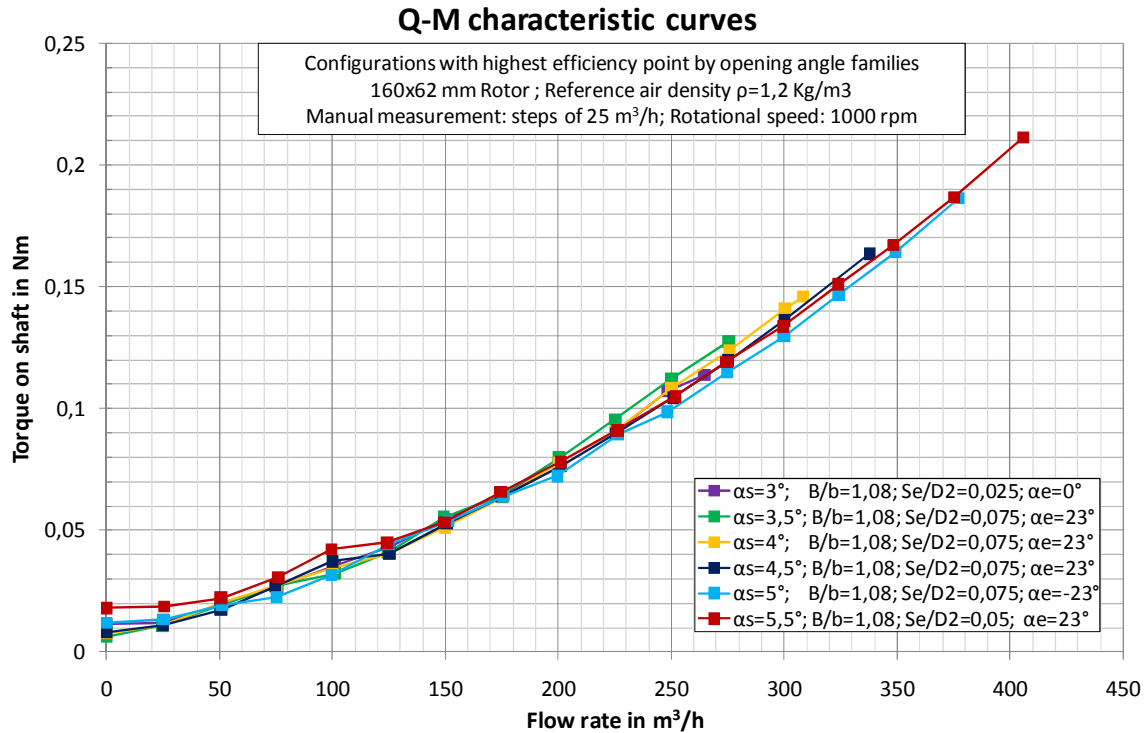


Figure 8.4: Torque on shaft vs. flow rate curves of the Sirocco type fan D160x62mm at 1000rpm, maximum static efficiency configuration by opening angle of families.

As a conclusion of this subsection, we can say that the most favorable value to obtain highest efficiencies for the opening angle of spiral curve is 5° . Additionally experimental data shows that an opening angle of $4,5^\circ$ is better than $5,5^\circ$. That could mean that if there is a maximum point for the efficiency is more plausible that this will be between $4,5^\circ$ - 5° than 5° - $5,5^\circ$.

8.1.3 Maximum static efficiencies by width families

Another parameter of study is the dimensionless ratio for the width of housing B/b . We have two values: $B/b = 1,08; 1,4$. In the next Figure 8.5, we can appreciate the best configurations for these two values.

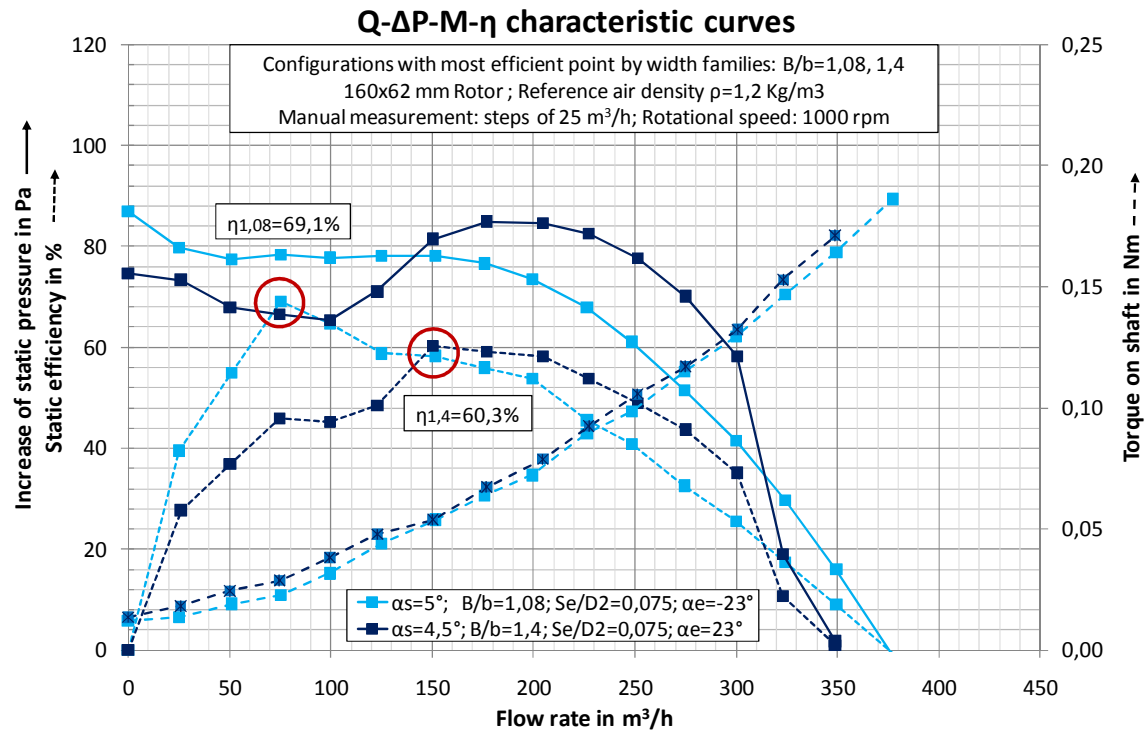


Figure 8.5: Performance curves of the Sirocco type fan D160x62mm at 1000rpm, maximum static efficiency configuration by width of housing families.

As we see in the picture, the maximum static efficiency for the thick housing is 60,3% and for the thin one is 69,1%. That means that the most properly value for B/b parameter is 1,08. In Table 8-3, we can see the details.

Table 8-3: Maximum static efficiencies by width of housing families.

η_{\max} by families of B/b		Configuration			
B/b	η_{\max}	α_s	Se/D2	α_e	data file
-	%	°	-	°	-
1,08	69,1	5	0,075	-23	110126_67_5_160x62_-23_12_1000
1,4	60,3	4,5	0,075	23	110127_87_45_160x62_23_12_1000

About the behavior of the increase of pressure, they are complementary. Before the flow rate point of 150 cubic meters, the increase of pressure for the thick housing undergoes the thin one. After that point, we have the opposite behavior. This is also happening with the efficiency curves.

As a conclusion of subsection, we say that a width for housing of $B/b = 1,08$ give better efficiencies.

8.1.4 Maximum static efficiencies by gap rotor-housing families

The gap rotor-hosing is also an important parameter on the Sirocco type fans. In this study we have arranged 5 values for this parameter: $Se/D_2 = 0,025; 0,05; 0,075; 0,1; 0,125$.

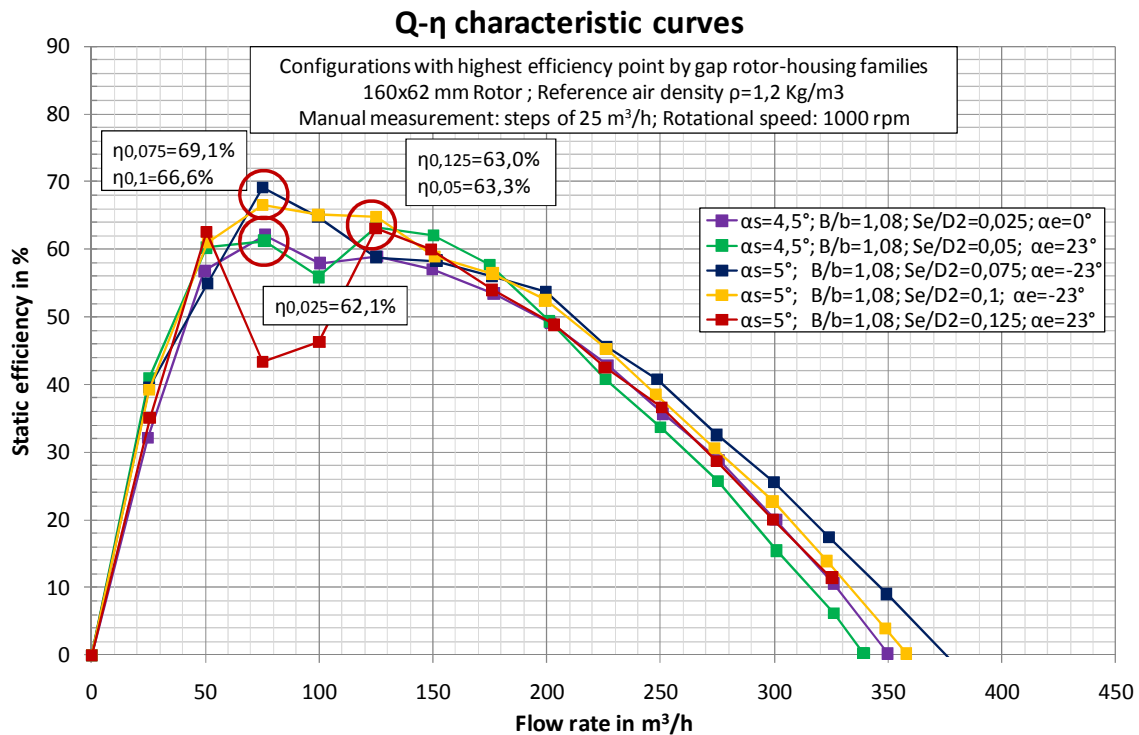


Figure 8.6: Static efficiency vs. flow rate curves of the Sirocco type fan D160x62mm at 1000rpm, maximum static efficiency configuration by gap rotor-housing families.

In Figure 8.6 are shown the efficiency curves by this grouping family. The highest efficiency is for the value of $Se/D_2 = 0,075$. We can observe that the three higher points are for curves with 5° opening angle and the last two one for $4,5^\circ$. So we can attend to the same considerations than the previous part: if there is a maximum point for the efficiency is more plausible that this will be between $4,5^\circ$ - 5° .

All of them belongs to the thin housing $B/b = 1,08$. As said before, this relation is providing always the best values for static efficiency.

About the parameter α_e , we can't give a clear recommendation because as we see in Table 8-4., it is fluctuating all over the range.

Table 8-4: Maximum static efficiencies by gap rotor-housing families.

η_{\max} by families of Se/D_2		Configuration			
Se/D_2	η_{\max}	α_s	B/b	α_e	data file
-	%	$^\circ$	-	$^\circ$	-
0,025	62,1	4,5	1,08	0	110125_67_45_160x62_0_4_1000
0,05	63,3	4,5	1,08	23	110125_67_45_160x62_23_8_1000
0,075	69,1	5	1,08	-23	110126_67_5_160x62_-23_12_1000
0,1	66,6	5	1,08	-23	110126_67_5_160x62_-23_16_1000
0,125	63,0	5	1,08	23	110126_67_5_160x62_23_20_1000

8.1 Maximum efficiencies found

Subsequently we show the characteristic curves for these configurations providing the maximal static efficiencies by gap rotor-housing families.

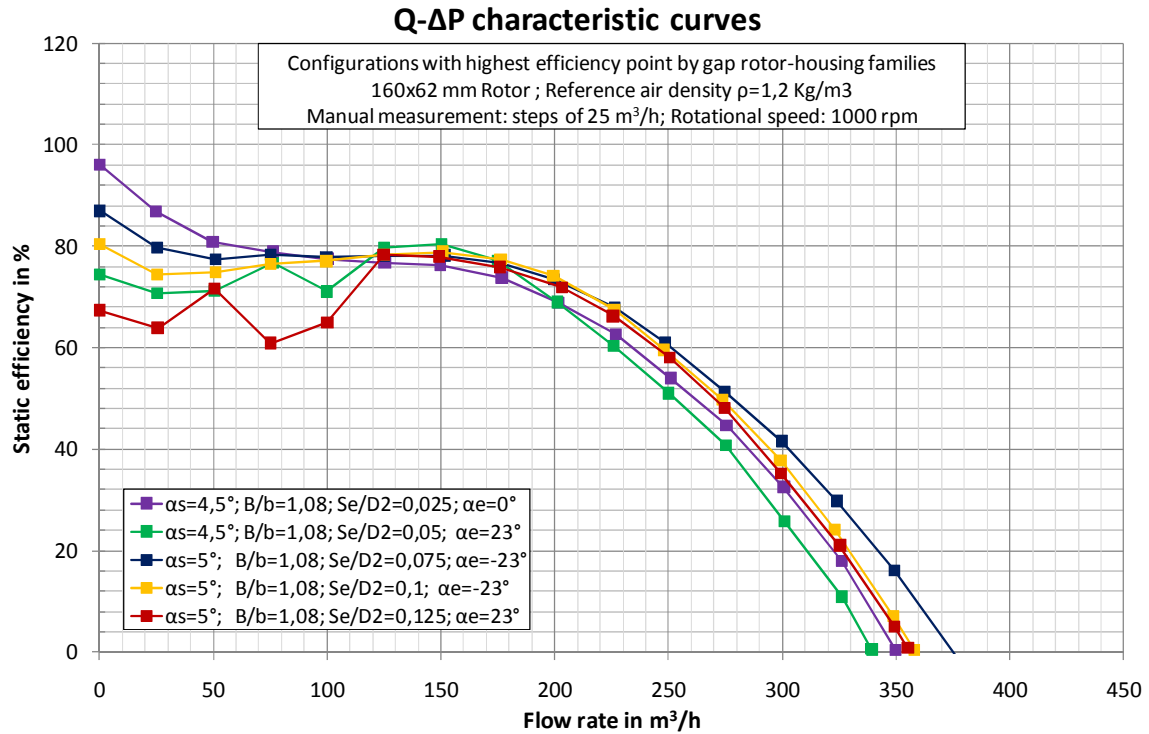


Figure 8.7: Increase of static pressure vs. flow rate curves of the Sirocco type fan D160x62mm at 1000rpm, maximum static efficiency configuration by gap rotor-housing families.

In Figure 8.7 we have the curves relative to the increase of static pressure vs. flow rate. All of them present smooth behavior but the red line ($Se/D_2=0,125$). In fact, when that relation is so big, we can observe strong vibrations from 50 to 100 m^3/h flow rate. When these curves were recorder, it was evident this behavior according to the intense noise according to the measurement. We can say that for $Se/D_2 = 0,125$, the air stream is not properly guided along the spiral housing, and subsequently for this range the fan is operating bad conditions.

We can see as well in Figure 8.8 that the smaller distance rotor-housing, the bigger torque on shaft required. This fact can be explained also knowing that the higher pressure the higher torque required on shaft.

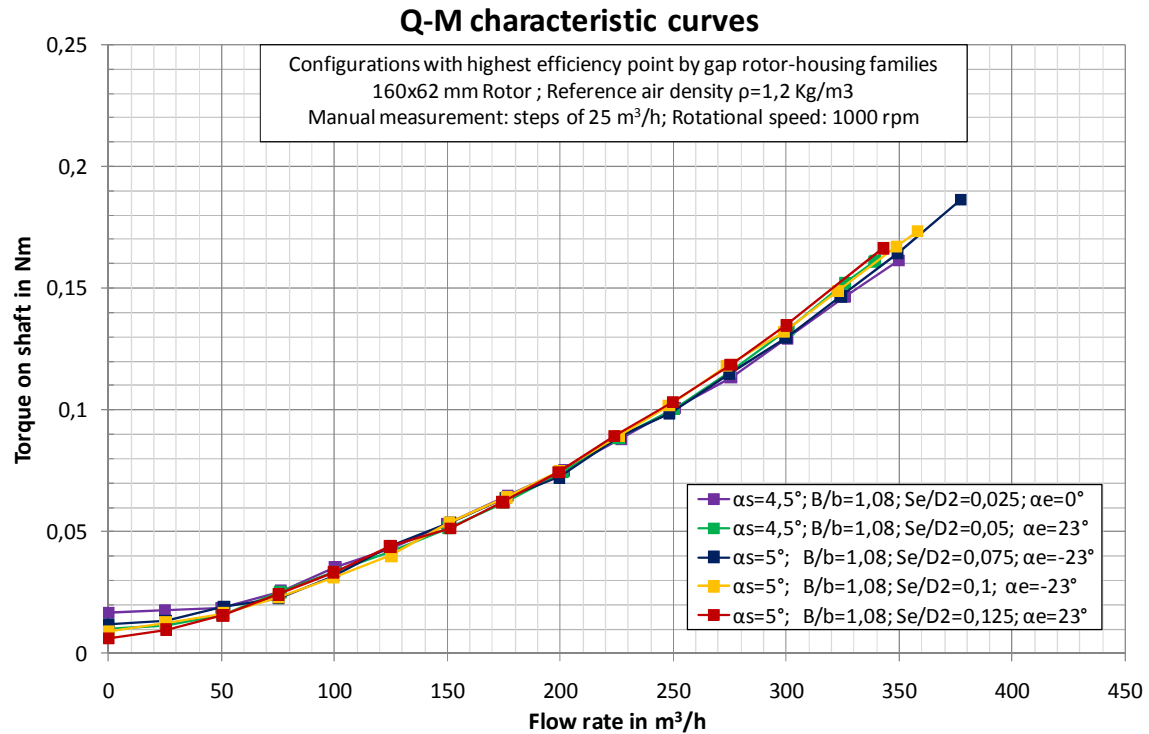


Figure 8.8: Torque on shaft vs. flow rate curves of the Sirocco type fan D160x62mm at 1000rpm, maximum static efficiency configuration by gap rotor-housing families.

8.1.5 Maximum static efficiencies by angle of eccentricity families

This parameter is the most controversial of all of the design parameters. Its study in the previous sections, does not disclose any appreciable trend.

In the next Table 8-5 we can see the detailed results:

Table 8-5: Maximal static efficiencies by angle of eccentricity families

η_{\max} by families of α_e		Configuration			
α_e	η_{\max}	α_s	B/b	$Se/D2$	data file
$^\circ$	%	$^\circ$	-	-	
23	65,7	4,5	1,08	0,075	110125_67_45_160x62_23_12_1000
0	65,4	5	1,08	0,075	110126_67_5_160x62_0_12_1000
-23	69,1	5	1,08	0,075	110126_67_5_160x62_-23_12_1000

The next Figure 8.9, shows the higher static efficiencies for this family group.

8.1 Maximum efficiencies found

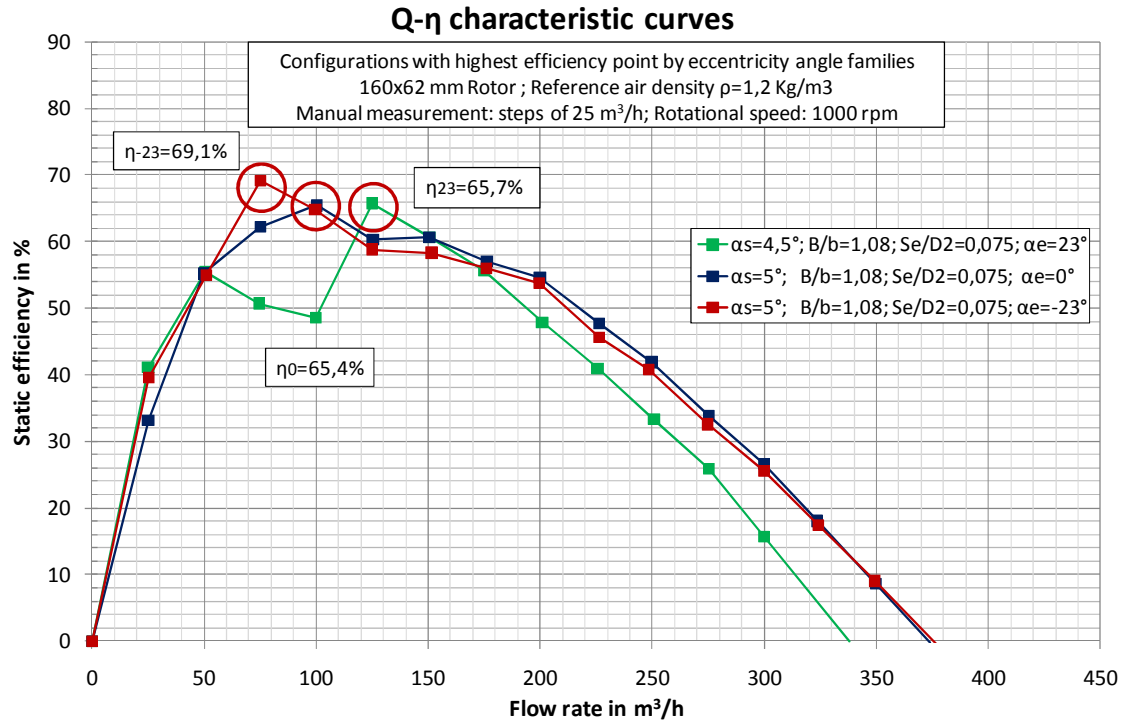


Figure 8.9: Static efficiency vs. flow rate curves of the Sirocco type fan D160x62mm at 1000rpm, maximum static efficiency configuration by angle of eccentricity families.

The highest efficiency point is for the configuration with $\alpha_e = -23$. By the way the rest efficiencies are also very high. As a conclusion I would say that this parameter is as not much relevant as the others. Its influence to obtain high efficiencies is lower than the other three parameters.

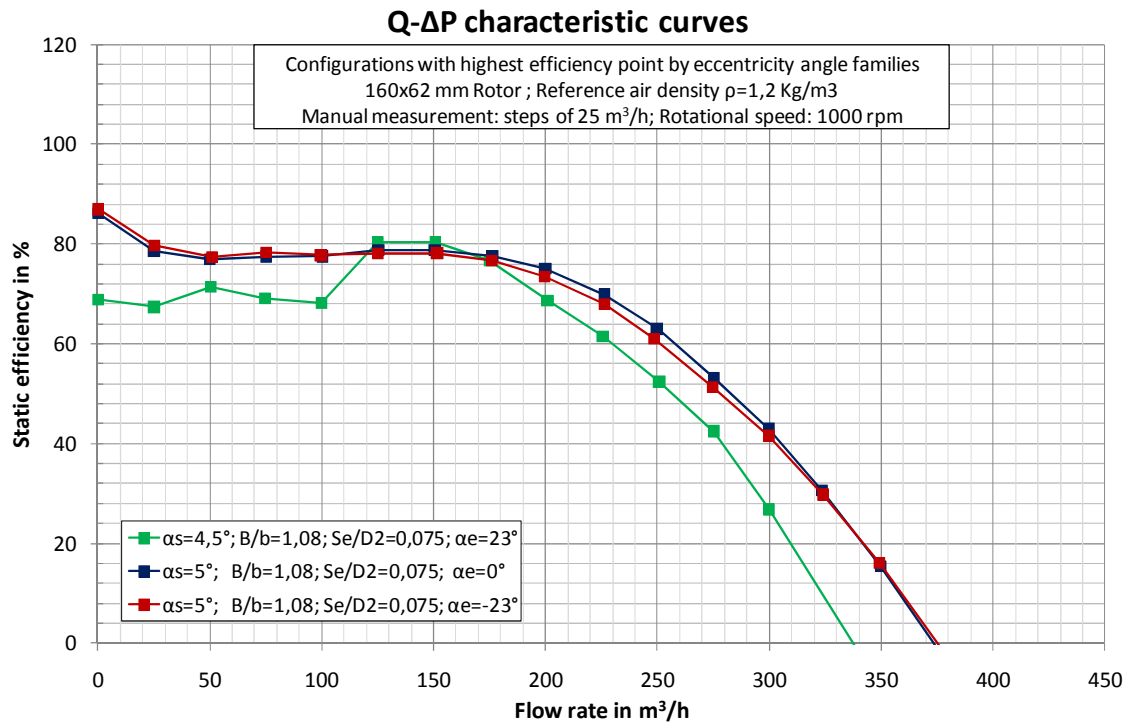


Figure 8.10: Increase of static pressure vs. flow rate curves of the Sirocco type fan D160x62mm at 1000rpm, maximum static efficiency configuration by angle of eccentricity families.

If we observe Figure 8.10, we can see one effect of this parameter. For all the three curves we have the same relation $B/b=1,08$ and $Se/D_2=0,075$, as well as similar α_s angles. The green line responds to the a special configuration: independent from α_s or B/b coming from the variables $Se/D_2=0,07$ and $\alpha_e = 23^\circ$. This configuration normally presents pressure oscillations in the range 50 – 100 m³/h. As we see in the figure, if we set this parameter to the values 0° or -23° the oscillations are avoided.

Finally in Figure 8.11 the curves of torque on shaft are displayed.

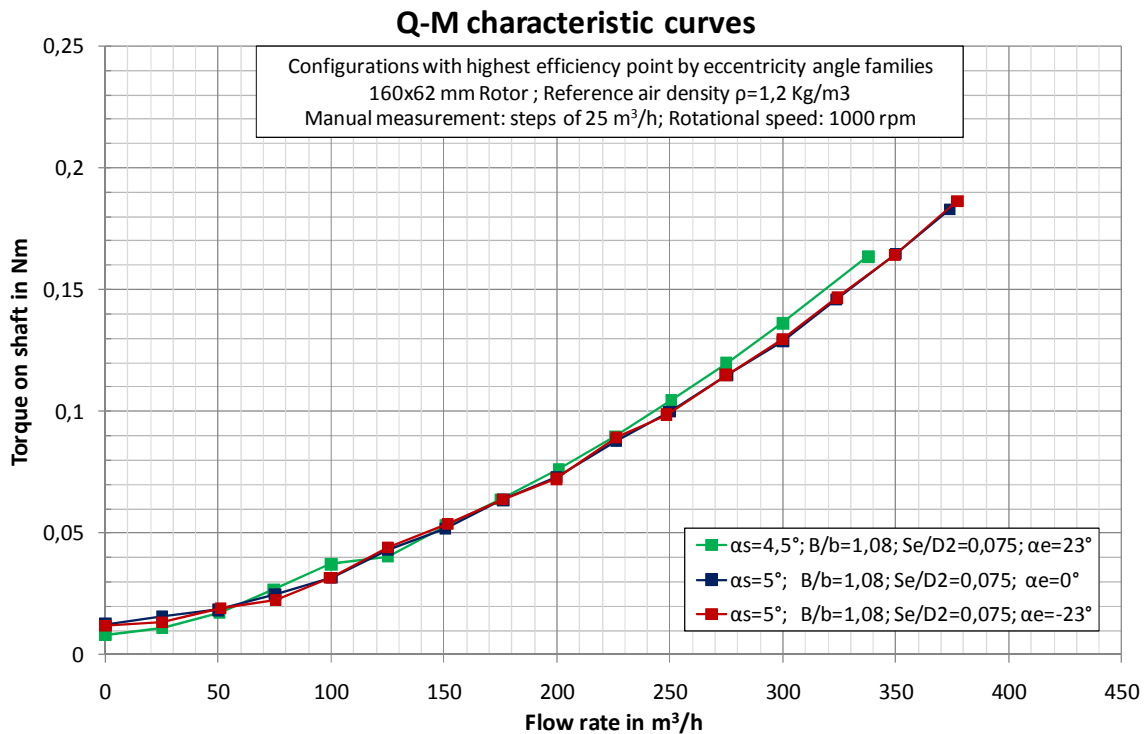


Figure 8.11: Torque on shaft vs. flow rate curves of the Sirocco type fan D160x62mm at 1000rpm, maximum static efficiency configuration by angle of eccentricity families.

8.1.6 Maximum static efficiencies for each point of flow rate

Until this section, we analyzed the curves of static efficiency by using the next criteria: Searching for the maximal efficiency point of the curve. But we can think that a device like a fan could work in different points of its characteristic curves. It depends on how matches the system characteristic curve and the characteristic curve of the fan. According to that possibility, the variation of the working point of the fan can allow a high decrease of the maximal efficiency. Consequently could be interesting to find the configuration that maintains the best efficiencies all along its characteristic curve.

8.1 Maximum efficiencies found

To find this configuration, we evaluate each flow rate point searching for the highest static efficiency from 0 to 450 m³/h. As the measurement is done by steps of 25 m³/h we have 18 points to evaluate.

Table 8-6: Maximal static efficiencies for each point of flow rate

η_{\max} by each point of flow rate		Configuration			
Flow rate	Max efficiency	B/b	Se/D2	α_e	data file
m ³ /h	%	-	-	°	
0	0,0				-
25	48,7	1,08	0,125	-23	110126_67_5_160x62_-23_20_1000
50	62,6	1,08	0,125	23	110126_67_5_160x62_23_20_1000
75	69,1	1,08	0,075	-23	110126_67_5_160x62_-23_12_1000
100	65,4	1,08	0,075	0	110126_67_5_160x62_0_12_1000
125	65,4	1,08	0,075	23	110125_67_45_160x62_23_12_1000
150	63,3	1,08	0,075	23	110126_67_5_160x62_23_12_1000
175	59,3	1,4	0,075	23	110127_87_45_160x62_23_12_1000
200	59,8	1,4	0,075	23	110128_87_55_160x62_23_12_1000
225	57,3	1,4	0,075	23	110128_87_55_160x62_23_12_1000
250	55,3	1,4	0,075	23	110128_87_55_160x62_23_12_1000
275	52,7	1,4	0,075	23	110128_87_55_160x62_23_12_1000
300	46,0	1,4	0,075	23	110128_87_55_160x62_23_12_1000
325	40,6	1,4	0,075	23	110128_87_55_160x62_23_12_1000
350	34,9	1,4	0,075	23	110128_87_55_160x62_23_12_1000
375	20,3	1,4	0,05	0	110128_87_5_160x62_0_8_1000
400	14,9	1,4	0,05	0	110128_87_5_160x62_0_8_1000
425	6,9	1,4	0,05	0	110128_87_5_160x62_0_8_1000
450	0,7	1,4	0,05	0	110128_87_5_160x62_0_8_1000

In Table 8-6, we can see the configurations with the highest static efficiency for each point of flow rate. The best efficiencies correspond to the first part of the table, that is, for small flow rates. In the previous section, all the values correspond to this part of small flow rate.

In the table we can observe this trend: the highest efficiencies come from small flow rates for the scroll housings with relation $B/b = 1,08$. For better performance on a large flow rates, the scroll housings with $B/b = 1,4$ are requested.

The full table of this efficiency study can be found in *Appendix D. Study of maximal static efficiencies*.

8.2 Resume of trends and influences found

After evaluating all the curves and the data recorded in the measurements, some clear trends and influences of the parameters of design have been found. We expose that ones in this section.

8.2.1 Influence of the opening angle

Concerning the opening angle of spiral curve (α_s), we can announce two main points. The first one is related about the maximum flow rate achieved and the second is about the location of the best efficiency points on the curves on the performance in sirocco type fan.

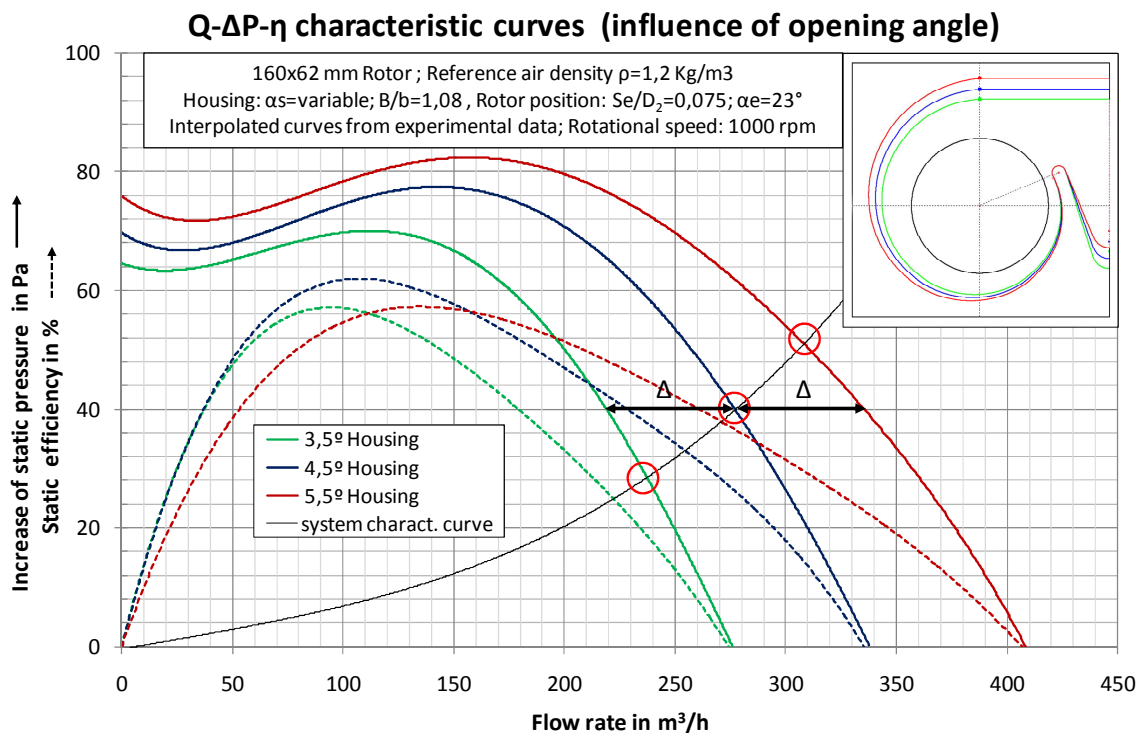


Figure 8.12: Influence of the opening angle on the flow rate

- 1) *The bigger opening angle, the bigger maximal flow rate achieved. One increase of the opening angle value produces a proportional step Δ on the pressure rise curve.*

In Figure 8.12 this influence is clearly shown by drawing the pressure rise curves of three consecutive opening angles. For instance, in this example, the increase of 0,5 degree on the opening angle produces an increase on the pressure rise of about 60 m^3/h . The curves are crossed by one random system characteristic curve to show the operating points of the system and the distance Δ between performance curves.

This influence of the opening angle means that we can expect bigger flow rates if we design with bigger opening angles on sirocco type fan. The alternative point of view of this influence is related with the best static efficiency point. As we see in the same figure, the increase of the opening angle value doesn't answer with an increase of the static efficiency. In fact, the location of the best efficiency points follows a parabolic

curve trend. That means that there is a maximum value of static efficiency that depending on the opening angle. This fact is explained more clearly in the next point.

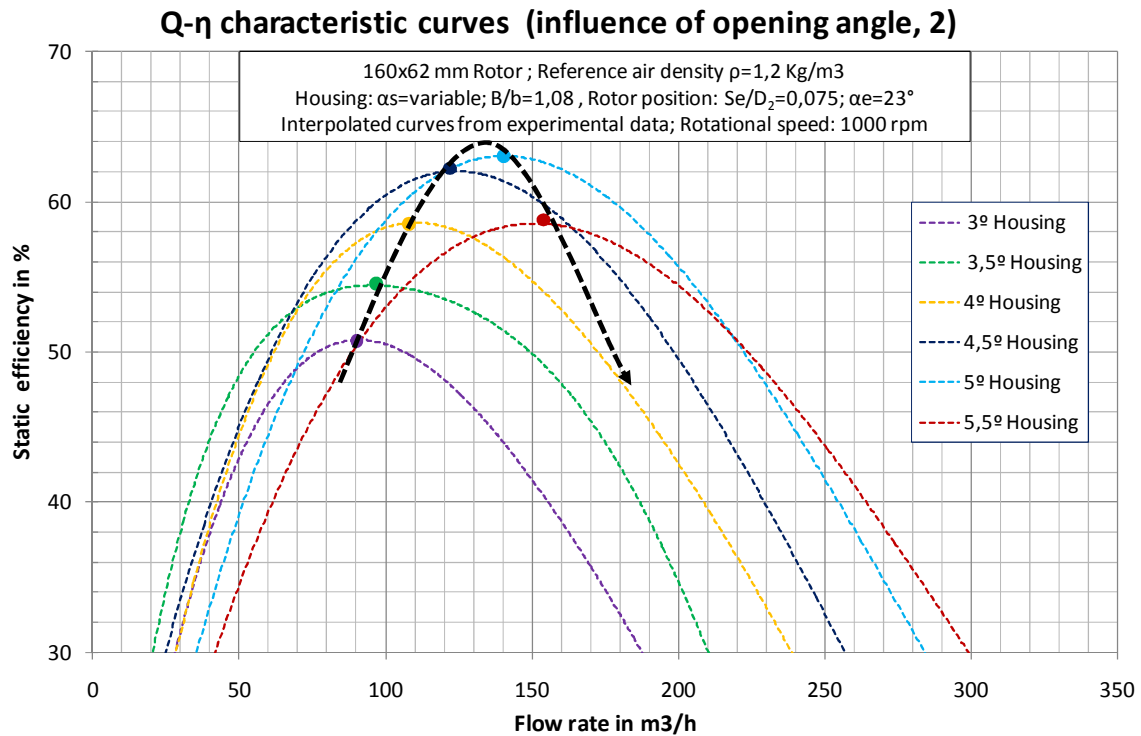


Figure 8.13: Location of the best static efficiency points for Sirocco type fan

- 2) *The best static efficiency points for each value of opening angle present an approximate parabolic distribution with a maximum around 5°.*

In Figure 8.13, we can appreciate the static efficiency curves for the entire opening angle values recorded in the measurements (3,0 to 5,5 degree). The best efficiency point is highlighted with a dot according the same color. A trend curve has been drawn to collect the distribution of these points.

The maximum efficiency is rising from the opening angle of 3° since it reaches the upper point. This maximum is for 5° opening angle. Afterwards, there is a drop, as we see for the angle of 5,5°. The flow rate responsible of each point is increasing according the influence that we explain in the previous point.

The location of the best static efficiency points means that there is an optimum in the design according the parameter of opening angle. In our measurement the best value for this parameter is 5 degree. But according on the trend line drawn in the figure, it is probable that the real maximum could be located between 4,5 and 5,0 degree.

8.2.2 Influence of the width of housing

We have observed a clear influence of the width of housing (B/b) on the performance of the fan that is explained below.

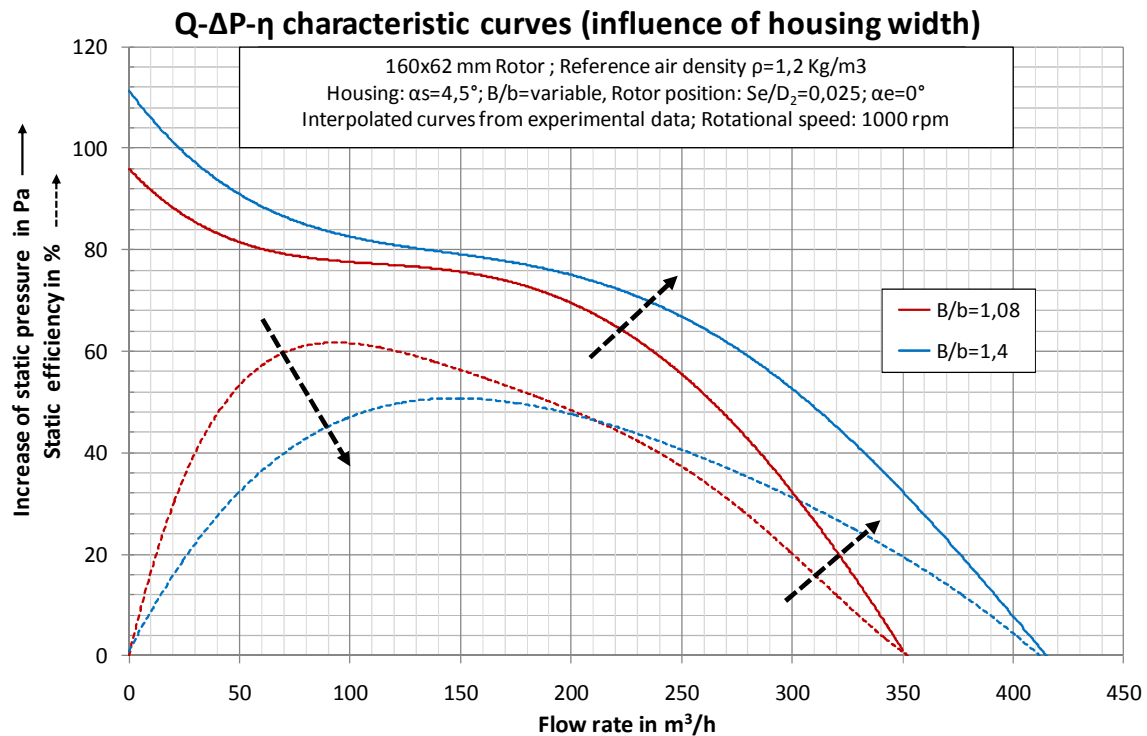


Figure 8.14: Influence of the width of housing on the performance of Sirocco type fan

- 3) *Maximal static efficiencies on Sirocco type fan can only be expected by designing scroll housings as thinner as possible in relation to the width of the rotor.*

The positive effect of increasing the width of housing is the bigger flow rate achieved and a rise of the static pressure provided by the fan, as we see in Figure 8.14. On the other hand this fact produces a decrease of the maximum static efficiency for smaller flow rates where the maximum is located.

The increase of the maximum flow rate provided by the fan displaces the best efficiency point to the right as it occurs when increasing the value of opening angle.

When a housing much broader than the rotor is requested, the best performance is achieved by placing the rotor as much closer as possible from the inlet of the fan. Proceeding this way, the distribution of the air stream is the most homogeneous according to the measurements.

8.2.3 Influence of decentering the rotor

Decentering the rotor from the original position was one of the parts included in the measurements. It had an important influence on the results for instance because the maximum static efficiency was found with this procedure. Apart of this fact, we observed some influences on the performance of the fan that are explained subsequently.

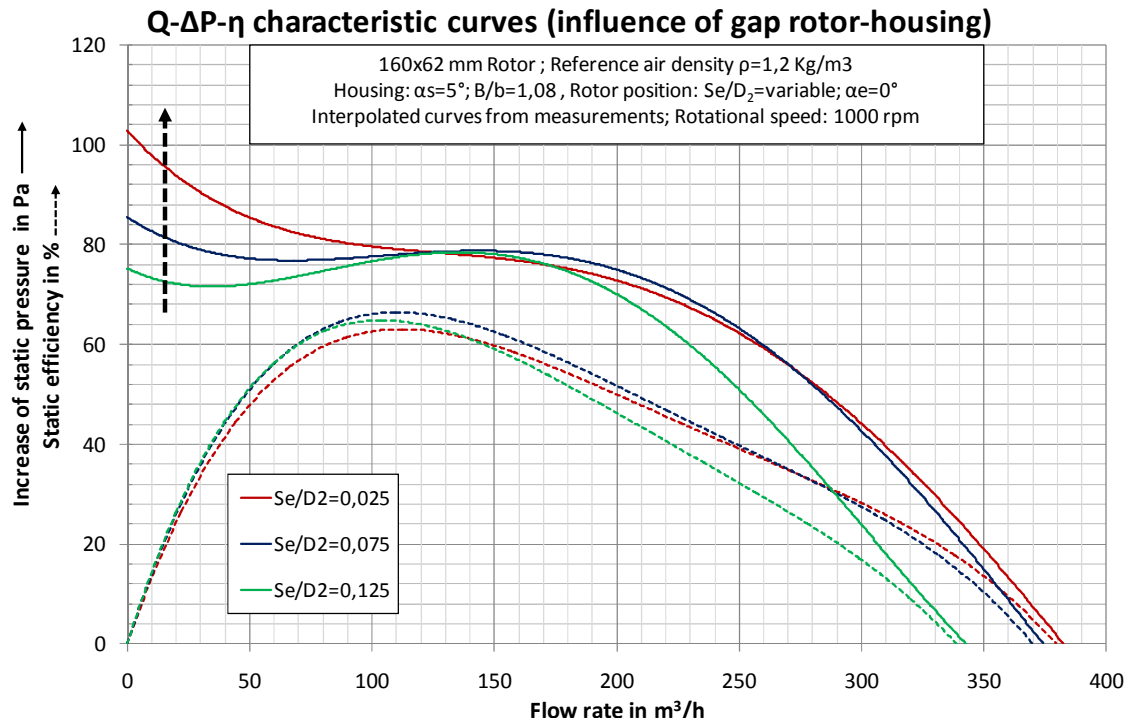


Figure 8.15: Influence of the gap rotor-housing on the pressure curve on Sirocco type fan

- 4) *The smaller gap between rotor-housing, the bigger pressure rise values for initial flow rate.*

In Figure 8.15 we can observe the curves of pressure rise and efficiency for three configurations where the only change from each other is the gap between rotor-housing. The initial pressure rise becomes higher when the gap decreases from 0,125 (green curve) to 0,025 (red curve) in about 35 Pa. That represents an increase of 35%.

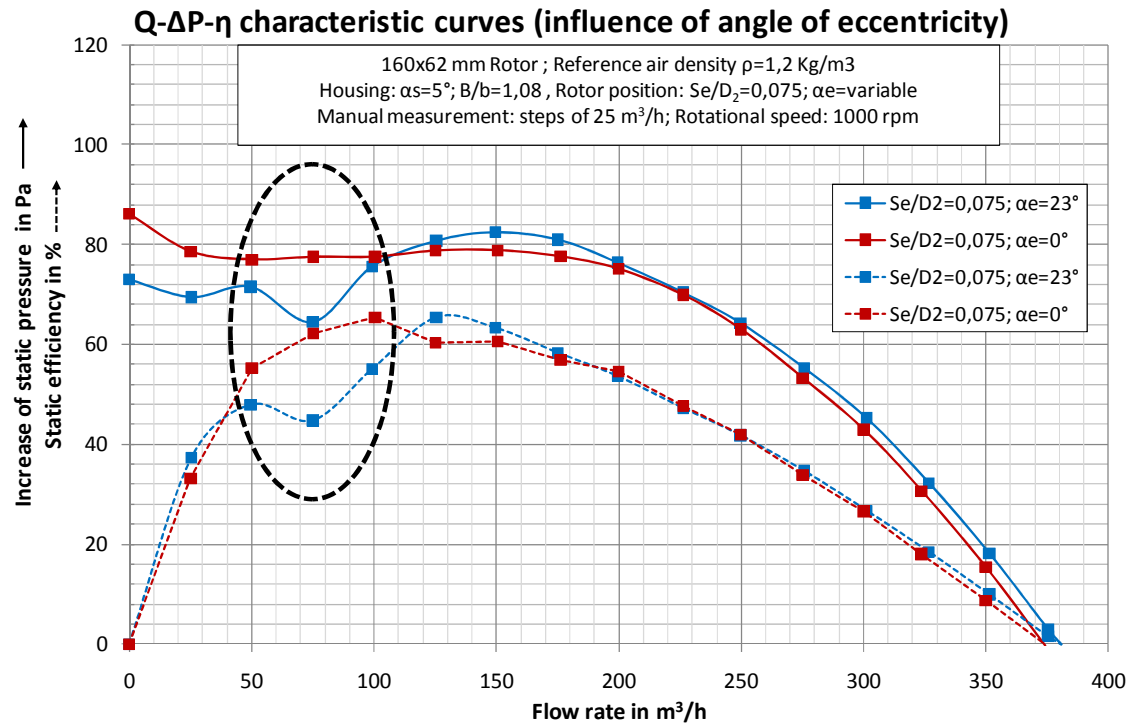


Figure 8.16: Influence of the angle of eccentricity in Sirocco type fan

- 5) *The parameter of angle of eccentricity α_e , can be used to avoid the pressure oscillations that appear for flow rates around $75 \text{ m}^3/\text{h}$ in some configurations of Sirocco type fan.*

According to the measurements, some configurations of sirocco type fan present big oscillations in the pressure rise curves at a flow rate at about $75 \text{ m}^3/\text{h}$, as we can appreciate in Figure 8.16. Particularly the configurations with the relations $Se/D_2 = 0,075$ and $\alpha_e = 23^\circ$.

By setting a smaller angle of eccentricity for this configuration the oscillations can be corrected obtaining smooth curves as we see in the figure above.

The last trend observed during the measurements is explained below.

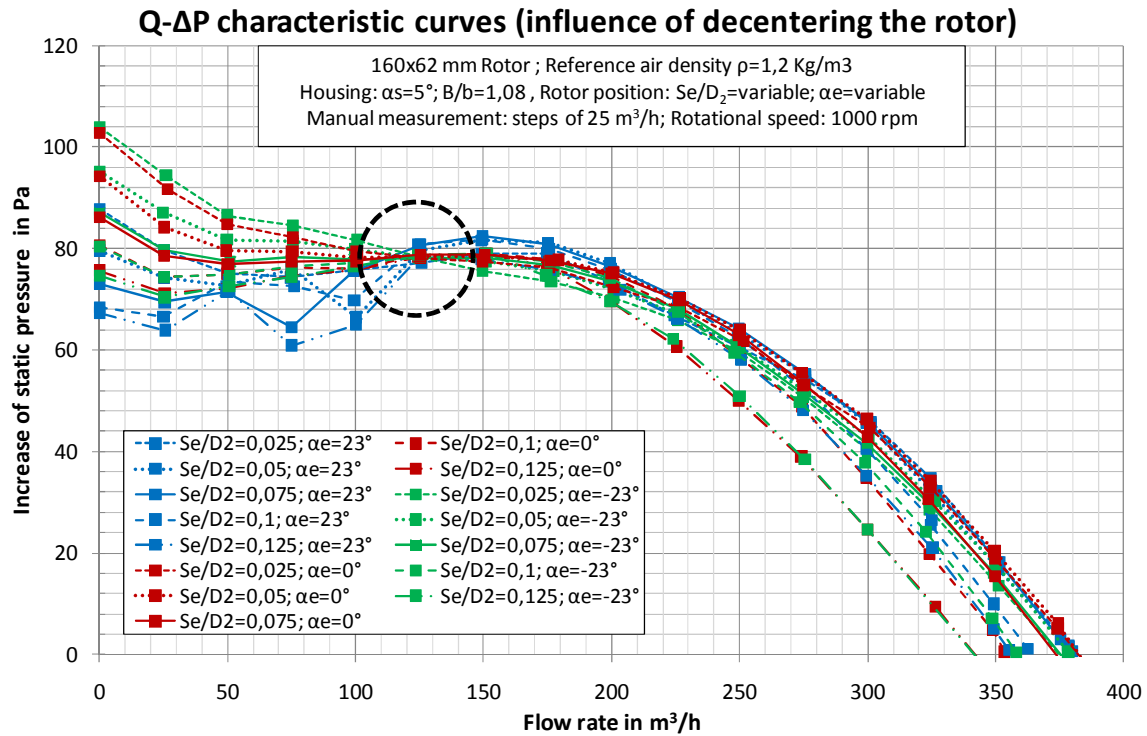


Figure 8.17: Common point in the configuration of Sirocco type fan.

- 6) *All the configurations of the fan concerning the same opening angle and same width of housing have a common point in the pressure rise curves.*

In figure Figure 8.17 we can appreciate that all the pressure rise curves have a point in common. The curves are drawn for opening angle of 5 degree and width of housing of 1,08.

This fact could mean that decentering the rotor have some effects on the performance of the fan related with the pressure rise, as the two ones explained above but is not as such difference as changing a principal parameter of design, for instance the opening angle or the width of housing.

9 Comparison of the results

So far we recorded our measurements by using one high-accuracy chamber test rig with known and accurate uncertainties (see *Chapter 5 Uncertainty of measurement*), we can compare the results obtained in this work with another sources of information.

We have mainly two references for comparing our results. The first one is to compare with the results of CFD simulations provided by a member of the team. The other is to compare with the figures that Roth obtained on his study of sirocco fans (Roth, 1980). We detail each one in the following parts.

9.1 Comparison with CFD's results

Computational fluid dynamics (CFD) is a branch of fluid mechanics that uses numerical methods and algorithms to solve and analyze problems that involve fluid flows. Computers are used to perform the calculations required to simulate the interaction of liquids and gases with surfaces defined by boundary conditions.

Experiments are used, in general, in order to validate CFD calculations and to provide starting values and boundary conditions. In addition, CFD allows obtaining details in the whole flow field: stream lines, shear stress, velocity and pressure distribution, particle tracks, etc.

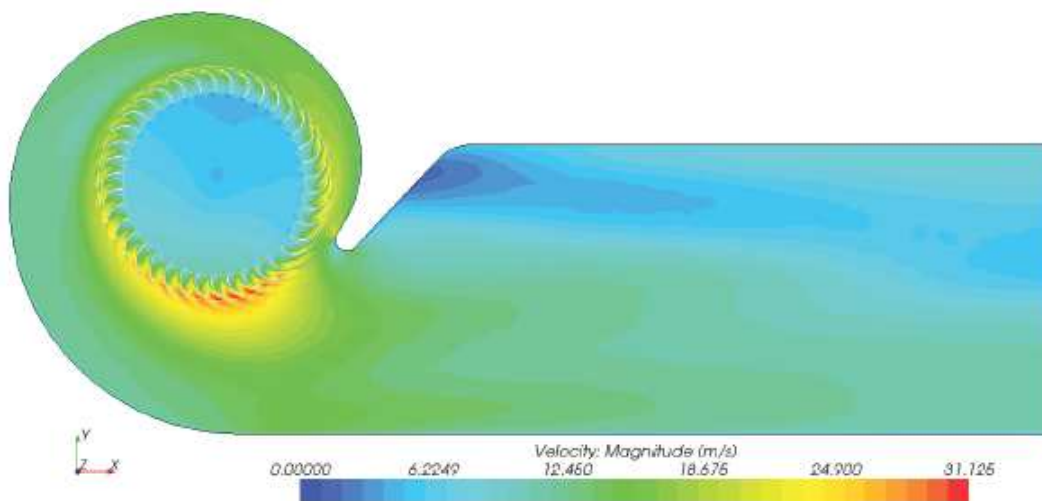


Figure 9.1: Sample illustration of velocity magnitude on Sirocco type fan $\alpha=7^\circ$ (source: Darvish, 2010)

An example of CFD simulation applied on Sirocco type fan is shown in Figure 9.1. We can see the velocity magnitude in m/s over the geometry of the fan.

We can obtain the necessary information from the simulations to establish a comparison. We applied CFD on one configuration of the Sirocco type fan evaluated in the measurement campaign:

$$\alpha_s = 5^\circ ; B/b = 1,08 ; Se/D_2 = 0,075 ; \alpha_e = 23^\circ$$

The results are shown in Figure 9.2 by using graphs. In this graph we present the habitual characteristic curves of pressure rise, torque on shaft and static efficiency vs. flow rate. In red-colored lines we have the curves for the experimental data and in blue-colored lines we have the curves provided by the CFD simulation.

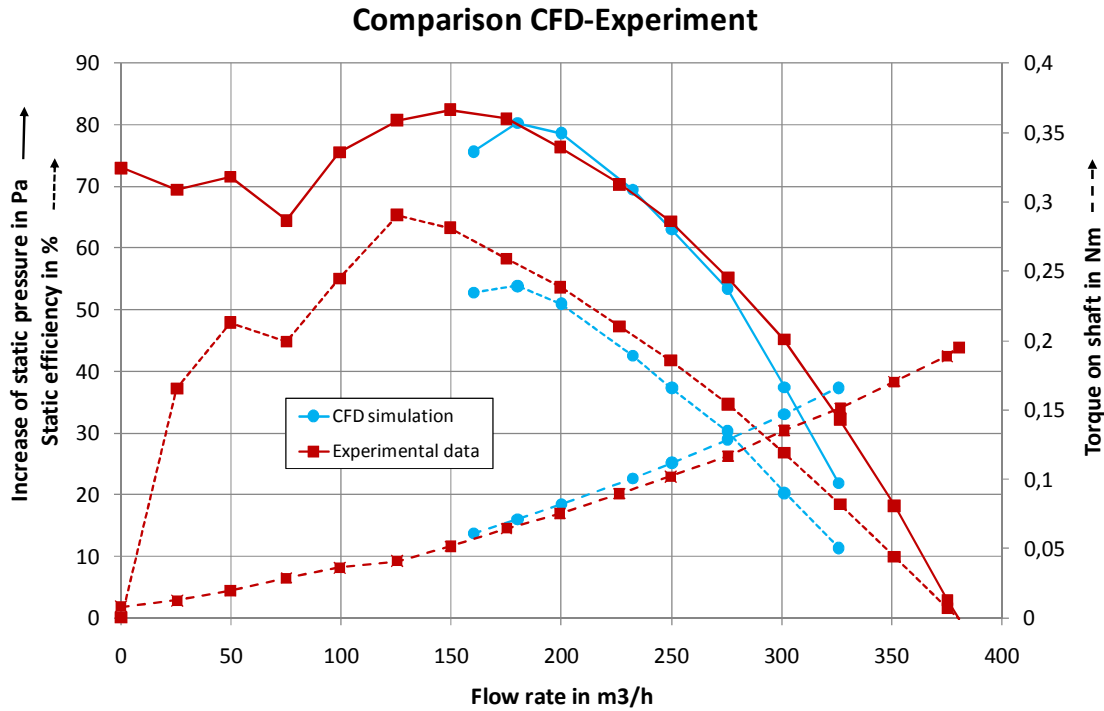


Figure 9.2: Comparison between Experimental data and CFD simulations for 5° housing

The data is qualitatively and quantitatively in good accordance with each other. The deviation amount is less than 5 to 10 %.

The pressure curve matches with high-accuracy in the range of flow rate from 175 to 275 m³/h. For higher values of flow rate, the differences are growing, as well for the initial point. The average deviation considering the pressure rise is 4,0 %.

The torque is the curve with the highest affinity. The deviation starts at the initial point with a deviation of 1,5 % but is slightly increasing with the flow rate to rise 5 %. The experimental torque is always slightly smaller than the simulated. The average deviation considering the full range of the torque is 3,4 %.

The static efficiency has the highest deviation from all three characteristic curves. This can be assumed by considering the differences in pressure rise and torque. In fact, we calculate the static efficiency by using both the pressure rise and torque in the

calculations. When there are deviations in these two values it have repercussions on the finally value of static pressure.

The deviation for the static efficiency in the range of flow rate from 175 to 275 m³/h is contained around 6 %. This one is increasing for further flow rate values and for the first point, where the differences are higher than 15 %. Considering the full range, the average of the deviation of static efficiency is 8,7 %.

For more detailed info about the deviations in each point, refer to Table 9-1.

Table 9-1: Deviation between Experimental and CFD simulations for 5° housing

CFD simulation					Experimental data			Deviations		
Point	Flow Rate	ΔP norm.	Torque	η_{st}	ΔP norm.	Torque	η_{st}	Deviations [%]		
	m ³ /h	Pa	Nm	%	Pa	Nm	%	ΔP norm.	Torque	Efficiency
7	160,06	75,6	0,061	52,8	81,4	0,060	60,8	7,1	1,5	13,2
8	180,04	80,3	0,071	53,8	79,2	0,069	56,9	1,4	2,6	5,4
9	200,05	78,6	0,082	51,0	75,8	0,079	52,6	3,7	2,9	3,2
10	232,28	69,5	0,101	42,5	68,3	0,097	44,9	1,8	3,7	5,4
11	250,16	63,0	0,112	37,3	62,9	0,107	40,2	0,0	4,0	7,2
12	275,35	53,4	0,129	30,3	54,0	0,123	33,0	1,0	4,5	8,2
13	301,29	37,4	0,147	20,3	43,1	0,140	24,9	13,1	4,9	18,5
								Average deviations [%]		
								4,0	3,4	8,7

To finish this comparison between our experimental results and the data obtained from the CFD simulations, we conclude that the concordance between each other is very good, both qualitatively and quantitatively.

9.2 Comparison with Roth's results

Roth obtained, after his extensive study on sirocco fans, a big amount of tables where he reflected the influence of the different variables on the performance of the fan. The most interesting for us in our study are shown in Figure 9.3.

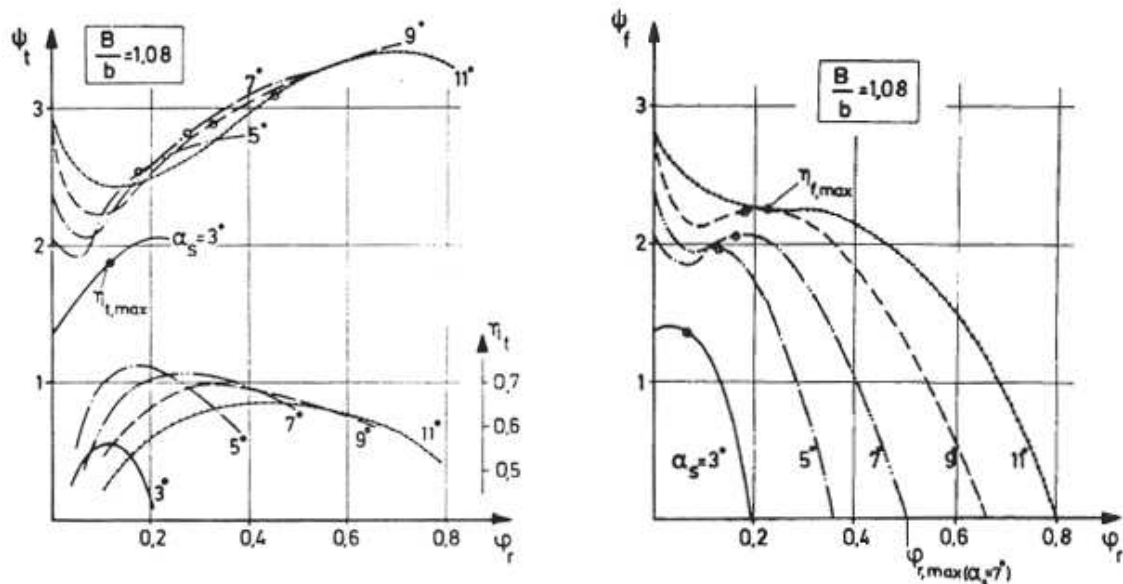


Figure 9.3: Graphs given by Roth on his study

In these two graphs we have the characteristics curves for Sirocco type fan for different opening angles of spiral curve (3° , 5° , 7° , 9° , 11°) all of them according to dimensionless ratio of width of housing $B/b = 1,08$.

The characteristic curve that we could use for the comparison is the one with 5° . Due to the difficulty to compare both results coming from different graphs, we merge them in a single one. To achieve this objective, the points from the curves of Roth have been read carefully by hand and a table has been created. For the details of this table of points please refer to *Appendix F. Data collected from Roth's graphs*.

Afterwards this list of points was inserted in a sheet to merge all the curves in the same graph.

We apply the comparison with this experimental configuration (same as previous comparison with CFD):

$$\alpha_s = 5^\circ ; B/b = 1,08 ; Se/D_2 = 0,075 ; \alpha_e = 23^\circ$$

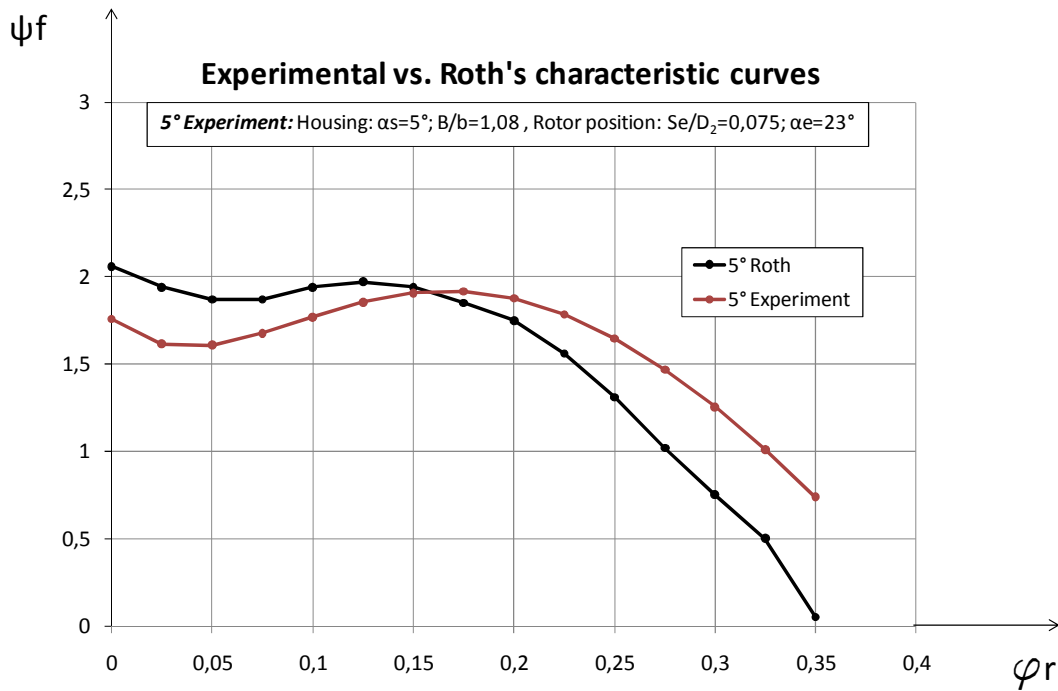


Figure 9.4: Comparison between experimental and Roth's curves for Sirocco type fan

In Figure 9.4, we can appreciate the pressure rise curves together in the same graph. The values to draw the characteristic curves are according ϕ_r (flow rate dimensionless ratio) and ψ_f (static pressure rise dimensionless ratio). We use the same parameters that Roth used to show his curves. For more details about these parameters, please refer to *Chapter 4 Mathematical foundations*.

These two curves are in good qualitative accordance. The experimental curve measured in this work presents the same trend as the one from Roth besides better performance due to the fact that higher flow rate is achieved.

To have a more accurate comparison we have built the next table that contains the deviation between each measured point.

Table 9-2: Deviation between Experimental and Roth's data for 5° housing

Comparison with Roth's data				
5° Roth		5° Experiment		deviation
φ_r	ψ_f	φ_r	ψ_f	%
0,000	2,06	0,000	1,759	17,1
0,025	1,94	0,025	1,616	20,1
0,050	1,87	0,050	1,609	16,2
0,075	1,87	0,075	1,676	11,6
0,100	1,94	0,100	1,769	9,7
0,125	1,97	0,125	1,854	6,3
0,150	1,94	0,150	1,908	1,7
0,175	1,85	0,175	1,917	3,5
0,200	1,75	0,200	1,876	6,7
0,225	1,56	0,225	1,784	12,6
0,250	1,31	0,250	1,646	20,4
0,275	1,02	0,275	1,468	30,5
0,300	0,75	0,300	1,255	40,2
				Avg. dev. [%]
				15,1

As we can appreciate in Table 9-2, the average deviation between our experimental results and the Roth's data is substantial for the initial and the final points defined. The average deviation for these points is about 25 %. The deviation concerning the full range is 15,1 %

From Roth's curve for 5° opening angle, we know exactly the values of two parameters that he used to obtain this curve. The opening angle is $\alpha_s = 5^\circ$ and the width ratio is $B/b = 1,08$. But it is not written on his work all the details of this curve. One of the most important is the value of the length of the outlet. (See Figure 2.1)

On the other hand, the affinity of the experimental curve for the opening angle of 5 degree is in good accordance for the middle points, that is in the range of flow ratio (φ_r) from 0,1 to 0,2. The average deviation for these points is about 6 %.

As a conclusion of this chapter, we can say, after comparing the deviations with CFD simulations and Roth's data, that we have:

- Good agreement of CFD with experiments
- Good agreement of Roth with this the measurements of this work for middle points of the characteristic curve.

10 Conclusions

The scroll housing of sirocco fan is highly responsible to achieve the best efficiencies for this type of fan. Assuming that the design of the rotor is nowadays strongly optimized, the influence on the design of the scroll housing plays a definitive roll to allow the fan unit to raise high-efficiency levels. In such a scroll housing about 75% of the dynamic energy produced by the rotor is converted into static pressure.

After the measurements applied to the new housings designed in this work and according to the obtained results, a maximal static efficiency of 69% has been achieved for a rotational speed of 1000 rpm. That could represent an outstanding increment in comparison with common sirocco fans.

The best efficiencies are achieved by designing the contour of the scroll housing according to an ideal logarithmic spiral curve. The most suitable opening angles to build the curve were $4,5^\circ$ and $5,0^\circ$ according to the results of this investigation. There was a significant drop in the efficiency by using $5,5^\circ$ opening angle as well as for smaller ones. Even by designing the contour of the housing in steps of $0,5^\circ$, that is from 3° to $5,5^\circ$, is not possible to conclude that in 5° there is the summit of the efficiency. It could be desirable to develop more accurate designs to check out where exactly the optimum value is according this parameter of design. For example, designing contours from α $4,5^\circ$ to $5,5^\circ$ in smaller steps.

The opening angle of spiral curve has an evident influence on the maximum flow rate provided by the fan. The bigger opening angle, the higher maximum flow rate achieved. The results of this study show that an increment $\Delta\alpha$ in the opening angle is corresponded with an increment ΔQ for the maximum flow rate.

High efficiency can be only expected if the width of the scroll housing is not much broader than the rotor. For instance, by designing according to dimensionless ratio of width of housing $B/b < 1,1$. When the designing condition could not satisfy this requirement, the best efficiency is achieved positioning the rotor as closer as possible to the inlet of the fan.

Decentering the rotor from the designed position had positive effects on the efficiency of the fan. The most suitable rotor positioning was for $Se/D_2 = 0,075$ and $\alpha_e = -23^\circ$. As mentioned above, could be interesting to perform and more detailed study on this parameter. For example, to check out smaller divisions from $Se/D_2 = 0,05$ to $0,1$.

The minimum gap between rotor and housing has a clear influence on the pressure rise for low flow rates. The smaller the gap, the higher increase of the pressure rise.

Some of the configurations of the fan presented big oscillations on the pressure when operating in the range from 50 to 125 m³/h. It happened mainly when $S_e/D_2 = 0,075$ and $\alpha_e = 23^\circ$. The angle of eccentricity of the rotor (α_e) could be used to avoid the oscillations of pressure.

11 Bibliography

11.1 Written references

- [1] ROTH, H.W.: *Improvement of sirocco fan* (in German: *Optimierung von Trommelläufer Ventilatoren*). Ph.D. Thesis, TH Karlsruhe, 1980.
- [2] LÜCKEMANN, A.: *Laser optical flow measurements of sirocco fans* (in German: *Laseroptische Strömungsmessungen an Trommelläufern*). Master-thesis, HTW Berlin, 2009.
- [3] BLEIER, FRANK P.: *Fan handbook: Selection, application and design*. McGraw-hill, 1997.
- [4] WHITE, FRANK M.: *Fluid mechanics*, 4th edition. McGraw-hill, 1998.
- [5] CAROLUS, T.: *Fans* (in German: *Ventilatoren*). Teubner Verlag, 2003.
- [6] LÓPEZ MARTÍNEZ, J.R.: *Analysis and design of Sirocco fans using different philosophies*. Master-thesis, HTW Berlin, 2009.
- [7] SALINAS CORTÉS, D.: *Measurement of Velocity and Turbulence in the Scroll housing of a Sirocco type fan by means of Laser Doppler Velocimetry*. Master-thesis, HTW Berlin, 2010.
- [8] DARVISH, M.: *Numerical Investigations on the Performance Characteristic of Radial Fans with Froward curved blades by means of CFD*. Master-thesis, HTW Berlin, 2010.
- [9] STUCHLIK, A. FRANK, S. and THAMSEN, P.: *Performance investigations of sirocco fans by means of computational fluid dynamics*. Isromac, 2010.
- [10] FRANK, S. STUCHLIK, A.: *Numerical analysis and design of sirocco fans with ideal and disturbed inflow and outflow*. (in German: *Numerische Berechnung und Auslegung von Trommelläufer-Ventilatoren bei idealer und gestörter Zu- und Abströmung*). Final Report, 2011.

11.2 Electronic references

- [11] www.punker.de
- [12] www.kistler.com
- [13] www.sew-eurodrive.com

- [14] www.tramec.it
- [15] www.rw-america.com
- [16] www.snr-bearings.com
- [17] www.jouning-blower.com

12 Nomenclature

Symbol	Meaning	Unit
D_1	Inner diameter of the rotor	m
D_2	Outer diameter of the rotor	m
b	Width of the rotor	m
R_b	Radius of the blade of the rotor	m
B	Width of the scroll housing	m
R_t	Radius of the tongue	m
S_e	Minimum gap between rotor-housing	m
β_{s1}	Inlet blade angle	°
β_{s2}	Outlet blade angle	°
α_s	Opening angle of spiral curve	°
α_t	Angle for positioning the tongue	°
α_e	Angle of eccentricity of gap rotor-housing	°
Q	Flow rate	m ³ /s
ΔP_{st}	Increase of static pressure	Pa
M	Torque	Nm
φ	Flow rate dimensionless ratio	-
ψ	Pressure rise dimensionless ratio	-
σ	Speed of the fan dimensionless ratio	-
δ	Geometry of the fan dimensionless ratio	-
η_{st}	Static efficiency	%
ρ	Density of the fluid	Kg/m ³
n	Rotational speed	u/s
P_{mec}	Mechanical power	W
P_{hyd}	Hydraulic power	W

Appendices

Appendix A. Tool for obtaining the points of the spiral curve

Points of the logarithmic spiral (tool)

equation: $r(\theta) = r_0 \cdot \text{EXP}(b \cdot \theta)$

r_0 = Initial radius

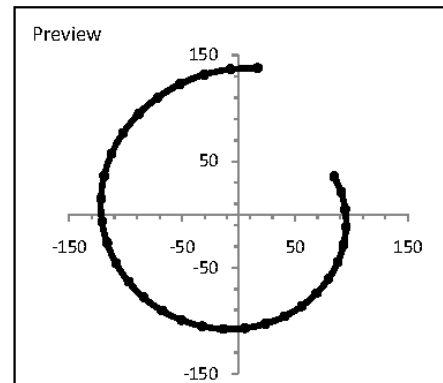
$b = \tan(\alpha)$

r_0 [mm]	92
α [°]	4,5

1) Obtaining spiral points
from an increment of angle

Angle increment [°]	10
Starting angle [°]	23
Direction *	-1

* (-1) = clockwise or 1 = anticlockwise



Final points				
#	Polar coordinates		Cartesian coordinates	
	Angle [°]	Radius [mm]	X [mm]	Y [mm]
0	23	92,0	84,7	35,9
1	13	93,3	90,9	21,0
2	3	94,6	94,4	4,9
3	-7	95,9	95,2	-11,7
4	-17	97,2	92,9	-28,4
5	-27	98,5	87,8	-44,7
6	-37	99,9	79,8	-60,1
7	-47	101,3	69,1	-74,1
8	-57	102,7	55,9	-86,1
9	-67	104,1	40,7	-95,8
10	-77	105,5	23,7	-102,8
11	-87	107,0	5,6	-106,9
12	-97	108,5	-13,2	-107,7
13	-107	110,0	-32,2	-105,2
14	-117	111,5	-50,6	-99,4
15	-127	113,0	-68,0	-90,3
16	-137	114,6	-83,8	-78,2
17	-147	116,2	-97,5	-63,3
18	-157	117,8	-108,4	-46,0
19	-167	119,4	-116,4	-26,9
20	-177	121,1	-120,9	-6,3
21	-187	122,8	-121,8	15,0
22	-197	124,5	-119,0	36,4
23	-207	126,2	-112,4	57,3
24	-217	127,9	-102,2	77,0
25	-227	129,7	-88,5	94,9
26	-237	131,5	-71,6	110,3
27	-247	133,3	-52,1	122,7
28	-257	135,2	-30,4	131,7
29	-267	137,0	-7,2	136,8
30	-277	138,9	16,9	137,9

Figure 12.1: Sheet tool created for obtaining the points of the logarithmic spiral curve

Appendix B. Values for decentering the rotor

Rotor160x62mm Positioning according to α_s , α_e and α_r

Increments x,y [mm] $\alpha_s [^\circ] = 3$						
	Angle direction [°]					
	23		0		-23	
Gap [mm]	Δx	Δy	Δx	Δy	Δx	Δy
4	7.4	3.1	10.1	-4.4	9.5	-8.5
8	3.7	1.6	6.1	-4.6	5.7	-7.2
12	0.0	0.0	2.1	-4.8	2.0	-5.8
16	-3.7	-1.6	-1.9	-5.0	-1.8	-4.4
20	-7.4	-3.1	-5.9	-5.2	-5.5	-3.0
Increments x,y [mm] $\alpha_s [^\circ] = 3,5$						
	Angle direction [°]					
	23		0		-23	
Gap [mm]	Δx	Δy	Δx	Δy	Δx	Δy
4	7.4	3.1	10.4	-5.1	9.8	-9.7
8	3.7	1.6	6.4	-5.4	6.0	-8.4
12	0.0	0.0	2.4	-5.6	2.2	-7.0
16	-3.7	-1.6	-1.6	-5.9	-1.5	-5.7
20	-7.4	-3.1	-5.6	-6.1	-5.3	-4.4
Increments x,y [mm] $\alpha_s [^\circ] = 4$						
	Angle direction [°]					
	23		0		-23	
Gap [mm]	Δx	Δy	Δx	Δy	Δx	Δy
4	7.4	3.1	10.8	-5.9	10.2	-10.7
8	3.7	1.6	6.8	-6.1	6.4	-9.4
12	0.0	0.0	2.8	-6.4	2.6	-8.1
16	-3.7	-1.6	-1.2	-6.7	-1.2	-6.8
20	-7.4	-3.1	-5.2	-7.0	-5.0	-5.5
Increments x,y [mm] $\alpha_s [^\circ] = 4,5$						
	Angle direction [°]					
	23		0		-23	
Gap [mm]	Δx	Δy	Δx	Δy	Δx	Δy
4	7.4	3.1	11.2	-6.6	10.6	-11.6
8	3.7	1.6	7.2	-6.9	6.8	-10.4
12	0.0	0.0	3.2	-7.2	3.0	-9.1
16	-3.7	-1.6	-0.8	-7.5	-0.8	-7.8
20	-7.4	-3.1	-4.8	-7.8	-4.6	-6.6
Increments x,y [mm] $\alpha_s [^\circ] = 5$						
	Angle direction [°]					
	23		0		-23	
Gap [mm]	Δx	Δy	Δx	Δy	Δx	Δy
4	7.4	3.1	11.6	-7.3	11.0	-12.6
8	3.7	1.6	7.6	-7.7	7.2	-11.4
12	0.0	0.0	3.6	-8.0	3.4	-10.1
16	-3.7	-1.6	-0.3	-8.4	-0.5	-8.9
20	-7.4	-3.1	-4.3	-8.7	-4.3	-7.7
Increments x,y [mm] $\alpha_s [^\circ] = 5,5$						
	Angle direction [°]					
	23		0		-23	
Gap [mm]	Δx	Δy	Δx	Δy	Δx	Δy
4	7.4	3.1	12.0	-8.1	11.4	-13.6
8	3.7	1.6	8.0	-8.4	7.6	-12.4
12	0.0	0.0	4.0	-8.8	3.8	-11.2
16	-3.7	-1.6	0.1	-9.2	-0.1	-10.0
20	-7.4	-3.1	-3.9	-9.6	-3.9	-8.8

Figure 12.2: Displacements in X-Y axes from the origin position for all the configurations

Rotor160x62mm Positioning according to α_s , α_e and α_c

Increments ready to insert in Rsterm $\alpha_s [^\circ] = 3$						
	Angle direction [°]					
	23		0		-23	
Gap [mm]	Δx	Δy	Δx	Δy	Δx	Δy
4	592	496	808	-704	760	-1360
8	296	256	488	-736	456	-1152
12	0	0	168	-768	160	-928
16	-296	-256	-152	-800	-144	-704
20	-592	-496	-472	-832	-440	-480
Increments ready to insert in Rsterm $\alpha_s [^\circ] = 3,5$						
	Angle direction [°]					
	23		0		-23	
Gap [mm]	Δx	Δy	Δx	Δy	Δx	Δy
4	592	496	832	-918	784	-1552
8	296	256	512	-972	480	-1344
12	0	0	192	-1008	176	-1120
16	-296	-256	-128	-1062	-120	-912
20	-592	-496	-448	-1098	-424	-704
Increments ready to insert in Rsterm $\alpha_s [^\circ] = 4$						
	Angle direction [°]					
	23		0		-23	
Gap [mm]	Δx	Δy	Δx	Δy	Δx	Δy
4	592	496	864	-944	816	-1712
8	296	256	544	-976	512	-1504
12	0	0	224	-1024	207	-1296
16	-296	-256	-96	-1072	-96	-1088
20	-592	-496	-416	-1120	-400	-880
Increments ready to insert in Rsterm $\alpha_s [^\circ] = 4,5$						
	Angle direction [°]					
	23		0		-23	
Gap [mm]	Δx	Δy	Δx	Δy	Δx	Δy
4	592	496	896	-1056	848	-1856
8	296	256	576	-1104	544	-1664
12	0	0	256	-1152	240	-1456
16	-296	-256	-64	-1200	-66	-1248
20	-592	-496	-384	-1248	-368	-1056
Increments ready to insert in Rsterm $\alpha_s [^\circ] = 5$						
	Angle direction [°]					
	23		0		-23	
Gap [mm]	Δx	Δy	Δx	Δy	Δx	Δy
4	592	496	928	-1168	880	-2016
8	296	256	608	-1232	576	-1824
12	0	0	288	-1280	272	-1616
16	-296	-256	-24	-1344	-36	-1424
20	-592	-496	-344	-1392	-344	-1232
Increments ready to insert in Rsterm $\alpha_s [^\circ] = 5,5$						
	Angle direction [°]					
	23		0		-23	
Gap [mm]	Δx	Δy	Δx	Δy	Δx	Δy
4	592	496	960	-1296	912	-2176
8	296	256	640	-1344	608	-1984
12	0	0	320	-1408	304	-1792
16	-296	-256	8	-1472	-8	-1600
20	-592	-496	-312	-1536	-312	-1408

Figure 12.3: Values of the displacements in X-Y axes translated into code for RSTerm software

Appendix C. Data provided by the chamber test rig

Datum / Uhrzeit:

Mittwoch, 26. Januar 2011

15:33

Prüfstand zur Messung von Ventilator- und Widerstandskennliniensen

www.ilkdresden.de

Software:

ILK-Volmess Version HTWB 4.07 / September 2010

Datum der letzten Kalibrierung:

30.04.10

Einstellungen:

manuelle Messung

Gewählter Messbereich:

Messbereich 1 (12..120 m³/h) / Kennlinienmessung /saugende Messung

Messung Nr.:

12

Bezugsdrehzahl für V1_K:

2940

Bezugsdichte für dpta_K:

1,2 kg/m3

Unloaded torque

0,011 Nm

Anmeldename:

TFDAdmin

Bearbeiter:

Te

Bezeichnung Prüfling:

160x62 - January camp.

Versuchsnummer:

110126_67_5_160x62_0_12_1000

Gewähltes Messsystem:

Kennlinienmessung

Scroll housing: 5° opening angle, 67mm width. Rotor position: at 0° angle direction, with 12mm gap. Manual measurement: steps of 25m³/h.

Unloaded torque: 0,011 Nm. File: 110126_Unloadedtorque.dat Rotational velocity: 1000rpm.

Negativer Volumenstrom bedeutet, dass das Seedingventil geöffnet war.

Die Gültigkeit in der Spalte nach dem Volumenstrom gibt an, ob bei der Volumenstrommessungen die Bedingungen der DIN EN ISO 5167 erfüllt wurden.

Anzahl der Messwerte

16

Messzeit	s	Volumenstro	m³/h	Gültigkeit	Pa	ISO 5167	kg/m³	Temp Kam.	°C	phi Kam.	%	Massestrom	kg/h	p_Baro	Pa	Wassergehalt	g/kg	Raumtemper	°C	Drehzahl	1/min	Drehmoment	Nm
6,5	0	0,5	84,95184	1,18384	21,70469	24,81995	0	100515,159	4,03691	20,93577	1000	0,02368											
42,5	25,0956	1	77,55903	1,18393	21,69893	24,85741	29,71135	100513,683	4,04137	20,96556	1000	0,02679											
71,5	50,08459	1	75,98218	1,18398	21,69444	24,8592	59,29937	100515,444	4,04041	20,96306	1000	0,02953											
102,5	75,16968	1	76,46747	1,18399	21,69668	24,82246	89,00043	100517,159	4,03491	20,94153	1000	0,03584											
131,5	100,37712	1	76,50213	1,18398	21,69861	24,8346	118,84438	100516,73	4,03739	20,95213	1000	0,04256											
251,5	125,30301	1	77,71639	1,18398	21,70437	24,86479	148,35647	100520,538	4,04366	20,97875	1000	0,05442											
285,5	150,44573	1	77,77706	1,18397	21,70598	24,81777	178,12384	100520,063	4,03638	20,94737	1000	0,06292											
313,5	176,18417	1	76,52991	1,18397	21,71046	24,84291	208,59703	100520,443	4,04155	20,96873	1000	0,07464											
344,5	199,83953	1	74,08911	1,18404	21,7127	24,85812	236,61706	100524,348	4,04434	20,97541	1000	0,08386											
376,5	226,25173	1	68,94792	1,18403	21,71815	24,87764	267,88803	100520,586	4,04884	20,98359	1000	0,09906											
409,5	249,79686	1	62,18117	1,1841	21,72584	24,85514	295,78554	100522,919	4,0467	20,97616	1000	0,11074											
447,5	275,10197	1	52,56916	1,18422	21,73225	24,86049	325,77991	100525,014	4,0487	20,98375	1000	0,12566											
479,5	300,01065	1	42,35289	1,18436	21,73385	24,8237	355,3209	100527,347	4,04256	20,96014	1000	0,13963											
512,5	323,54706	1	30,28524	1,18444	21,74475	24,82006	383,22142	100525,633	4,04426	20,95622	1000	0,15697											
550,5	349,89871	1	15,15118	1,18459	21,75628	24,81464	414,48565	100527,204	4,04557	20,95555	1000	0,17562											

Figure 12.4: Example of data table provided by the chamber test rig for a measurement on the scroll housing of 5°

Appendix D. Study of maximal static efficiencies

Table 12-1: Summary of the best static efficiencies found by different criteria

0. Max static efficiency found

η_{\max}		Configuration			
α_s	η_{\max}	B/b	Se/D2	α_e	data file
°	%	-	-	°	
5	69,1	1,08	0,075	-23	110126_67_5_160x62_-23_12_1000

1. Max static efficiencies by opening angle families

η_{\max} by families of α_s		Configuration			
α_s	η_{\max}	B/b	Se/D2	α_e	data file
°	%	-	-	°	
3	56,5	1,08	0,025	0	110125_67_3_160x62_0_4_1000
3,5	60,0	1,08	0,075	23	110125_67_35_160x62_23_12_1000
4	65,0	1,08	0,075	23	110125_67_4_160x62_23_12_1000
4,5	65,7	1,08	0,075	23	110125_67_45_160x62_23_12_1000
5	69,1	1,08	0,075	-23	110126_67_5_160x62_-23_12_1000
5,5	60,2	1,08	0,05	23	110127_67_55_160x62_23_8_1000

2. Max static efficiencies by width families

η_{\max} by families of B/b		Configuration			
B/b	η_{\max}	α_s	Se/D2	α_e	data file
-	%	°	-	°	
1,08	69,1	5	0,075	-23	110126_67_5_160x62_-23_12_1000
1,4	60,3	4,5	0,075	23	110127_87_45_160x62_23_12_1000

3. Max static efficiencies by gap rotor-housing families

η_{\max} by families of Se/D2		Configuration			
Se/D2	η_{\max}	α_s	B/b	α_e	data file
-	%	°	-	°	
0,025	62,1	4,5	1,08	0	110125_67_45_160x62_0_4_1000
0,05	63,3	4,5	1,08	23	110125_67_45_160x62_23_8_1000
0,075	69,1	5	1,08	-23	110126_67_5_160x62_-23_12_1000
0,1	66,6	5	1,08	-23	110126_67_5_160x62_-23_16_1000
0,125	63,0	5	1,08	23	110126_67_5_160x62_23_20_1000

4. Max static efficiencies by angle of eccentricity families

η_{\max} by families of α_e		Configuration			
α_e	η_{\max}	α_s	B/b	Se/D2	data file
°	%	°	-	-	
23	65,7	4,5	1,08	0,075	110125_67_45_160x62_23_12_1000
0	65,4	5	1,08	0,075	110126_67_5_160x62_0_12_1000
-23	69,1	5	1,08	0,075	110126_67_5_160x62_-23_12_1000

5. Max static efficiencies by each point of flow rate

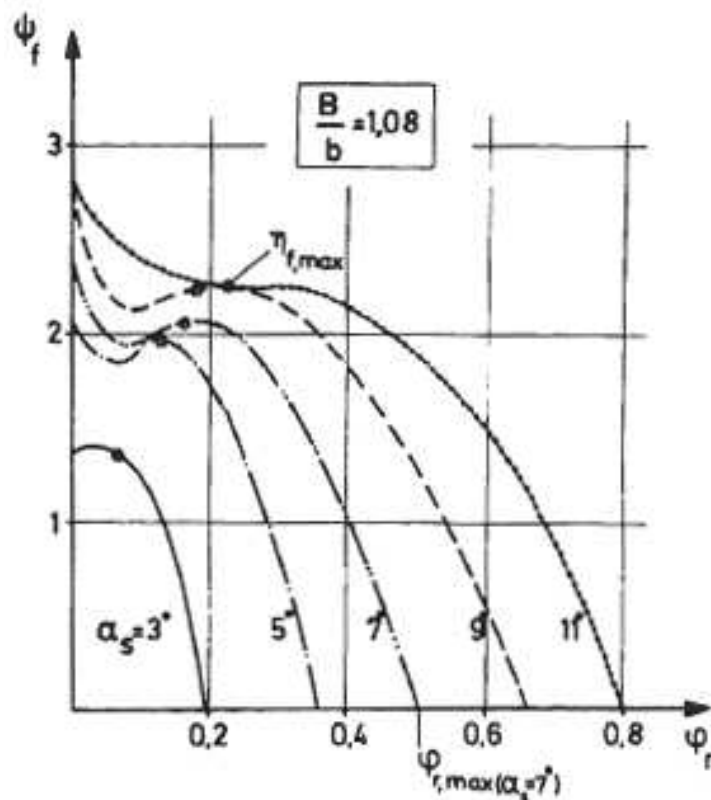
η_{\max} by each point of flow rate		Configuration			
Flow rate	Max efficiency	B/b	Se/D2	α_e	data file
m3/h	%	-	-	°	
0	0,0				-
25	48,7	1,08	0,125	-23	110126_67_5_160x62_-23_20_1000
50	62,6	1,08	0,125	23	110126_67_5_160x62_23_20_1000
75	69,1	1,08	0,075	-23	110126_67_5_160x62_-23_12_1000
100	65,4	1,08	0,075	0	110126_67_5_160x62_0_12_1000
125	65,4	1,08	0,075	23	110125_67_45_160x62_23_12_1000
150	63,3	1,08	0,075	23	110126_67_5_160x62_23_12_1000
175	59,3	1,4	0,075	23	110127_87_45_160x62_23_12_1000
200	59,8	1,4	0,075	23	110128_87_55_160x62_23_12_1000
225	57,3	1,4	0,075	23	110128_87_55_160x62_23_12_1000
250	55,3	1,4	0,075	23	110128_87_55_160x62_23_12_1000
275	52,7	1,4	0,075	23	110128_87_55_160x62_23_12_1000
300	46,0	1,4	0,075	23	110128_87_55_160x62_23_12_1000
325	40,6	1,4	0,075	23	110128_87_55_160x62_23_12_1000
350	34,9	1,4	0,075	23	110128_87_55_160x62_23_12_1000
375	20,3	1,4	0,05	0	110128_87_5_160x62_0_8_1000
400	14,9	1,4	0,05	0	110128_87_5_160x62_0_8_1000
425	6,9	1,4	0,05	0	110128_87_5_160x62_0_8_1000
450	0,7	1,4	0,05	0	110128_87_5_160x62_0_8_1000

Appendix E. Details of the configuration with highest static efficiency

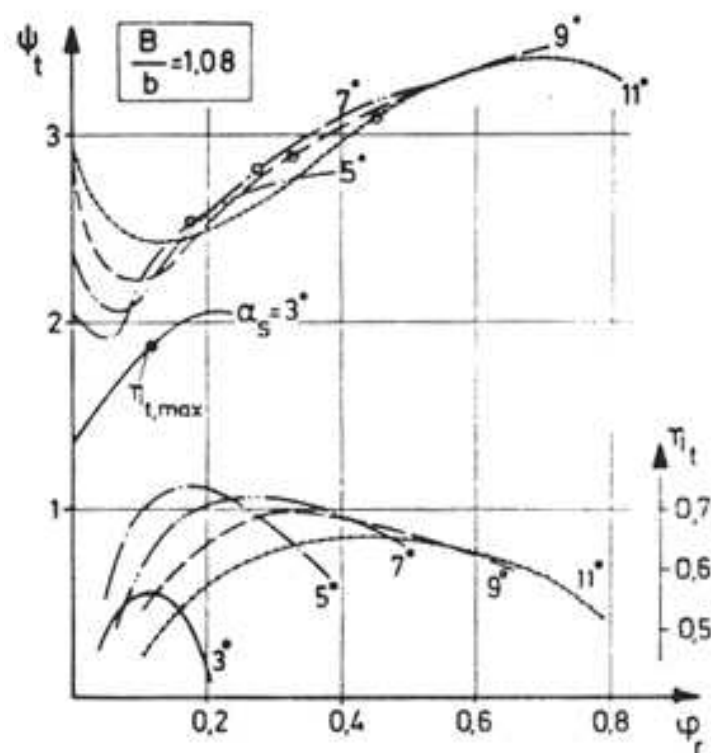
Highest static efficiency configuration:													$\alpha_s=5^\circ$ $B/b=1,08$ $Se/D2=0,075$ $\alpha_e=-23^\circ$			
Point	V	ΔP norm.	n	Torque	P mec	ΔP_t norm.	φ_r	ψ_t	ψ_f	η_t	η_f	σ	δ			
	m3/h	Pa	U/min	Nm	W	Pa	-	-	-	-	-	-	-			
1	0,0	87,0	1000	0,012	1,268	87,0	0,000	2,07	2,07	0,000	0,000	0,000	-			
2	25,2	79,7	1000	0,013	1,412	79,9	0,027	1,90	1,89	0,396	0,395	0,102	7,16			
3	51,1	77,4	1000	0,019	2,000	78,1	0,054	1,85	1,84	0,554	0,549	0,148	5,00			
4	75,3	78,3	1000	0,023	2,371	79,8	0,080	1,89	1,86	0,704	0,691	0,178	4,13			
5	99,6	77,8	1000	0,032	3,322	80,3	0,106	1,91	1,85	0,669	0,648	0,205	3,58			
6	125,0	78,1	1000	0,044	4,613	82,2	0,133	1,95	1,86	0,618	0,588	0,229	3,20			
7	151,5	78,2	1000	0,054	5,644	84,1	0,161	2,00	1,86	0,627	0,583	0,252	2,91			
8	175,9	76,7	1000	0,064	6,687	84,6	0,187	2,01	1,82	0,618	0,560	0,276	2,69			
9	199,6	73,4	1000	0,072	7,574	83,7	0,212	1,99	1,74	0,613	0,538	0,304	2,49			
10	226,3	68,0	1000	0,089	9,369	81,2	0,241	1,93	1,61	0,545	0,456	0,343	2,30			
11	248,4	61,1	1000	0,099	10,325	77,0	0,264	1,83	1,45	0,514	0,408	0,389	2,13			
12	274,7	51,4	1000	0,115	12,039	70,9	0,292	1,68	1,22	0,449	0,326	0,465	1,94			
13	299,8	41,5	1000	0,130	13,562	64,7	0,319	1,54	0,99	0,397	0,255	0,570	1,76			
14	324,2	29,8	1000	0,147	15,371	56,9	0,345	1,35	0,71	0,333	0,174	0,762	1,56			
15	349,3	16,0	999,3	0,164	17,169	47,5	0,372	1,13	0,38	0,268	0,091	1,257	1,29			
16	377,2	-1,2	999,4	0,186	19,489	35,5	0,402	0,84	-0,03	0,191	-0,006	-	-			

Figure 12.5: Performance details for the configuration with highest static efficiency

Appendix F. Data collected from Roth's graphs



Roth's experiment $\alpha_s = 3^\circ$		
φ_r	ψ_f	η_t
0,000	1,37	-
0,025	1,40	0,43
0,050	1,37	0,49
0,075	1,32	0,53
0,100	1,23	0,56
0,125	1,10	0,56
0,150	0,80	0,54
0,175	0,45	0,50
0,200	0,00	0,43



Roth's experiment $\alpha_s = 5^\circ$		
φ_r	ψ_f	η_t
0,000	2,06	-
0,025	1,94	-
0,050	1,87	0,55
0,075	1,87	0,63
0,100	1,94	0,68
0,125	1,97	0,71
0,150	1,94	0,73
0,175	1,85	0,74
0,200	1,75	0,73
0,225	1,56	0,72
0,250	1,31	0,71
0,275	1,02	0,69
0,300	0,75	0,67
0,325	0,50	0,64
0,350	0,05	0,62
0,375	0	0,59

Figure 12.6: Tables created after reading manually the points of Roth's curves

Appendix G. Specifications of the components

Torque Sensor – Mini-Smart Torque Sensor, Type 4502A...



Technical Data

Mechanical Basic Data

Measuring range	N·m	±0,5 ... 1 000
Rated torque M_{nom}	N·m	0,5 ... 1 000
Overload capacity		
Service torque		1,5 x M_{nom}
Limiting torque		1,5 x M_{nom}
Rotational angle/- speed measurem. (Version QA, HA, RA, RAU)	pulses/ revolut.	2x360, 90° displaced, TTL
Nominal speed		
≤18 N·m	1/min	12 000
20 ... 160 N·m	1/min	9 000
250 ... 1 000 N·m	1/min	7 000
Version QA, HA, RA, RAU (rotational angle measurement)	1/min	7 000
Housing material		Anodized aluminum
Protection class		IP40

General Electrical Specifications

Cut-off frequency -3 dB	kHz	3
Accuracy class		0,2

Linearity error including hysteresis	% FSO	<±0,2
Output signal	VDC	±0 ... 5
at rated torque (rated value)	VDC	5
Load resistance	kΩ	>10
Temp. influence on the zero point	% FSO/°C	<±0,015
Temp. influence on the nominal value	% FSO/°C	<±0,015
Control signal	%	100 ±0,2
100 % control input	VDC	"On" 5 ... 30 "Off" 0 ... 2
Operating temperature range (Rated temperature range)	°C	10 ... 60
Service temperature range	°C	0 ... 70
Storage temperaure range	°C	-25 ... 80
Electrical connection		12 pin built-in connector
Supply voltage	VDC	11 ... 26
Power consuption	W	<1



Figure 12.7: Technical data of the Torque sensor by KISTLER

Torque Sensor – Mini-Smart Torque Sensor, Type 4502A...



Dimensions

Torque sensor with shaft end and integral mounting base,
Version RAU

- This version can be used as functional check on tilt procedure or rotation monitoring
- Variable mounting positions, applications for left and right hand torque readings as well as the static and dynamic conditions are possible
- All RAU type sensors have an integrated rotational angle measurement

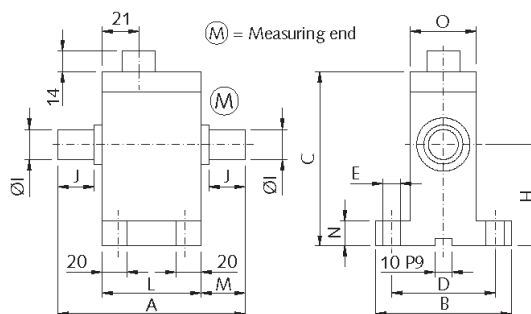


Table Version RAU (with rotational angle measurement)

Type	Measuring range N-m	A	B	C	D	E	H	øI g6	J	L	M	N	O	Size	Axial force N max.	Radial force N max.
04502A1RAU	1	90	58	83	45	7	45	10	15	58	16	12	28	1	20	15
4502A2RAU	2	90	58	83	45	7	45	10	15	58	16	12	28	1	50	25
4502A5RAU	5	90	58	83	45	7	45	10	15	58	16	12	28	1	100	50
4502A10RAU	10	90	58	83	45	7	45	10	15	58	16	12	28	1	150	50
4502A20RAU	20	106	85	102	60	9	63	17	22	59	23	15	38	2	150	150
4502A50RAU	50	106	85	102	60	9	63	17	22	59	23	15	38	2	200	150

Electrical Connections

Pin Allocation of the 12 Pin Built-in Connector

Function	PIN	Description	
Supply	F	+U _s	11 ... 26 VDC, power consumption <1 W
	E	GND	Ground relating to U _s and angle of rotation pulses
Shield	M	In sensor connected to housing	
Torque output	C	U _a	±5 VDC at M _{nom} at >2 kΩ 5 VDC at control signal activation R _{iC} = 10 Ω, output short circuit proof relating to AGND
	D	AGND	Ground relating to U _a
Angle of rotation sensor Supply	H	+U _s	5 VDC
Angle of rotation pulses	B	Track A	Open collector output Internal 1 kΩ resistance to 5 VDC (pull up), TTL-level
	G	Track B	As Track A, 90° displaced
100 % control input	K	Control	Off: 0 ... 2 VDC On: 5 ... 30 VDC
	A	KGND	Ground relating to control input
	J	Not connected	

Figure 12.8: Dimensions and electrical connections for the torque sensor by KISTLER



Radabmessung dimension of wheel dimension de roue								Standardnabe standard hub moyeu standard			Betriebsdaten inklusiv Nabe operating data inclusive of hub valeurs d'opération moyeu inclus			
Type	ØD ₂	B	ØD ₀	ØD ₁	Ød ₂	z	x _{ca}	Type	Ød _{max}	kg	max. n _{min} ⁻¹	J · 10 ⁻³ kg m ²	kg	
140 ●	140	42 52 62	115	109	16	33	2	4 □	12,7	0,029	5.450 4.850 4.300	0,725 0,809 0,893	0,24 0,26 0,28	
140 ●	140	42 52 62	115	109	25	33	2	5c □	16	0,085	5.450 4.850 4.300	0,734 0,818 0,902	0,29 0,31 0,34	
146 ●	146	42 52 62 74	123	115	25	33	2	5c □	16	0,085	5.880 5.230 4.640 4.120	0,821 0,913 1,006 1,116	0,30 0,32 0,34 0,37	
160 ●	160	42 52 62 74 82	137	129	25	36	2	5c □	16	0,085	5.965 5.370 4.770 3.760 3.340	1,122 1,245 1,369 1,515 1,613	0,33 0,36 0,38 0,41 0,42	
180 ●	180	52 62 74 82 92	157	149	25	40	2	5e □	16	0,11	5.310 4.780 4.250 3.345 2.970	1,854 2,030 2,241 2,381 2,557	0,43 0,46 0,49 0,51 0,53	
200 ●	200	62 74 82 92 102	171	161	30 25	38	2	21e ■ 20 5e □ 16	0,31 0,11		4.780 4.300 3.820 3.390 3.010	3,755 4,134 4,387 4,703 5,019	0,83 0,87 0,90 0,94 0,98	
215 ●	215	62 74 82 92 102	187	177	30 25	42	2	21e ■ 20 5e □ 16	0,31 0,11		4.440 4.000 3.550 3.150 2.800	4,995 5,487 5,815 6,225 6,635	0,91 0,96 0,99 1,03 1,07	
225 ●	225	74 82 92 102 114	196	187	30 25	42	2	21e ■ 20 5e □ 16	0,31 0,11		4.250 3.820 3.400 3.020 2.675	6,262 6,624 7,077 7,528 8,070	0,99 1,02 1,06 1,10 1,15	
240 ●	240	74 82 92	206	193	25	38	2	5e □	16	0,11	3.980 3.580 3.180	10,74 11,49 12,42	1,10 1,17 1,24	
240 ●	240	74 82 92 102 114	206	193	42 30	38	2	20a ■ 30 21e ■ 20	0,58 0,31		3.980 3.580 3.180 2.825 2.505	11,03 11,77 12,70 13,64 14,75	1,57 1,63 1,71 1,78 1,87	
250 ●	250	82 92 102	215	203	25	38	2	5e □	16	0,11	3.820 3.440 3.055	12,85 13,87 14,88	1,20 1,28 1,36	
250 ●	250	82 92 102 114 127	215	203	42 30	38	2	20a ■ 30 21e ■ 20	0,58 0,31		3.820 3.440 3.055 2.715 2.410	13,14 14,15 15,17 16,39 17,71	1,67 1,74 1,82 1,91 2,01	
280 ●	280	92 102 114 127 142	244	233	42 30	42	2,5	20a ■ 30 21e ■ 20	0,58 0,31		3.410 3.070 2.730 2.420 2.150	20,42 21,85 23,57 25,44 27,59	1,93 2,01 2,11 2,22 2,35	

● Schlüsselöffnung

● Socket screw key hole

● Trou de la serrure

Nabenausführung siehe Blatt 4.1.1.01-02

Material: verzinktes Stahlblech

□ Standardausführung ohne Keilnut

■ mit Keilnut

design of hub see page 4.1.1.01-02

material: galvanized sheet steel

□ standard type without keyway

■ with keyway

modèle de moyeu, voir fiche 4.1.1.01-02

matière: tôle d'acier galvanisée

□ type standard sans rainure de clavette

■ avec rainure de clavette

Figure 12.9: Specifications of the rotor by Punker

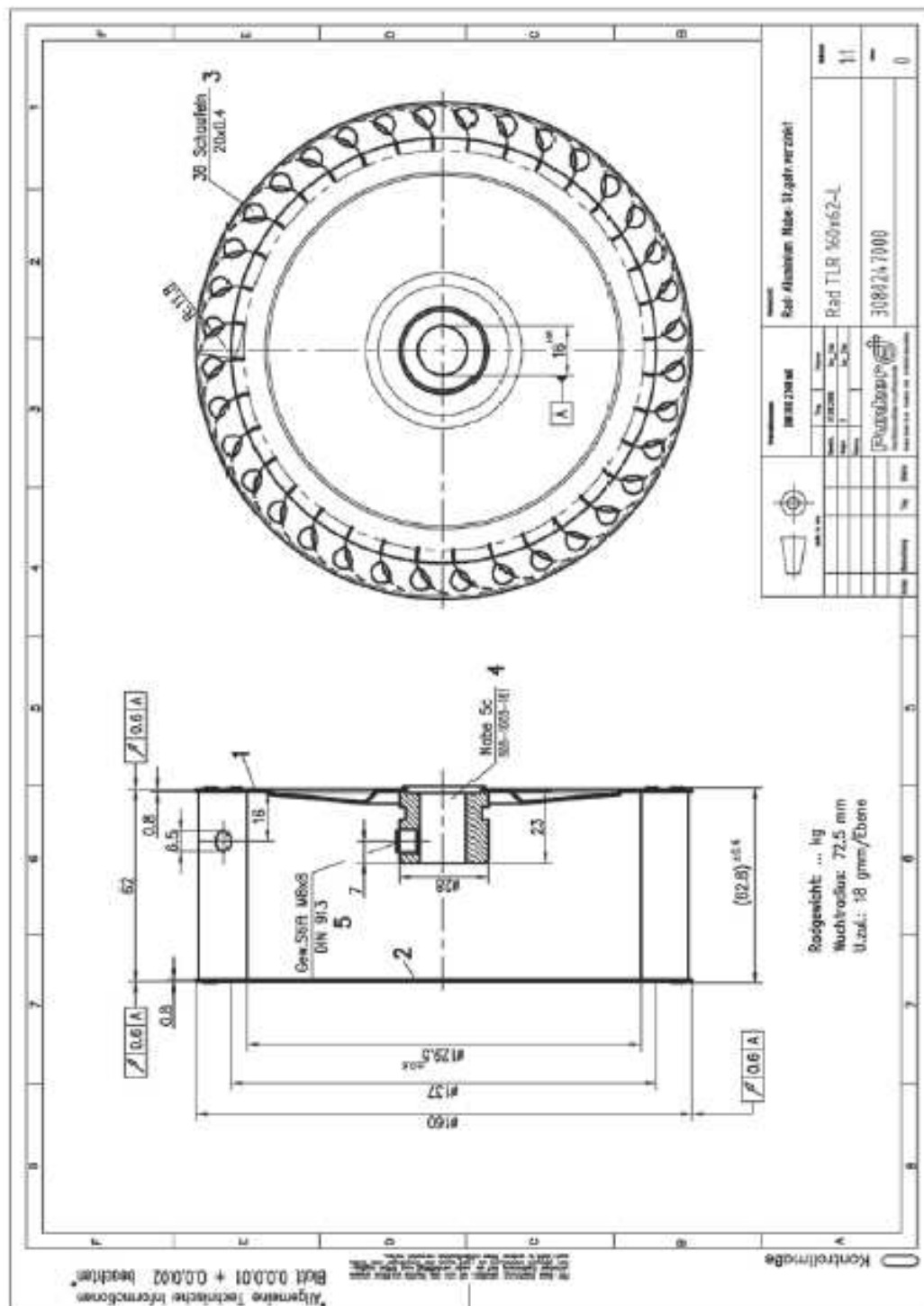


Figure 12.10: Dimensions of the rotor by Punker

RINVII ANGOLARI
RIGHT ANGLE GEARS
WINKELGETRIEBE

FATTORE DI SERVIZIO FS

SERVICE FACTOR FS

BETRIEBSFACTOR FS

A	0.7	0.9	1	1.3
B	0.9	1	1.3	1.8

h/d
ore di funzionamento giornaliere
hours of operation per day
Tägliche Betriebszeit in Std.

A
carico uniforme
uniform load
Gleichmäßiger Betrieb

B
carico con urti modesti
load with moderate shocks
Mittelstarke Stöße beim Betrieb

C
carico con urti
load with shock
Starke Stöße beim Betrieb

N.B.
Verificare che la temperatura di esercizio non superi i valori da -20°C a +80°C.

N.B.
Check that the operating temperature is not outside the range -20°C / +80°C.

N.B.
Die Betriebstemperatur sollte nicht außerhalb des folgenden Bereichs liegen: -20°C / +80 °C.

Nel caso del rapporto 2:1 non usare il rinvio in moltiplicazione (cioè entrando dall'albero B o C) oltre 700 giri al minuto.

If you require a 2:1 ratio, do not use a speed multiplier (i.e. with inputs on shaft B or C) which operates at more than 700 rpm.

Falls die Getriebe als Übersetzungsgetriebe (ins Schnelle) verwendet werden sollen, ist darauf zu achten, dass die Antriebsdrehzahl an der welle B oder C 700 Upm nicht überschreiten darf.

PRESTAZIONI

PERFORMANCES

LEISTUNG

	T2 [Nm]	2.0	—	7.7	—	20.2	—	33	—	5.7	—
	P1 [kW]	0.63	—	2.5	—	6.5	—	11	—	1.7	—
	T2 [Nm]	2.4	0.9	8.6	4.2	25.2	17.9	42	29.5	8.4	6.7
	P1 [kW]	0.37	0.14	1.3	0.65	3.9	2.8	6.5	4.5	1.2	0.94
	T2 [Nm]	2.6	1.0	9.2	4.5	27.1	19	46	33	9.8	8.0
	P1 [kW]	0.29	0.11	1.0	0.50	3.0	2.1	5.1	3.6	0.98	0.80
	T2 [Nm]	2.9	1.1	10	5	29.7	21	53	37	12.4	10.2
	P1 [kW]	0.19	0.07	0.67	0.33	2.0	1.4	3.5	2.5	0.75	0.62
	T2 [Nm]	3.4	1.3	11.6	5.6	34.7	23	63	41	16.4	13.9
	P1 [kW]	0.11	0.04	0.39	0.19	1.2	0.77	2.1	1.4	0.50	0.42
	T2 [Nm]	4.2	1.5	14.5	6.2	44	26	79	44	25.4	22
	P1 [kW]	0.05	0.02	0.16	0.07	0.49	0.29	0.89	0.49	0.25	0.22
	T2 [Nm]	4.7	1.7	16.5	6.7	50.5	27	89	46	33	25.7
	P1 [kW]	0.03	0.01	0.09	0.04	0.28	0.15	0.5	0.26	0.17	0.13

Simbolo Symbol Symbol	Definizione	Definition	Definition
n ₂	Giri uscita	Output revs	Umdrehungen Abtrieb
i	Rapporto	Ratio	Untersetzung
T ₂	Coppia uscita max.	Max. output torque	Max. Abtriebsdrehzahl
P ₁	Potenza entrata	Input power	Antriebsleistung

CARICHI RADIALI E ASSIALI

RADIAL AND AXIAL LOADS

RADIALE UND AXIALE BELASTUNGEN

	Fr	Fa
RL31	210	110
RL32	410	200
RL33	760	430
RL34	880	490

Fr:
Carico radiale max. (N) applicato a metà della sporgenza dell'albero
Max. radial load in N
Radial - Belastung (max.) in N

Fa:
Carico assiale max. (N)
Max. axial load in N
Axial - Belastung (max) in N

Figure 12.11: Specifications of the right angle gear by TRAMEC



RINVII ANGOLARI
RIGHT ANGLE GEARS
WINKELGETRIEBE



DIMENSIONI

DIMENSIONS

ABMESSUNGEN

RL 31

3FL

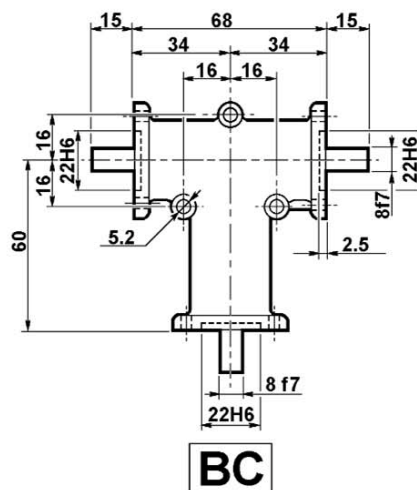
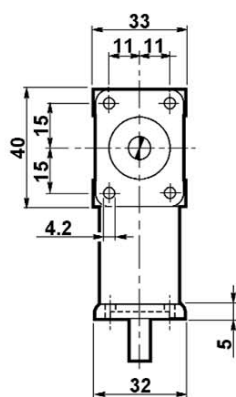
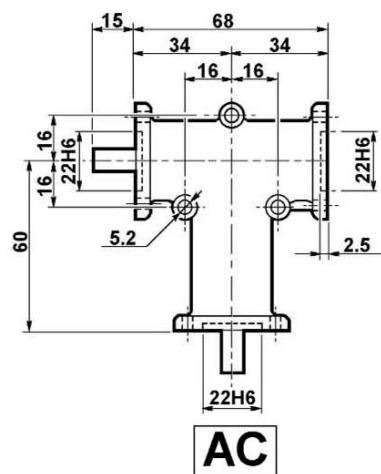
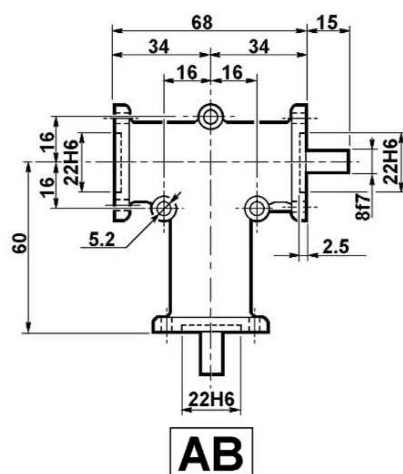
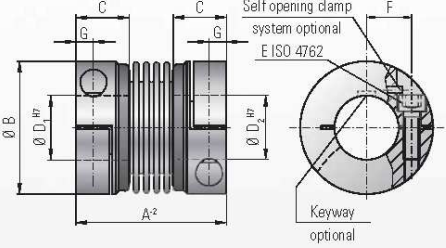


Figure 12.12: Dimensions of the right angle gear by TRAMEC



Ordering example

BKL / 80 / 26 / 22 / XX

Model
Series/Nm
Ø D1 H7
Ø D2 H7
non standard

MODEL BKL

BACKLASH-FREE, TORSIONALLY STIFF METAL BELLOWS COUPLINGS

with clamping hub

Properties:

- easy to mount
- low moment of inertia
- economically priced

Material:

BelloWS made of highly flexible high-grade stainless steel. Hub material see table

Design:

With a single ISO 4762 radial clamping screw per hub.

Self opening clamp system optional:
Loosening the clamping screw applies force to the pin, which will force the clamp into the open position for easy mounting and dismounting.

Temperature range:

-30 to +100° C (-22 F to 212 F)

Speeds:

Up to 10,000 rpm, in excess of 10,000 with a finely balanced version.

Backlash:

Absolutely backlash-free due to frictional clamped connection.

Brief overloads:

Acceptable up to 1.5 times the value specified.

Service life:

These couplings have an infinite life and are maintenance-free if the technical ratings are not exceeded.

Tolerance:

On the hub/shaft connection 0.01 to 0.05 mm.

Non standard:

Custom designs with varied tolerances, keyways, non-standard material, bellows and ATEX designs are available upon request.

Model BKL		Series									
		2	4,5	10	15	30	60	80	150	300	500
Rated torque (Nm)	T _{rn}	2	4.5	10	18	30	60	80	150	300	500
Overall length (mm)	A ²	30	40	44	58	68	79	92	92	109	114
Outer diameter (mm)	B	25	32	40	49	56	66	82	82	110	123
Fit length (mm)	C	10.5	13	13	21.5	26	28	32.5	32.5	41	42.5
Inner diameter possible from Ø D1 to Ø D2 (mm)	D _{1/2}	4-12.7	6-16	6-24	8-28	10-32	14-35	16-42	19-42	24-80	35-82
Fastening screw ISO 4762	E	M3	M4	M4	M5	M6	M8	M10	M10	M12	M16
Tightening torque of the fastening screw (Nm)	F	2.3	4	4.5	8	15	40	70	85	120	200
Distance between centers (mm)	G	8	11	14	17	20	23	27	27	39	41
Distance (mm)	H	4	5	5	6.5	7.5	9.5	11	11	13	17
Moment of inertia (10 ⁻³ kgm ²)	J _{rel}	0.002	0.007	0.016	0.065	0.12	0.3	0.75	1.8	7.5	11.7
Hub material		AL optional steel	AL optional steel	AL optional steel	AL optional steel	AL optional steel	AL optional steel	AL optional steel	steel optional AL	steel optional AL	steel optional AL
Approx. weight (kg)		0.02	0.05	0.08	0.16	0.25	0.4	0.7	1.7	3.8	4.9
Torsional stiffness (10 ³ Nm/rad)	C _t	1.5	7	9	23	31	72	80	141	157	290
axial ± (mm)		0.5	1	1	1	1	1.5	2	2	2	2.5
lateral ± (mm)	Max values	0.2	0.2	0.2	0.2	0.2	0.2	0.2	0.2	0.2	0.2
angular ± (degree)		1	1	1	1	1	1	1	1	1	1
axial spring stiffness (N/mm)	C _a	8	35	30	30	50	67	44	77	112	72
lateral spring stiffness (N/mm)	C _l	50	350	320	315	368	679	590	960	2940	1450

(1 Nm = 8.85 in lbs)

Figure 12.13: Specifications of the couplings by R+W



Technisches Datenblatt

Teile Nr 16003

einreihiges Radialrillenkugellager offen

Hauptmerkmale

Bohrungsdurchmesser (d) : 17 mm (+0, -8) μ
 Außendurchmesser (D) : 35 mm (+0, -11) μ
 Innenring-Breite (B) : 8 mm (+0, -120) μ
 Außenring-Breite (C) : (+0, -120) μ
 Gesamtbreite (T) :
 Gewicht : 0.032 kg
 Empfohlene Mindesttemperatur : -40 ° C
 Empfohlene Höchsttemperatur : 120 ° C
 Grenzdrehzahl Schmierfett : 20000 tr/min
 Grenzdrehzahl Öl : 24000 tr/min
 Ab-Dichtung/Deckung : Keine
 Käfig : Stahl

Anwendungsbedingungen

Betriebstemperatur : -
 Betriebsdrehzahl : -

Lebensdauer

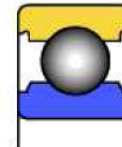
Dynamische Kapazität ISO (C) : 600 daN
 Dynamische Radiallast : -
 Dynamische Axiallast : -
 Lebensdauer L10 (ISO) : -
 Koeffizient a2 : 1

Sicherheitsfaktor

Statische Kapazität ISO (Co) : 325 daN
 Statische Radiallast (Fro) : -
 Statische Axiallast (Fao) : -
 Sicherheitsfaktor (Fs) : -

Einstellungen

Einstellung Innenring : -
 Einstellung Außenring : -



Charakteristische Frequenzen (Hz) bei 60 tr/min mit sich drehendem Innenring

Käfig-Frequenz : 0.408
 Rollkörper-Frequenz : 5.275
 Außenring-Frequenz : 4.084
 Innenring-Frequenz : 5.915
 Im Fall eines sich drehenden Außenrings sollten Sie sich an SNR wenden.

Schmierung

Öl : -

Fett : -

Mindestfördermenge Öl : -
 Anfangsgewicht des Schmierfetts : -

Nachschmierung

Gewicht des zu erneuernden Schmierfetts : -
 Nachschmierhäufigkeit : -

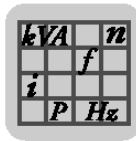
Figure 12.14: Specifications of the bearings by SNR

Drehstrommotor DFT80K2/TF

Motor-Drehzahl [R/min] 2700
Bauform IM B5
Motor-Moment [Nm]/ED [%] S1
Motor-Spannung [V] 230/400
Motor-Leistung [kW] 0,75
LS-Anzahl (Satz je Antrieb) 1
Sprache D/LNI
Sachnummer 1 Typenschild 01818686
Motor-Frequenz [Hz] 50
Motor-Spannung [V]/Schaltart 230/400 Dreieck/Stern
Nennstrom [A] 3,50/2,00
cos PHI 0,86
wärmeklasse/Schutzart [IP] F/54
Nettogewicht [kg] 9,087
[Fabrikationsnummer 01.1259527401.0001X08]



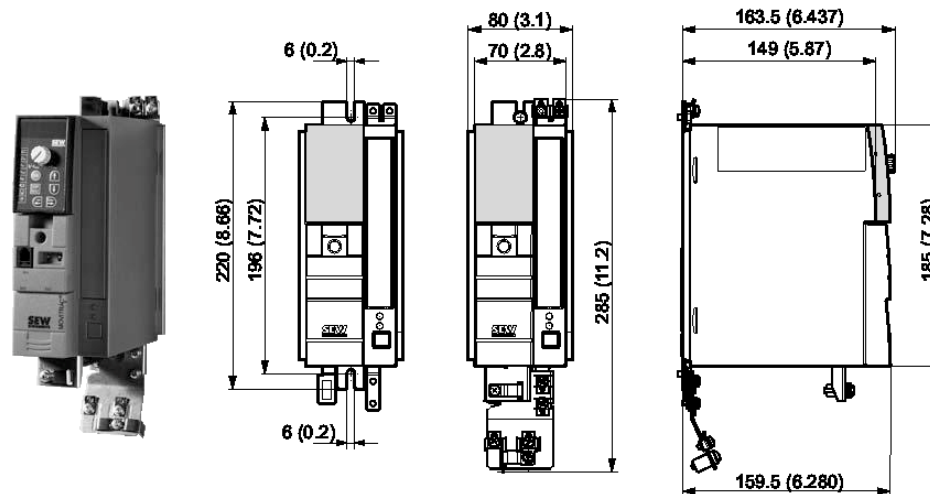
Figure 12.15: Specifications for the motor by SEW-EURODRIVE



Technical Data

Technical data of MOVITRAC® B

4.4.11 AC 230 V / 1-phase / size 0S / 0.55 / 0.75 kW / 0.74 / 1.0 HP



MOVITRAC® MC07B (1-phase power supply)		0005-2B1-4-00	0008-2B1-4-00
Part number		828 494 6	828 495 4
INPUT			
Rated mains voltage	V _{mains}	1 × AC 200 – 240 V	
Rated mains frequency	f _{mains}	50 / 60 Hz ± 5 %	
Rated mains current, 100 % operation	I _{mains}	AC 8.5 A	AC 9.9 A
Rated mains current, 125 % operation	I _{mains 125}	AC 10.2 A	AC 11.8 A
OUTPUT			
Output voltage	V _O	3 × 0 – V _{mains}	
Recommended motor power 100 % operation	P _{Mot}	0.55 kW / 0.74 HP	0.75 kW / 1.0 HP
Recommended motor power 125 % operation	P _{Mot 125}	0.75 kW / 1.0 HP	1.1 kW / 1.5 HP
Rated output current 100 % operation	I _N	AC 3.3 A	AC 4.2 A
Rated output current 125 % operation	I _{N 125}	AC 4.1 A	AC 5.3 A
Apparent output power 100 % operation	S _N	1.4 kVA	1.7 kVA
Apparent output power 125 % operation	S _{N 125}	1.7 kVA	2.1 kVA
Minimum permitted braking resistance value (4 quadrant operation)	R _{BW_min}	27 Ω	
GENERAL INFORMATION			
Power loss 100 % operation	P _V	45 W	50 W
Power loss 125 % operation	P _{V 125}	50 W	65 W
Current limitation		150 % I _N for at least 60 seconds	
Terminal cross section / tightening torque	Terminals	4 mm ² / AWG12 / 0.5 Nm / 4 lb in	
Dimensions	W × H × D	80 × 185 × 163.5 mm / 3.1 × 7.28× 6.437 in	
Mass	m	1.5 kg / 3.3 lb	

Figure 12.16: Specifications of the frequency inverter Movitrac by SEW-EURODRIVE

